NEXT-GENERATION DEWATERING FABRICS

DEVELOPMENT OF DEWATERING FABRICS INCORPORATING SLIT-PORE GEOMETRIES

By KURT JAMES WESTHAVER, B.ENG

A Thesis Submitted to the School of Graduate Studies
in Partial Fulfillment of the Requirements for the Degree
Master of Applied Science

MASTER OF APPLIED SCIENCE (2018) McMaster University

(Chemical Engineering) Hamilton, Ontario

TITLE:	Development of Dewatering Textile Materials Incorporating Slit-Pore Geometries
AUTHOR:	Kurt James Westhaver, B. Eng. (Laurentian University)
SUPERVISOR:	Dr. D. Latulippe
NUMBER OF PAGES:	xviii, 116

LAY ABSTRACT

The treatment of municipal, industrial and agricultural wastewater produces a semi-liquid mixture known as sludge. The costs associated with pumping, transporting, treating, storing, and disposing of sludge are significant. Therefore, sludge dewatering techniques are employed to increase the solids content of the material by separating the solid and liquid components, thus reducing the overall volume requiring further handling. Non-mechanical dewatering methods require large areas of land and favorable climatic conditions, while mechanical dewatering technologies require significant capital investment and ongoing operation and maintenance by highly trained personnel. Due to these shortcomings, the conventional methods of sludge dewatering are not applicable to scenarios where: the quantity of sludge is small, there is limited budget, there are land restrictions, or dewatering is performed seasonally. An alternative approach that has recently attracted considerable attention is the use of dewatering fabrics; specially engineered textiles supplied in the form of very large bags into which the sludge is pumped. The concept itself is simple, pressure inside the bag pushes the free water through the fabric while the solid material is retained within. Unfortunately, these products have exhibited poor dewatering performance for certain feed materials. In this work, a series of ‘next-generation’ engineered dewatering fabrics featuring elongated ‘slit’ pores were produced using laser cutting techniques. A comprehensive analysis of the effect of the filter properties on dewatering performance was performed using sludge sourced from two different operations: municipal wastewater treatment and precious metal mining.

ABSTRACT

In recent years, the use of engineered dewatering fabrics has emerged as a viable alternative to conventional methods of sludge dewatering in numerous application areas including municipal wastewater, mining, and pulp and paper. Previous studies have focused on the development of empirical ratios between dewatering performance and the porous properties of the textile material. The limitation of this approach is that the latter is difficult to characterize using currently available techniques due to the complex, nonuniform pore structure of conventional woven and nonwoven dewatering fabrics. In this study, a series of dewatering fabrics were produced using advanced microfabrication techniques featuring well-defined slit-pore geometries. Full-factorial design-of-experiment frameworks were employed to evaluate the effects of slit-pore dimensions and slit-pore spacing on cake layer development and key dewatering performance metrics. Laboratory scale dewatering performance tests were performed using both anaerobic digested sludge from the Woodward Avenue Wastewater Treatment Plant in Hamilton, Ontario and metal precipitate sludge from a nickel-copper mine in Ontario, Canada. The results from this study provide new insights into the importance of the cake layer in geotextile dewatering and the impact of pore geometry, porosity, and polymer performance on cake layer development.

ACKNOWLEDGEMENTS

It is my pleasure to thank the many people who made this thesis possible. I would like to start by expressing my gratitude to my supervisor Dr. David Latulippe of the Department of Chemical Engineering at McMaster University. His passion for innovation, dedication to his students, and trust in the research process allowed me to explore the many facets of my project and ultimately produce a body of work of which I am very proud. His sound advice, constructive feedback, and strong ideas helped me to work through numerous engineering challenges over the past two years. I am truly thankful for the countless hours he spent putting together grants and reference letters, meeting to discuss and edit my work, and encouraging me to set and achieve goals I would not have pursued otherwise. Most importantly, David taught me to trust in my abilities as a novice researcher and gave me the confidence to take my project in directions that reflect my passion for environmental applications within the mining sector.

I would also like to thank the undergraduate students -Morgan Archer, Karl Zimmermann, and Noel Devaere- who contributed to this research. I would especially like to thank Morgan; your assistance in the lab was essential to completing the many experiments which went into this work. The debates, lunches spent playing basketball as well as editing advice, and general help and friendship were all greatly appreciated.

I also want to extend my gratitude to Roozbeh Mafi, Emanuel Ausch, and the whole team at Canadian General-Tower Ltd. for the amazing opportunity you provided me with to learn and grow as an aspiring professional engineer. This project has broadened my understanding of sludge dewatering, water treatment, PVC formulation,

and micro fabrication. Our biweekly meetings provided me with valuable feedback, helped to keep the project on track, and provided me with the opportunity to further develop my presentation skills.

I want to thank SNF and Kemira for generously providing the polymer flocculants employed in this work, as well as Mark Solomon and the operations staff at the Woodward Avenue Wastewater Treatment Plant for providing the anaerobic digested sludge samples throughout this project.

I am grateful to Paul Gatt for his assistance in the design and construction of the dewatering performance test apparatus, Dr. Jake Nease for providing helpful resources related to the development of the multiple linear regression model, and the staff at the McMaster Manufacturing Research Institute for their technical assistance with the Keyence VHX Digital Microscope.

The funding for this work was provided by Canadian General-Tower Ltd. and the Ontario Centres of Excellence through their Voucher for Innovation and Productivity I Program. Financial support was also provided by Natural Sciences and Engineering Research Council (NSERC) through the Canada Graduate Scholarships-Master's (CGS M) Program and by the Province of Ontario and the Thomson-Gordon Group through the Ontario Graduate Scholarship (OGS). Additional funding was provided by the Water Environment Association of Ontario (WEAO) Scholarship Program.

I would also like to thank the many professors who taught me the fundamentals of chemical engineering, my undergraduate professors at the Bharti School of Engineering at Laurentian University as well as my graduate professors at the Faculty of Engineering at

McMaster University. Their kind assistance, advice and encouragement were critical to my growth as an aspiring engineer.

Lastly, the encouragement and love provided to me by my family throughout my time in the Master of Applied Science in Chemical Engineering Program cannot be overstated. I would like to thank my parents -Gary and Shelley- who support me in whatever I choose to pursue. You have always believed in my abilities and encouraged me to take on new and exciting challenges. To Teghan, my incredibly supportive partner, thank you for making this journey with me over the past two years. The love and support you have provided me during my undergraduate studies, post graduate internship, and my return to school to obtain a master's degree has been invaluable. I look forward to the next chapter of my life with you by my side.

TABLE OF CONTENTS

LIST OF TABLES

LIST OF FIGURES

LIST OF ABBREVIATIONS

ADS	Anaerobic Digested Sludge
AMD	Acid Mine Drainage
AOS	Apparent Opening Size
BT	Breakthrough
CST	Capillary Suction Time
DE	Dewatering Efficiency
DMAEA-Q	Quaternized-N,N Dimethylamino Ethylacrylate
DOE	Design-of-Experiments
DPT	Dewatering Performance Test
FBRM	Focused Beam Reflectance Measurement
MFT	Microscale Flocculation Test
MLR	Multiple Linear Regression
MPS	Metal Precipitate Sludge
OPD	Optimum Polymer Dose
PFT	Pressure Filtration Test
SC	Solids Content
TS	Total Solids
TSS	Total Suspended Solids
WQA	Water Quality Analysis
WWTP	Wastewater Treatment Plant

Chapter 1: Introduction

1.1 Sludge Dewatering

The term ‘sludge’ refers to a slurry-like mass, deposit, or sediment which is generated through the treatment of municipal, industrial, or agricultural wastewater. The implementation of efficient sludge dewatering processes prior to the further treatment or final disposal of these high-water-content materials is critical to the economic and environmental sustainability of these operations [1]. Dewatering processes apply solid-liquid separation principles in order to increase the solids content (SC) of the sludge, thus reducing the overall volume of material requiring further handling. As a result, substantial cost savings are generated with respect to sludge pumping, transportation, treatment, storage, and disposal. Furthermore, environmental concerns related to the long-term storage of sludge -such as leachate production during landfilling operations- are mitigated [2].

Dewatering processes are classified according to the solid-liquid separation principle employed. There are four primary classifications: sedimentation, flotation, filtration, and screening. In sedimentation and flotation processes, the liquid phase of the sludge is constrained, and the solid particles can move freely within in it. Sedimentation can be applied when there is a significant difference in the specific gravities of the liquid and the suspended solids; the solids particles ‘settle’ out of suspension due to gravity or a centrifugal force. Conversely, the flotation process uses bubbles to transport the solids particles to the surface where they are collected using a mechanical system. In filtration and screening processes, a driving force is applied to the system, causing the liquid phase to pass through a medium which serves to constrain the solid particles [3].

1.2 Conventional Sludge Dewatering Technologies

A description of the conventional technologies used to perform sludge dewatering is presented herein. Note this section is not exhaustive and only includes some of the most common methods.

1.2.1 Sludge drying bed

Sludge drying beds represent a straightforward approach to sludge dewatering that offers low capital and operating costs and is ideally suited for small wastewater treatment plants (WWTP) [4]. This non-mechanical dewatering technology consists of a layer of sand -approximately 10 to 23 cm thick- overtopping 20 to 46 cm of granular material [5]. Earthen embankments or concrete foundation walls are used to contain the sand and gravel (i.e. the filter media) and serve as a perimeter for the sludge drying area. Additional embankments are used to subdivide this region into individual 'sludge drying beds'. In order to prevent erosion of the sand layer and evenly distribute the sludge across the filter media -in a layer 20 to 30 cm thick- splash pads are installed below the sludge inlets [5]. A drainage system consisting of perforated clay pipes integrated into the layer of granular material allows excess water to discharge from the sludge drying bed via gravity. The surface of the sludge is exposed to the atmosphere allowing evaporation or 'drying' of the sludge to occur. A schematic of a sludge drying bed is presented in Figure 1.

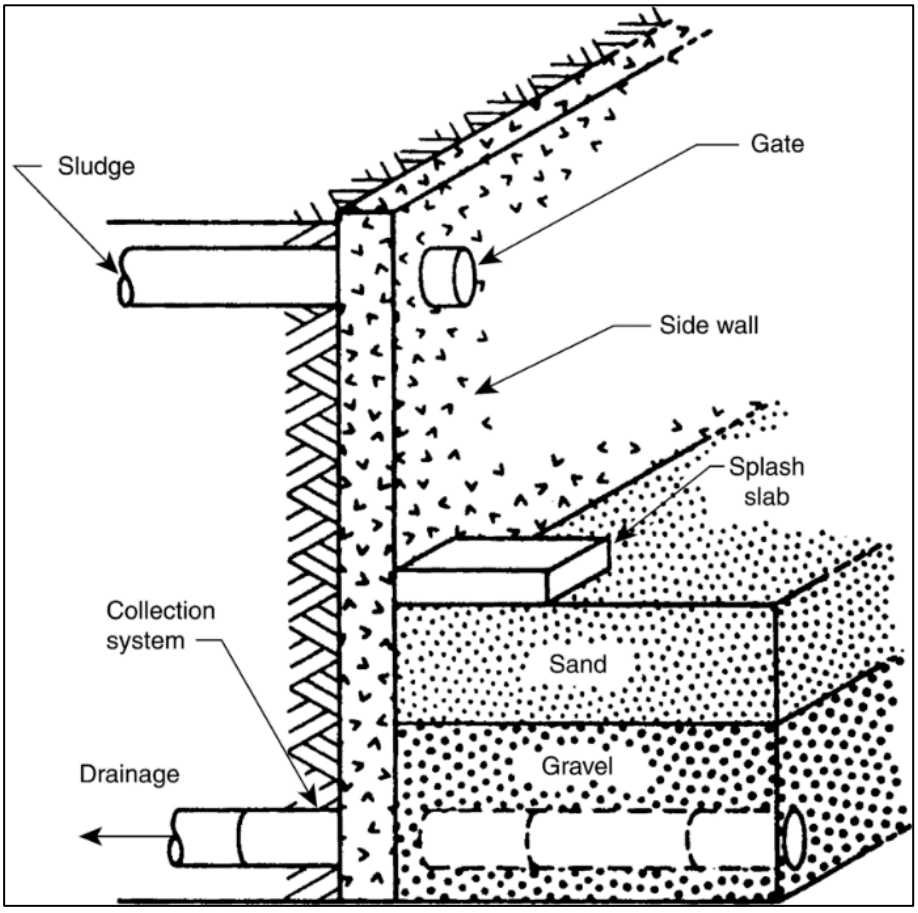

Figure 1. Schematic of a sludge drying bed [5].

A modification which can be made to the basic sludge drying bed is the implementation of common reeds, as shown in Figure 2. By planting these reeds in the sand layer, the resulting ‘reed bed’ is able to remove water from the sludge material via plant transpiration as well as evaporation and gravity filtration. Furthermore, previous studies have shown that as the reeds extend their roots into the growing sludge layer, localized aerobic zones are introduced into the typically anaerobic environment. These aerobic zones aid in the stabilization and mineralization of the sludge [6]. For the reed bed to properly operate during its entire life span -generally 30 years or more- emptying of each bed must be preformed every 8 to 12 years [4].

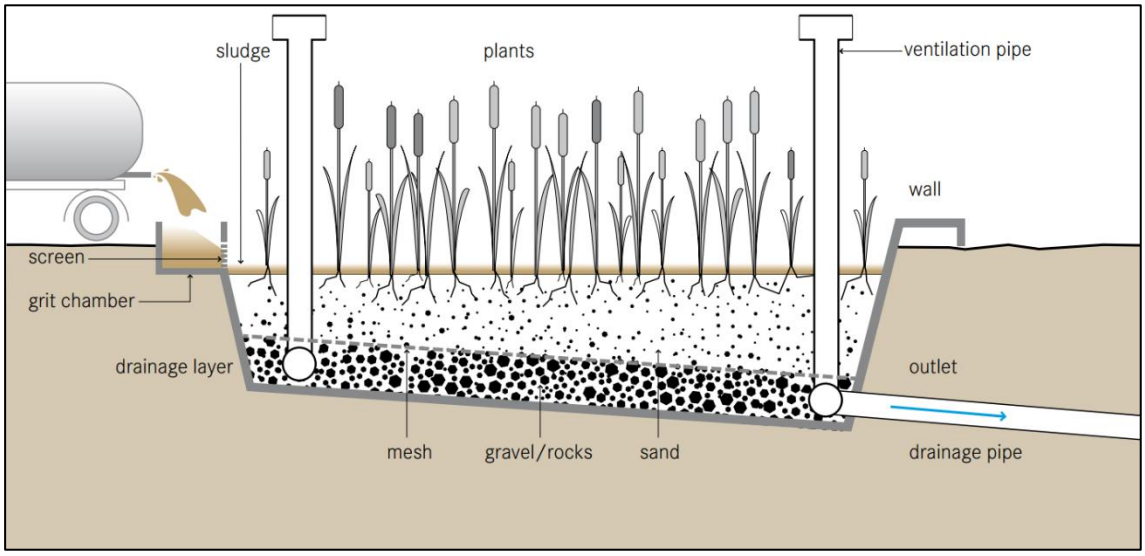

Figure 2. Schematic of a reed bed [7].

1.2.2 Decanter centrifuge

The decanter centrifuge -also referred to as the solid-bowl scroll-discharge centrifuge- is a dewatering technology used to treat a wide variety of sludge materials including mature fine tailings from oil sands processing [8]. Although mechanically complex, this piece of equipment exploits the same basic principles of sedimentation employed by many of the non-mechanical methods of sludge dewatering. For applications in which the specific gravity of the suspended solids is significantly greater than that of the liquid phase, the driving force provided by gravity is often sufficient to separate the solid and liquid phases of the sludge material in a reasonable amount of time [9]. However, when this differential is small -due to the solid and liquid fractions having similar densities or the presence of very small suspended particles- the apparent difference in specific gravity can be increased by applying an external force greater than that of gravity alone [3]. The decanter centrifuge employs a centrifugal force to accomplish this task.

As shown in Figure 3, the decanter centrifuge consists of a screw conveyor surrounded by a solid cylindrical enclosure referred to as the ‘bowl’. The sludge material is fed to a fixed position located along the horizontal axis of the device. The bowl and screw conveyor rotate at different speeds creating the centrifugal force which serves to transport the sludge from the ‘feed zone’ to the bowl wall, and to promote the sedimentation of suspended solids. The clarified liquid -referred to as the centrate- flows along the length of the bowl and exits the system at the far end of the centrifuge. The liquid discharge has an integrated weir which controls the depth of the liquid ‘pond’ held on the bowl wall during centrifugation. The other end of the bowl is tapered inwards, creating a slope up which the solids are transported by the screw conveyor. During this process, most of the liquid entrained within the solid material is removed. The dewatered solids exit the system at solids discharge located at the top of the tapered section of the bowl. In order to optimize dewatering performance, the dimensions of the screw conveyor, depth of the liquid pond, length of the bowl, rotational speeds, and the angle of the slope are chosen based on the dewatering characteristics of the feed material [9].

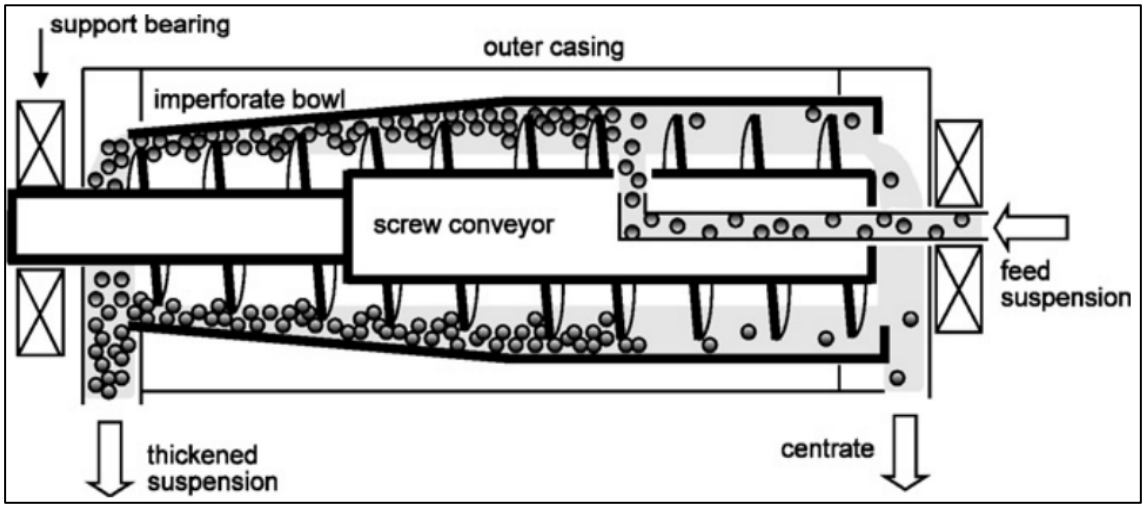

Figure 3. Schematic showing the essential features of a decanter centrifuge [10].

1.2.3 Plate and frame filter press

The plate and frame filter press -also referred to as a membrane filter plate- consists of a series of perforated plates and hollow frames which are arranged in alternating order to create separating chambers. A pair of rails are positioned along the length of the system which serve as a support structure. As depicted in Figure 4, each separating chamber features a hollow frame sandwiched between two filter plates covered with filter cloth. The chambers are held together using hydraulic or screw rams. To perform dewatering, slurry is forced into the separating chambers under pressure using a centrifugal pump. The solids are retained by the filter cloth, and the filtrate is discharged into engineered drainage points. Filter cake accumulates within the separating chambers and -when these chambers are filled- the perforated plates and hollow frames are pulled apart to discharge the solid material. This process is often performed manually, thus the operating costs associated with the use of this technology are significant. Plate and frame filter presses can also employ separating chambers with integrated washing plates which

facilitate cake washing; a wash liquor is passed through the filter cake to collect residual dissolved solids entrapped within the solid material [3].

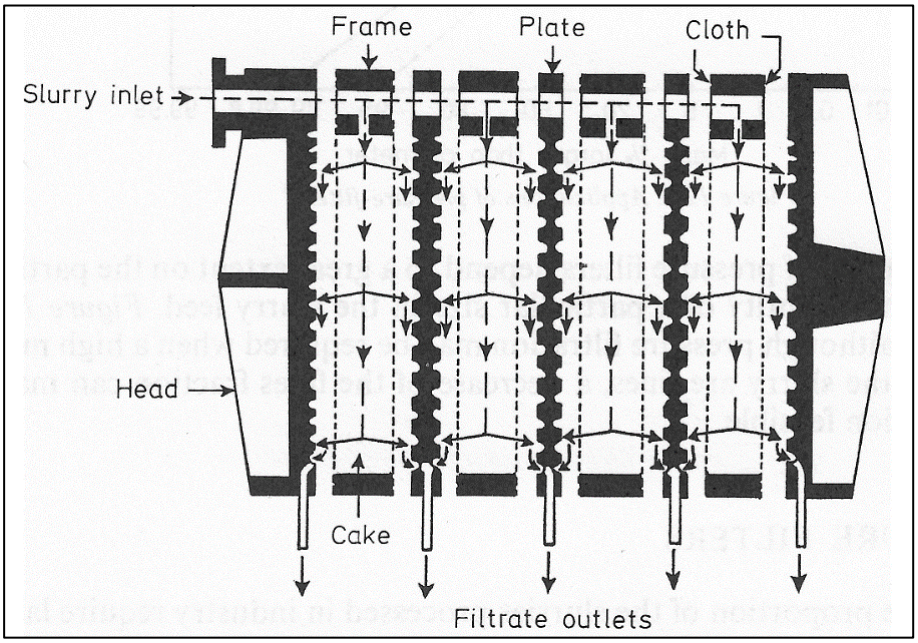

Figure 4. Schematic of a plate and frame filter press assembly [3].

1.2.4 Belt filter press

The belt filter press consists of an upper and a lower filter cloth -or belt- tensioned around a series of rollers. As shown in Figure 5, these cloths continuously rotate in opposite directions. The sludge is first fed onto the lower filter cloth where initial dewatering occurs; gravity forces free water to pass through the cloth, while the solid material is retained. The arrangement of the rollers is designed such that the distance between the upper and lower filter cloths decreases along the feed material's path, creating what is referred to as a 'consolidation zone'. As a result, the pressure applied to the sludge is continuously increased as it is carried through the system. Shear forces created by the relative movement of the filter cloths causes additional water to be

removed, and ultimately creates a filter cake with SC ranging from 12 to 50 % by weight [10].

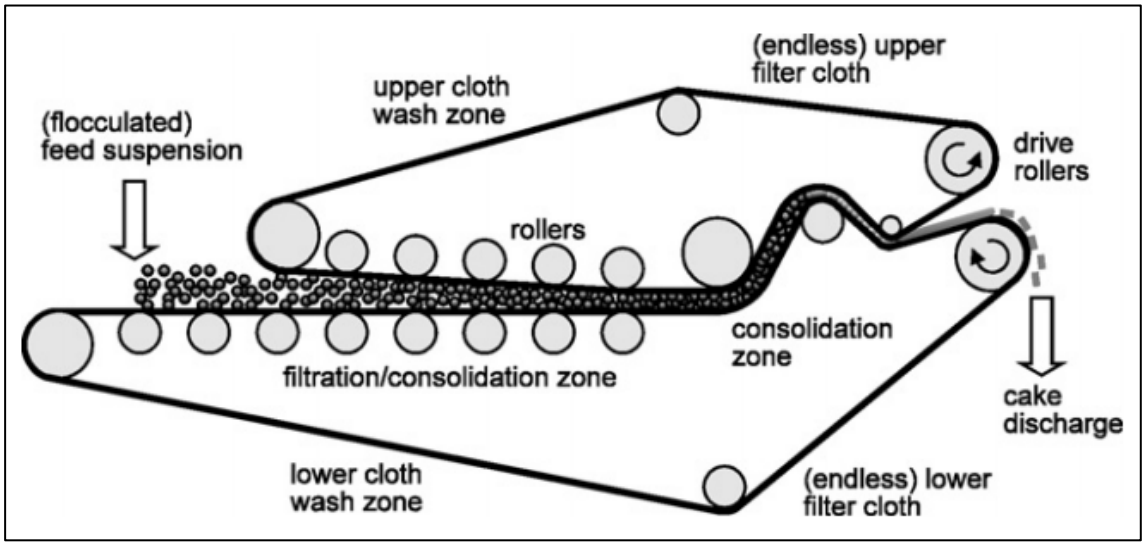

Figure 5. Schematic of a typical belt filter press [10].

1.3 Flocculation

Separating very small particles from a suspension is less efficient than separating larger particles. Thus, 'flocculating' procedures are often applied to increase particle size prior to performing sludge dewatering. In these procedures chemical additives are used to modify the solid-liquid interface such that small particles aggregate creating larger particles or flocs [3]. The development of polyelectrolytes which exhibit excellent flocculation performance at low concentrations represents a significant breakthrough in solid-liquid separation technology. These water-soluble polymer molecules, often referred to as polymer flocculants, can be nonionic, anionic, or cationic, and are characterized by their average molecular weight and the charge density distribution along the polymer chain [3]. The mechanism by which polymer flocculants induce the aggregation of small particles involves two distinct processes: charge neutralization and particle bridging. In

aqueous suspensions, small particles are electrostatically stabilized; osmotic pressure caused by overlapping electrical double layers create repulsive interparticle interactions which prevent aggregation [11]. Charge neutralization refers to the adsorption of an oppositely charged polymer flocculant to the surface of the suspended particles to lower zeta potential and, in turn, reduce repulsive interactions. Based on this principle, the optimum polymer dose (OPD) corresponds to a zeta potential of zero, which is achieved when the charged groups adsorbed to the particle surface neutralize the initial surface charge of the particle. If additional polymer is added beyond this point the particles can be re-stabilized. This phenomenon is referred to as charge reversal and can be detrimental to sludge dewatering operations [12]. If the adsorbed configuration of the polymer flocculant extends beyond the electrical double layer of the produced flocs, particle bridging can occur. In this process, a single polymer molecule adsorbs to the surface of multiple flocs creating a 'bridge'. In doing so, larger flocs are created which further improves the efficiency of separation and can increase floc strength [11].

There are a vast number of polymer flocculants available on the market; each with a unique combination of charge density, chemical composition, and molecular weight. The selection of an appropriate flocculant and the identification of the optimum dose are critical to minimizing treatment costs, optimizing flocculation performance, and mitigating the risk of environmental contamination. As reported by Cobbledick et al., flocculation performance varies widely based on the physiochemical properties of the flocculant employed [13]. Furthermore, the relationship between polymer dose and flocculation performance has been shown to be a strong function of flocculant type [14].

Therefore, identifying the ‘best’ flocculant can reduce the total quantity of polymer required to perform flocculation and thus minimize the associated costs. Unfortunately, no empirical model currently exists which allows the performance of a flocculant to be predicted based on its physiochemical properties [15]. Moreover, sludge materials originating from different industrial processes or WWTPs have diverse dewatering characteristics [14]. Thus, polymer flocculants must be screened on a case-by-case basis. Once the flocculant is selected, the OPD must be identified in order to maximize flocculation performance. The addition of too much flocculant -referred to as overdosing- can hinder flocculation performance through charge reversal and cause a variety of environmental toxicity issues; low concentrations of flocculant have been found to be toxic to aquatic lifeforms [16]. The addition of too little polymer -referred to as under dosing- can lead to poor flocculation performance.

Jar testing is the conventional method of screening polymer flocculants. In this approach, a number of beakers or ‘jars’ are filled with 1 to 2 L of the sludge material to be dewatered. These jars are equipped with independently controlled mixers which are used to stir the sludge samples at a desired rate. A unique dose of polymer flocculant is added to each beaker, and the settling characteristics of the sludge samples are subsequently compared. This process is repeated for each polymer to be screened. Thus, testing many polymer flocculants across a wide dose range is a laborious process for operations personnel and requires large volumes of sludge material. In response to these shortcomings, alternative methods of polymer screening (incorporating parallel and microscale processing techniques) have been developed to reduce the amount of time and

the volume of sludge material required to screen polymers and perform dosage optimization [14]. A thorough description of the high-throughput techniques for polymer screening employed in this work is provided in Section 2.5.

1.4 Geotextile Dewatering

An alternative approach to sludge dewatering that has recently attracted considerable attention is the use of engineered dewatering fabrics; specially designed geotextiles supplied in the form of enclosed bags typically 1 to 10 m in diameter [17]. In this process, a feed sludge source is first chemically conditioned using an appropriate polymer flocculant to maximize both the rate of dewatering and the retention of suspended solids [17]. As shown in Figure 6, the pre-treated sludge is fed to a geotextile dewatering bag using a positive displacement pump. The pressure within the bag forces the free water out through the pores of the fabric while keeping the solids contained within [18]. As dewatering proceeds, a permeable cake layer develops on the inner surface of the geotextile which contributes to the retention of fine particles and ultimately defines the overall permeability of the system [19].

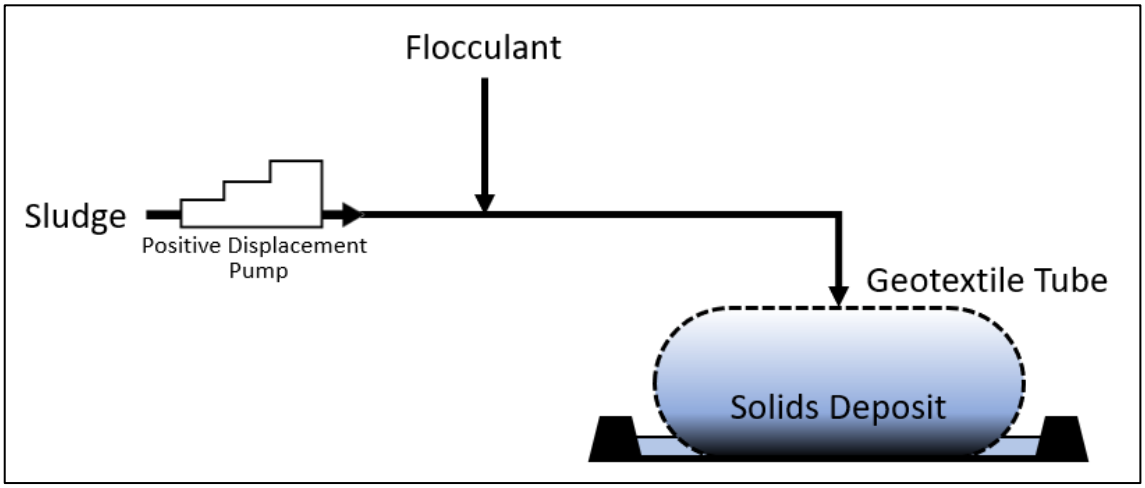

Figure 6. Schematic of the geotextile dewatering process. Sludge is chemically conditioned using in-line addition of a polymer flocculant, then pumped to an enclosed bag constructed of an engineered dewatering fabric.

Geotextile dewatering bags are typically operated in the semi-batch configuration shown in Figure 7. The bag is first filled to approximately 85% of its total capacity with pre-treated sludge. The feed pump is then turned off and the higher 'head pressure' (caused by the vertical column of fluid) inside the bag pushes the free water through the engineered dewatering fabric while the solid material is retained. The retained solids are then allowed to consolidate at the bottom of the bag. This process is repeated until 85% of the bag's capacity is filled with consolidated solids [20]. The dewatering rate, solids retention, and volume reduction achieved by a geotextile dewatering bag are a function of the dewatering characteristics of the sludge, the efficacy of the pre-treatment methods employed, and the pore structure of the engineered dewatering fabric. After the dewatering process is complete, there are multiple options:

- the bags are cut open and the retained solids are removed and transported to another location for disposal;
- the filled bags are trucked off-site; or

- the filled bags are left in place to be used as containment structures (diversion dams, dikes, etc.).

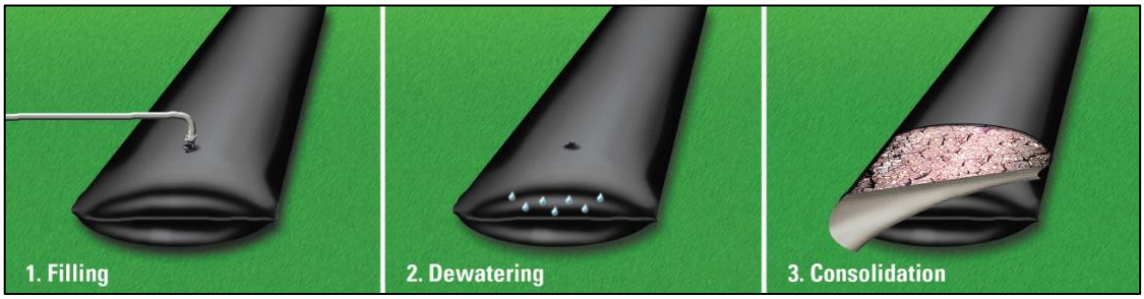

Figure 7. Schematic of the semi-batch operation of a geotextile dewatering bag; taken from https://www.tencategeo.us/en-us/products/geotube-systems/geotube-dewatering

The size, shape, and distribution of a dewatering fabric's pores are a function of the fiber type and manufacturing processes used in its development [21]. The currently available fabrics for geotextile dewatering applications fall into one of two categories: woven or nonwoven. Woven geotextiles are composed of monofilament, multifilament, or slit-film yarns that are produced using high-tenacity polypropylene or polyester [19]. As shown in Panel A of Figure 8, the weave patterns employed to interlace these yarns create a uniform array of pores which are approximately square in shape [22] [23]. Conversely, a nonwoven geotextile is a sheet, web, or batt of fibers or filaments that has been bonded using a combination of mechanical, thermal, or chemical processes creating a complex 3-dimensional pore structure [24] [25]. Panel B of Figure 8 depicts a needle-punched, nonwoven textile created using stable polypropylene fibers. Apparent opening size (AOS) refers to the largest pore opening of a geotextile and is measured via ASTM D4751-16, which combines the dry-sieving of glass beads and the use of a capillary porometer [26]. Typical AOS values reported in the literature range from 150 to 850 µm for woven textiles, and 75 to 210 µm for nonwoven textiles [23] [25].

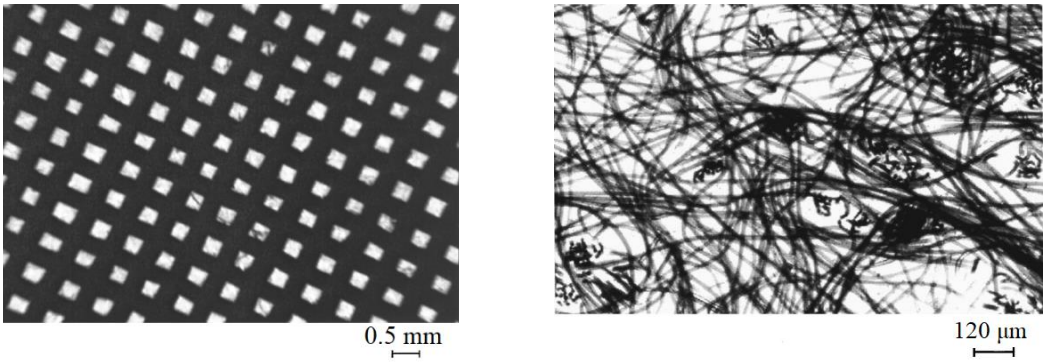

Figure 8. Images depicting the pore structure of conventional engineered dewatering fabrics. Panel A displays a woven textile constructed of monofilament polypropylene yarns [23], while Panel B depicts a needle-punched, nonwoven textile constructed of stable polypropylene fibers [25].

Geotextile dewatering bags are economical, mechanically simple, easily transported, and can be fabricated in site specific sizes. These attributes make them particularly attractive for applications where:

- the quantity of sludge requiring dewatering is relatively small;
- the available budget is limited;
- there are land restrictions;
- the sludge is produced at a remote location;
- dewatering is to be performed on a seasonal basis.

In contrast, the conventional methods of sludge dewatering are not applicable to the scenarios outlined above due to their respective limitations; non-mechanical dewatering methods require large areas of land and favorable climatic conditions, while mechanical dewatering technologies require significant capital investment and ongoing operation and maintenance by highly trained personnel [27]. These factors -combined with the intuitive advantages of a dewatering technology that is efficient, low cost, and simple to operate- make geotextile dewatering bags a viable alternative to conventional methods of sludge

dewatering. From rural wastewater treatment facilities to the dewatering of 2.65 million cubic yards of dredged sediment from Onondaga Lake in Syracuse, New York, geotextile dewatering has been shown to be a versatile technology capable of facilitating both small and large-scale operations [28].

The market for geotextile dewatering bags has been strengthened in recent years as result of increasing landfill fees and the development of strict environmental regulations governing the storage and disposal of waste materials [17]. Geotextile dewatering bags have been adopted to dewater sludge originating from municipal water and wastewater treatment facilities as well as mining and pulp and paper operations [19] [29] [30]. Geotextile dewatering has also been demonstrated to be a viable option for treating sludge sourced from the agricultural sector. A challenging aspect of fruit and vegetable farming is the treatment of 'washwater'; the wastewater produced through the washing, fluming or cooling of field produce [31]. A key component of washwater treatment is the removal of suspended solids (i.e. soil particles, vegetable pieces and other organics) to meet the regulations which govern effluent clarity. As part of the Holland Marsh Growers' Association Water Project, the geotextile dewatering process was shown to effectively remove suspended solids from vegetable washwater [32] [33]. Figure 9 displays images of the vegetable washwater and time-lapse photos of the dewatering process.

Figure 9.The image on the left depicts vegetable washwater, while the image on the right is a time-lapse of the geotextile dewatering process [33].

Geotextile dewatering bags also offer a unique approach to the progressive closure and reclamation of oil sands tailings ponds. Mature fine tailings -which are composed of water, sand, clay and residual bitumen- can be consolidated and dewatered within geotextile bags creating a ‘trafficable’ deposit. As shown in Figure 10, the bags can then be covered with an aggregate material followed by a layer of top soil. To complete the process, hydroseeding can be employed to create a vegetated cover. Previous studies have shown that geotextile dewatering bags can retain 99 % of the suspended solids, while significantly increasing the SC of the mature fine tailings when effective pre-treatment is employed [34].

Figure 10. Images of geotextile dewatering bags filled with consolidated MFT. These tubes can be covered with aggregate material and vegetated as part of an oil sands reclamation program [34].

1.5 Problem Statement

Dewatering fabrics are selected for a given application based on an empirical ratio between the median particle size of the sludge and the AOS of the fabric [22]. However, as previous studies have demonstrated, the size of the smaller pore openings has a direct effect on filtration performance [23] [25]. This is problematic as many currently available methods for measuring pore opening size distributions are unreliable, operator-dependent, or extremely time consuming [23]. Furthermore, this approach does not consider the relationship between the porosity of the fabric and the permeability of the filter cake, or its rate of development. Therefore, there is a need for an alternative approach to dewatering fabric selection which is based on well-defined relationships between filter properties, key dewatering performance metrics, and filter cake characteristics. Such a method -combined with effective screening of pre-treatment conditions- would allow for the optimization of the geotextile dewatering process based on the inherent dewatering characteristics of the sludge source.

Another limitation of the conventional dewatering fabrics is that -in certain applications- they are prone to foul or ‘blind’. Depending on the dewatering

characteristics of the feed material and the efficacy of the pre-treatment conditions employed, the pore openings of the fabric can become blocked with solid material and cause a premature end to the dewatering process. As a result, the liquid fraction of the feed material remains within the dewatering bag which behaves like a ‘waterbed like mattress’ [34]. This scenario reflects a classic trade-off between quality and quantity in the field of separation sciences; small pore openings effectively retain suspended solids but are prone to fouling, larger pore openings are less prone to fouling but do not effectively separate the solid and liquid fractions of the sludge. Thus, there is a market opportunity for a ‘next generation’ dewatering fabric that is able to retain suspended solids, is less prone to fouling, and -as a result- is applicable to a wider range of sludge sources.

1.6 Research Objectives

In this work, a series of ‘next-generation’ engineered dewatering fabrics featuring unique pore morphologies were produced using solid-state laser cutting; an advanced microfabrication technique capable of producing very small features with a high degree of accuracy. These advanced dewatering fabrics are referred to throughout this thesis as ‘thin-film dewatering filters’. A laboratory-scale geotextile filtration system was also designed and fabricated ‘in house’ to evaluate the dewatering performance of engineered dewatering fabrics under conditions of constant pressure or constant rate.

In contrast with the conventional dewatering fabrics, each of the thin-film dewatering filters featured a uniform array of elongated slit-pores. The width, length and interpore spacing of the slits -and therefore the total porosity of the fabric- were precisely

defined prior to fabrication using a full-factorial design-of-experiments (DOE) framework. The advantage to this approach is that it allows for a comprehensive analysis of the effect of pore morphology on dewatering performance to be made. Moreover, regression models can be developed which relate the design factors of the DOE framework to key dewatering performance metrics. These models can then be used to optimize the pore morphology of the dewatering fabric to achieve the desired objectives of a dewatering application. The use of solid-state laser technology, in combination with computer aided design software, also allows for a level of design flexibility and a rate of prototype development greater than that attainable for the conventional fabrics.

The concept of an engineered dewatering fabric incorporating slit-pore geometries was inspired by recent studies which explored the use of elongated pores to reduce fouling in microfiltration and ultrafiltration membrane applications. It was hypothesised that this concept could be applied to dewatering fabrics as they operate based on the principle of surface filtration; solids are deposited on the feed side of the filter medium. The concept of reducing fouling using elongated pores is illustrated in Figure 11. As particle bridging of the pore openings occurs, elongated pores provide additional filtration area for fluid flow relative to the conventional circular pores; reducing the decline in flux as filtration proceeds. Furthermore, if the designed width of the elongated pore is equal to the diameter of the circular pore the solids retention capacity of the fabric should remain unchanged as the transmission of solids through the material is governed by the smallest pore dimension.

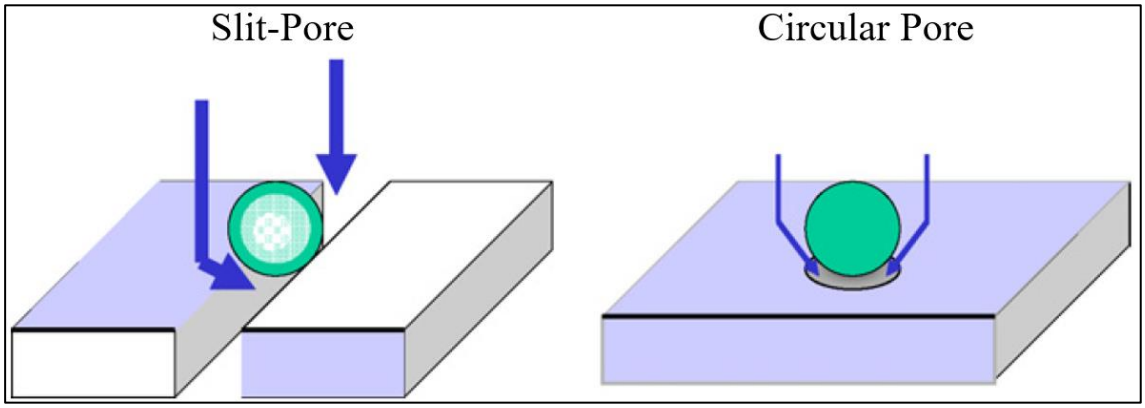

Figure 11. Schematic of the fluid flow around a spherical particle creating a blockage on a slit-pore compared to a cylindrical pore; adapted from [35].

This concept was first applied to the development of surface microfilters by Bromley et al. [36]. A custom filter having elongated pores 10 μm in width and 420 μm in length was produced using metal screen. Its performance was compared to that of a commercially available track-etched filter having 10 μm diameter pores. Constant rate filtration tests were performed in a stirred cell apparatus using a dilute suspension of latex particles. The results demonstrated that the filter with elongated pores was able to achieve a critical flux much greater than the filter with conventional circular pores. Critical flux is defined as the volumetric filtrate flowrate per unit filtration area above which fouling occurs. The track-etched filter experienced fouling at fluxes above 260 lm^{-2} h^{-1} while the custom filter with elongated pores was able to achieve fluxes as high as 1500 lm^{-2} h^{-1} without experiencing substantial fouling.

Moreover, work by Chandler & Zydney [35] demonstrated that microfilters possessing elongated pores were less prone to a decline in flux arising from fouling of the pore openings. Two microfilters were evaluated using Baker's yeast suspensions; one having circular pores 6 μm in diameter and the other having pores 6 μm in width by 400

μm in length. The microfilter with elongated pores had a filter porosity of 2.4 %, while the circular pore filter had a porosity of only 0.08 %. Constant pressure filtration tests (PFTs) revealed that the flux decline experienced by the filter with elongated pores was slower than that observed for the conventional filter with circular pores. Due to their high aspect ratio, the elongated pores were only partially blocked by the deposited yeast, whereas the circular pores were quickly fouled.

A more recent study by Kanani et al. [37] applied this concept to the development of ultrafiltration membranes. In doing so, they demonstrated that the use of elongated pores is a viable method of reducing fouling in a manner that does not compromise the very high selectivity achieved by conventional circular pores. The hydraulic permeabilities of custom silicon membranes were evaluated using phosphate buffered saline, while sieving data was obtained using both bovine serum albumin and polysaccharide dispersions. The silicon membranes were designed to have elongated nanopores approximately 45 μm in length and 10 to 60 nm in width. The obtained data was compared to that observed for commercial ultrafiltration membranes having circular pores. The results of this comparison clearly demonstrate that membranes with elongated pores achieve greater selectivity at a given permeability. In other words, increasing the length of the pore openings increased the permeability of the ultrafiltration membranes without degrading their ability to retain small particles.

To date, the concept of elongated pore openings has not been applied in the engineered dewatering fabric community and thus there exists an excellent opportunity for innovation.

1.7 Applications

This work focuses on two potential applications of the thin-film dewatering filters: anaerobic digestion of wastewater sludge and pond treatment of acid mine drainage. A description of these two processes is provided below.

1.7.1 Anaerobic digestion

Municipal wastewater is treated using a combination of physical, biological, and chemical processes in order to prevent the release of pollutants into waterways. Such pollutants include oxygen-demanding substances, pathogens, nutrients, and inorganic and synthetic organic chemicals. After initial screening of large suspended materials and the removal of sand, grit, cinder, and small stones using a grit chamber, wastewater proceeds to a primary clarifier. Herein, the flow rate of the wastewater is reduced allowing small particles of suspended matter to settle out. The material collected at the base of the clarifier is referred to as primary sludge. In order to remove dissolved constituents, the clarified water exiting the primary clarifier is fed to an aeration basin. The wastewater is mixed with air and, in turn, bacteria and microorganisms break down the organic matter resulting in further bacterial growth. The aerated mixture then flows to a secondary clarifier where the excess biomass -referred to as secondary or “activated” sludge- is removed [38].

The primary and activated sludge streams are then fed to an anaerobic digester where anaerobic bacteria stabilize the sludge and eliminate pathogens. This process gained widespread adoption in the 1970s as it provided a viable option for energy production through the combustion of the methane generated. There are four primary

stages of anaerobic digestion: hydrolysis, acidogenesis, acetogenesis, and methanogenesis. The complex organic matter entering the digester is first broken down into its individual monomers by hydrolytic enzymes. Next, fermenting bacteria convert these monomers into volatile fatty acids which are subsequently converted to acetate, hydrogen and carbon dioxide by acetogenic bacteria. Finally, methane is produced through the conversion of acetate and hydrogen by acetoclastic methanogens and the conversion of hydrogen and carbon dioxide by hydrogenotrophic methanogens [39]. The anaerobic digestion process results in the development of a sludge material -referred to in this work as anaerobic digested sludge (ADS)- with SC ranging from 2 to 6 % by weight [2]. The nutrient value and energy content of the ADS make it an ideal candidate for a variety of beneficial use management options including: forestry, mine reclamation, agriculture, disturbed land improvement, value added product development, energy capture, and cement manufacture. A key factor in determining the most appropriate management option for an ADS source is the concentration of trace elements, pathogens and other contaminants that may pose a risk to the environment or human health. When deemed unsuitable for beneficial use, ADS can be permanently disposed of through either combustion or landfilling.

Due to increasing tipping fees and a shortage of landfill availability, disposal of ADS has become more difficult in recent years [40]. Furthermore, due to increasing fuel costs, the transportation of ADS for beneficial use has become more expensive. To minimize the difficulties associated with ADS disposal -or the transportation costs associated with beneficial use practices- sludge dewatering of ADS is often performed

using either a belt filter press or a decanter centrifuge. As previously discussed, these mechanical dewatering technologies require significant capital investment and ongoing operation and maintenance by highly trained personnel. As such, they are not suitable for small rural WWTPs -which have limited resources- or for temporary operations to increase plant capacity during high flow periods. Dewatering fabrics represent a promising alternative to belt filter presses and decanter centrifuges for the dewatering of ADS. Their low cost and ease of operation make them ideally suited for use in small wastewater treatment facilities and for increasing the capacity of existing ADS dewatering systems.

1.7.2 Acid mine drainage treatment

Mining operations produce large volumes of hazardous wastes that can pose a significant threat to the environment and human health. The two most prevalent waste materials produced by base and precious metal mining operations are mine tailings and waste rock. 'Mine tailings' refers to the fine particulate matter left over after extractive processes have been used to remove valuable constituents from ore. 'Waste rock' refers to the broken rock or overburden –ranging in size from fine sand to large boulders– removed from the ground along with the ore which contains minerals in concentrations too low for economic recovery.

The ever-growing inventory of mine waste presents a major concern for the mining industry due to the potential environmental effects on receiving water bodies and inhibition of mine site reclamation strategies associated with Acid Mine Drainage (AMD). Mine tailings and waste rock contain sulphide minerals –such as pyrite– which

readily react with atmospheric oxygen and water to form AMD. These effluents contain elevated concentrations of toxic substances such as: cyanides, arsenic, heavy metals, and other by-products of ore extraction. The Kam Kotia Mine –located in Timmins, Ontario, Canada– is a notable example of the environmental and economic impacts of AMD. As shown in Figure 12, a ‘kill zone’ was created at this former copper mine in which nearly all vegetation was destroyed as AMD flowed through the groundwater and ultimately contaminated a nearby river [41]. Despite entering closure in the 1970s, AMD production onsite persists and is expected to continue for the indefinite future. The estimated cost to fully remediate the Kam Kotia Mine is $40.8 million [41]. In the United States and Canada alone, it is estimated that as much as $77 billion will be required to perform on-going care and maintenance of existing AMD sites to mitigate their environmental impact [42].

Figure 12. Photograph of the ‘kill zone’ created by acid mine drainage at the Kam Kotia Mine in Timmins, Ontario, Canada [41].

The conventional method of treating AMD is referred to as ‘pond treatment’. As shown in Figure 13, this process begins with the addition of an alkali –such as lime or caustic soda– to raise the pH [43]. The targeted pH is typically between 9.5 and 11 to precipitate metals out of solution as metal hydroxides [44]. Polymer flocculants or coagulants may also be added to the process to aggregate the solids into larger particles. The AMD is subsequently fed to a series of ponds. The first pond in the series -referred to as the ‘settling pond’- removes most of the metal hydroxide precipitates from the suspension via sedimentation. The second pond is significantly larger, providing a longer retention time and more laminar flow conditions. Referred to as the ‘polishing reservoir’, this pond provides further removal of contaminants to ensure the effluent meets regulatory requirements. Carbon dioxide is added to the effluent of the polishing reservoir

to return the pH to neutral conditions prior to discharge off-site. More advanced AMD treatment methods are available which provide greater control over treatment parameters and produce higher density sludge. However, pond treatment systems are widely adopted by mine site operators due to their simplicity and low capital costs; two characteristics which make pond treatment particularly advantageous after mine closure.

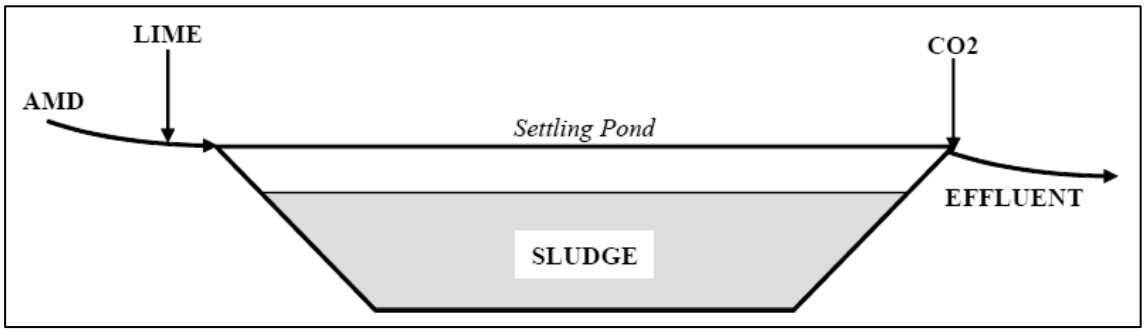

Figure 13. Schematic of the conventional pond treatment method of removing harmful substances from acid mine drainage prior to discharge off-site [44].

In order to maintain the capacity of the pond treatment system, the material which accumulates at the bottom of the settling pond and polishing reservoir –referred to in this work as metal precipitate sludge (MPS)– is removed periodically by means of dredging. A variety of disposal options are available for MPS ranging from on-site deposition in mine workings, waste rock piles or natural land depressions, to off-site disposal in third-party landfills. The optimal disposal method for an MPS source is a function of local regulations, the dewatering characteristics and production rate of the sludge, the size and topography of the site, as well as the budget of the mine site operator [44]. The MPS produced by conventional pond treatment systems are typically between 1 and 3 % solids by weight [44]. As a result, the land use requirements and handling costs associated with disposal can be substantial. To overcome these challenges, a pre-disposal sludge

dewatering process is often applied. For sites at which sufficient land is available for on-site disposal, sludge drying beds - referred to in the mining sector as engineered ponds- are used to perform sludge dewatering. Using this technique, the SC of the MPS can be increased by as much as a factor of 3 in some cases [44]. However, dewatering MPS using an engineered pond is a slow process; up to two years may be required to achieve the desired volume reduction [44]. Plate and frame filter presses are employed when on-site disposal is not a viable option and have been shown to increase the SC of MPS by more than a factor of 7 [45]. However, the capital investment and operating expenditure required to purchase and maintain a plate and frame filter press -in addition to third-party disposal fees– make this option cost prohibitive for many mine site operators.

Engineered dewatering fabrics represent a promising alternative to the conventional methods of dewatering MPS. As previously discussed, geotextile dewatering is especially practical for transitory dewatering applications. Dredging of AMD treatment ponds is typically performed on a yearly basis. During this period, the dewatering bags can be quickly deployed on-site, filled with the dredged material, left in place until the MPS is sufficiently dewatered and, finally, disposed of in a landfill or used as a dam or dike to contain mine waste. Due to their ability to be stacked, geotextile bags have significantly smaller land requirements than sludge drying beds. Moreover, their mechanical simplicity means they are significantly less expensive to purchase and operate than plate and frame filter presses. Engineered dewatering fabrics have been successful applied to MPS; increasing SC by up to 900% within several days [46]. Furthermore, geotextile bags have also been employed as a replacement for conventional pond

treatment; performing metal hydroxide precipitate removal and dewatering in a single unit operation. At the Kam Kotia Mine, geotextile bags were able to decrease the TSS of AMD from 29,300 mg/L to less than 30 mg/L [47].

1.8 Thesis Organization

This thesis is organized into five chapters. A brief description of the contents of each chapter is presented in the following section.

Chapter 2 describes the rapid prototyping techniques employed to develop a total of fourteen thin-film dewatering filters incorporating well-defined slit-pore geometries. A thorough description of the materials and methods employed in Chapter 3 and Chapter 4 to evaluate the effects of slit-pore dimensions and slit-pore spacing on dewatering performance is also provided.

The focus of Chapter 3 is the application of the thin-film dewatering filters to the dewatering of ADS from the Woodward Avenue WWTP in Hamilton, Ontario, Canada. A ‘microscale flocculation test’ (MFT) was first used to screen the effectiveness of six cationic polymer flocculants to pretreat the ADS. The fourteen thin-film dewatering filters were then evaluated using a ‘constant rate dewatering test’ to establish the fundamental correlation structure between the design factors of interest and four key performance metrics: medium resistance, maximum cake resistance, extent of dewatering, and solids retention. The effects of polymer dose on the respective performances of the thin-film dewatering filters were also evaluated. The work presented in this chapter will be published in an forthcoming issue of *Environmental Technology*.

The focus of Chapter 4 is the application of the thin-film dewatering filters to treat MPS from a nickel-copper mine in Ontario, Canada. A high-throughput screen of cationic and anionic polymer flocculants was performed using the LUMiFuge, an analytical centrifuge that measures real-time stability behaviour, to identify the 'best' pre-treatment condition to enhance the dewaterability of the MPS. Four thin-film dewatering filters - identified based on a full-factorial experimental design informed by the results obtained for the ADS- were evaluated with respect to dewatering rate, extent of dewatering, and solids retention via the standard PFT. A particular emphasis was placed on the effect of filter porosity on the rate of filter cake development and the implications this may have on full-scale applications. The work presented in this chapter has been accepted for publication as part of the proceedings of the Tailings & Mine Waste '18 Conference to be held October 1-2, 2018 in Keystone, Colorado.

Chapter 5 outlines the conclusions obtained through this work as well as recommendations for future research.

Chapter 2: Materials and Methods

2.1 Thin-film Dewatering Filters

A series of thin-film dewatering filters possessing well-defined slit-pore geometries were designed 'in house' using AutoCAD 2015 software (Autodesk Inc.) to perform a comprehensive analysis of the effect of the filter properties on dewatering performance. Each filter was a circular disc (85 mm in diameter) containing an array of pores with a particular combination of characteristic dimension, pore-to-pore spacing, and length-to-width aspect ratio. The filters were produced using a flatbed fiber laser cutting system by KJ Laser Micromachining (Etobicoke, Ontario) using Kapton® HN general-purpose polyimide (DuPont) having a nominal thickness of 5 mils (0.127 mm). This approach allowed for the development of pore dimensions as small as 40 μm in size. In this study, 'characteristic dimension' is defined as the designed width of a slit-pore or the diameter of a circular pore and is considered as being analogous to the AOS of conventional fabrics. Furthermore, 'pore-to-pore spacing' is defined as the edge-to-edge distance between adjacent pores in both the longitudinal and transverse directions. In order to fully evaluate the impact of pore dimensions and pore spacing on dewatering performance and cake layer permeability, a 2^3 full-factorial DOE approach (as shown in Table 1) was used.

Table 1. High and low values selected for the three design factors in the full-factorial DOE.

Factor	Description	High Value	Low Value
A	Characteristic Dimension	100 μm	80 μm
B	Pore-to-Pore Spacing	4 mm	1 mm
C	Pore Aspect Ratio (length:width)	50:1	15:1

In addition to the eight filters defined by the DOE framework, six additional filters were produced that featured characteristic dimensions, pore spacing, and aspect ratios that extended to a larger scope of filter conditions within the study. Specifically, these filters featured characteristic dimension values of 40 μm and 200 μm, pore-to-pore spacings of 1.5 mm, 2.83 mm and 3.65 mm, and an aspect ratio of 1:1 (i.e. circular pores). The naming of each filter is based on 'XX×YYY_Z' where XX is the characteristic dimension, YYY is the pore length (defined by the combination of characteristic dimension and length:width aspect ratio), and Z is the pore-to-pore spacing. For example, the '80×1200_4mm' filter possesses a characteristic dimension of 80 μm, slit-pore length of 1200 μm (15:1 aspect ratio), and pore-to-pore spacing of 4 mm. A complete list of the filters evaluated in this work can be found in Table 2**.**

In order to ensure that the size and distribution of the pores were consistent with the design specifications, a VHX-5000 series digital microscope (Keyence Corporation) was used to image the filters prior to the dewatering experiments. Microscope images of two representative filters (one from within the DOE framework featuring slit-pores and one from the expanded design space having conventional circular pores) are displayed in Figure 14.

Table 2. Technical details for the thin-film dewatering filters featuring slit-pore geometries that that were designed 'in house' and manufactured by KJ Laser Micromachining (Etobicoke, Ontario). These filters feature well-defined characteristic dimension, pore-to-pore spacing and pore aspect ratio which allowed for a comprehensive analysis of the effect of the filter properties on dewatering performance to be made.

Filter ID	Characteristic Dimension (µm)	Pore-to-Pore Spacing (mm)	Pore Aspect Ratio (length:width)	Porosity (%)
40×600_4mm	40	4	15:1	0.14
100×100_2.83mm	100	2.83	1:1	0.17
100×100_1.5mm	100	1.5	1:1	0.35
80×1200_4mm	80	4	15:1	0.47
80×1200_3.65mm	80	3.65	15:1	0.54
100×1500_4mm	100	4	15:1	0.69
100×100_1mm	100	1	1:1	0.79
100×5000_4mm	100	4	50:1	0.88
80×4000_4mm	80	4	50:1	1.03
200×3000_4mm	200	4	15:1	2.53
80×1200_1mm	80	1	15:1	4.32
80×4000_1mm	80	1	50:1	5.62
100×1500_1mm	100	1	15:1	6.03
100×5000_1mm	100	1	50:1	8.81

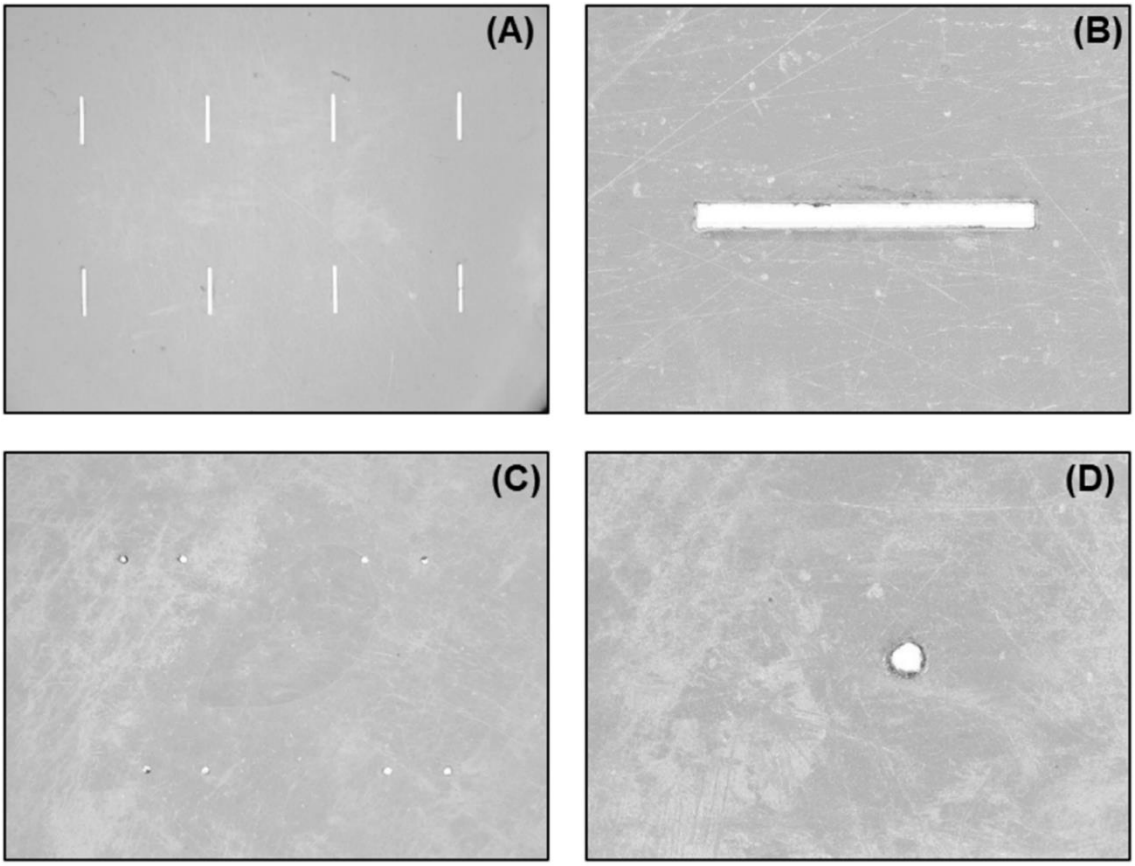

Figure 14. Images captured using the VHX-5000 series digital microscope (Keyence Corporation) of two representative thin-film dewatering filters. Panels A and B depict the '100×1500_4mm' filter (pore width = 100 µm; pore length = 1500 µm; pore-to-pore spacing = 4 mm) at magnifications of 30× and 200×, respectively. Panels C and D depict the '100×100_2.83mm' filter at 30× and 200× magnification.

2.2 Woven Textile

In order to compare the performance of the thin-film dewatering filters featuring well-defined slit-pore geometries to that of conventional engineered dewatering fabrics, samples of a commercially available woven textile were obtained. This fabric, referred to as 'Woven Commercial Textile' in the presented results, is constructed of multifilament, high-tenacity polypropylene yarns and was supplied in circular discs 85 mm in diameter. As reported by the manufacturer, the Woven Commercial Textile has an AOS of 430 µm, while the O_{50} and O_{95} pore opening sizes are 80 µm and 195 µm, respectively. The manufacturer does not report the fabric's total porosity which is defined as the ratio of the total area of the pores to the total area of the fabric. Figure 15 displays two images of the Woven Commercial Textile; a standard picture depicting one the 85 mm fabric discs supplied, and an image of the weave pattern obtained using the VHX-5000 series digital microscope at 30x magnification.

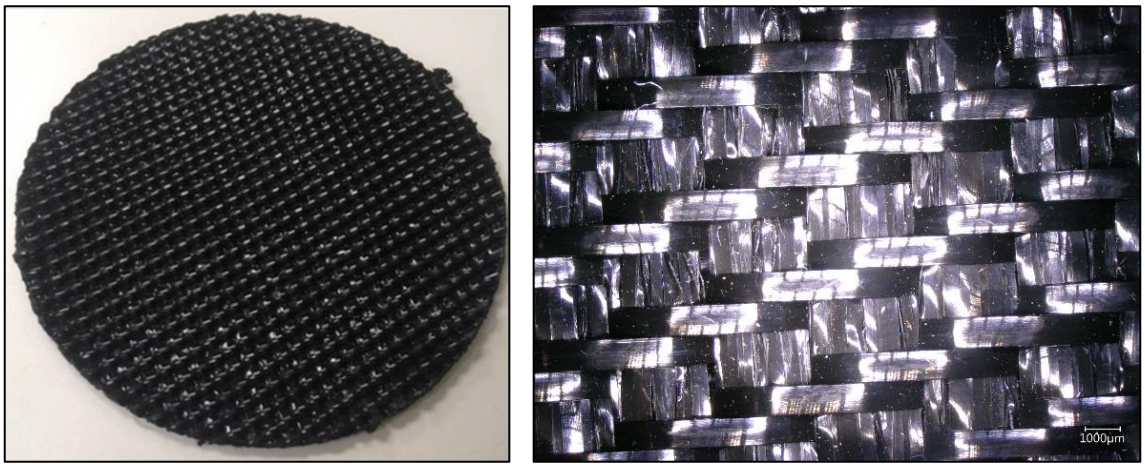

(A) **(B)**

Figure 15. Images of the Woven Commercial Textile samples evaluated in this work to compare the performance of the thin-film dewatering filters to that of conventional geotextiles. Panel A includes a picture of one of the 85 mm circular discs provided by the manufacturer, while Panel B displays a microscope image of the same disc obtained using a VHX-5000 series digital microscope (Keyence Corporation) at 30× magnification.

2.3 Sludge Material

2.3.1 Anaerobic digested sludge

The ADS employed in this research project was obtained at various times between January 2017 and August 2017 from the Woodward Avenue WWTP in Hamilton, Ontario. In total, four samples were collected: Sample 1 on January 30th, Sample 2 on March 14th, Sample 3 on May 29th, and Sample 4 on August 4th. Samples 1 and 2 were used during the initial stages of the project to test and refine the experimental setup, while Samples 3 and 4 were used to obtain the experimental results presented in Chapter 3. More specifically, Sample 3 was used in Sections 3.2 and 3.4, and Sample 4 was used in Section 3.3. Each of these samples were collected in 20 L plastic pails from the outlet of the anaerobic digester and subsequently transported to McMaster University. While not in use, the samples were stored at 4℃. In order to ensure the physical and chemical properties of the ADS remained consistent between subsequent experiments, all samples were used within 2 months of receipt from the WWTP. The images presented in Figure 16 depict the ADS sample collection process.

Figure 16. Images depicting the collection of an anaerobic digested sludge sample from the outlet of the anaerobic digester at the Woodward Avenue WWTP (Hamilton, Ontario).

The total solids (TS) of the ADS was relatively consistent between the four samples acquired, ranging from 1.7 % for Sample 3 to 2.7 % for Sample 1. Particle size analysis was performed for Samples 3 and 4 via focused beam reflectance measurement (FBRM). Refer to Section 2.3.4 below for a description of the FBRM technology. As shown in Figure 17, both ADS samples possessed log normal chord length distributions consisting primarily of silt (3.9 – 62.5 µm) and clay-sized (0.98–3.9 µm) particles. A thorough water quality analysis (WQA) was performed on the liquid fractions of Samples 3 and 4 by AGAT Laboratories (Mississauga, Ontario). The supernatant sample for analysis was prepared at McMaster University via batch centrifugation at 6000 RPM using an Allegra 25R centrifuge. The analytical results for these two samples are

summarized in Table 3; Sample 4 was determined to have a greater quantity of dissolved constituents.

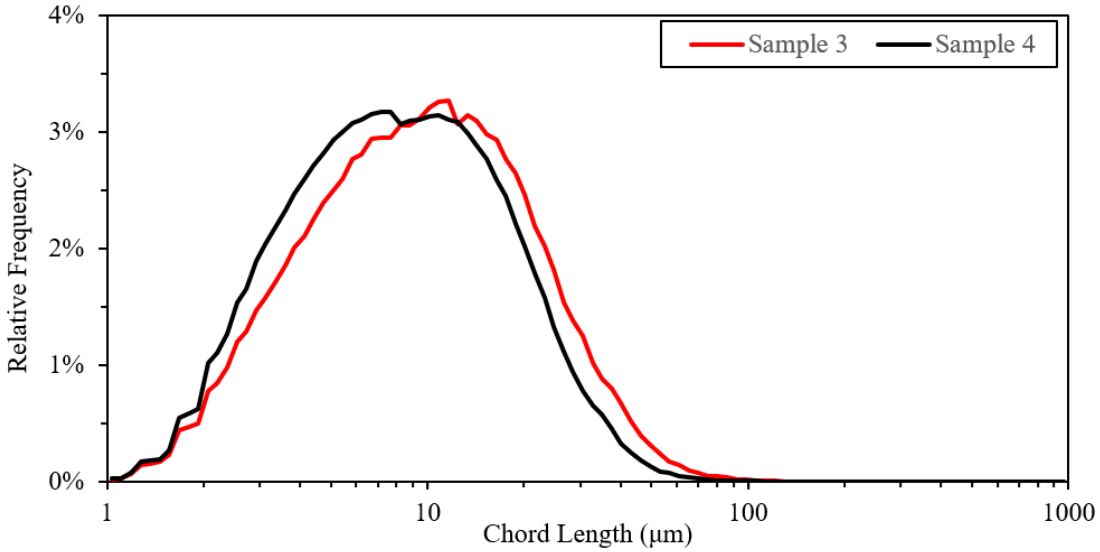

Figure 17. Chord length distributions for Samples 3 and 4 of the ADS obtained via focused beam reflectance measurement using a Particle Track G400 instrument (Mettler Toledo).

Table 3. Summary of the analytical results for the ADS samples used for the dewatering tests as described in Chapter 3.

Property	Sample 3	Sample 4
Total Solids (%) [a]	1.7	2.4
Electrical Conductivity (µS/cm) [b]	4080	7730
pH [b]	8.37	8.01
Total Hardness (mg/L) [b]	832	403
Total Dissolved Solids (mg/L) [b]	2000	1650
Alkalinity (mg/L) [b]	4080	3190
Chloride (mg/L) [b]	187	166
Reactive Silica (mg/L) [b]	15.0	30.8
Ammonia as N (mg/L) [b]	909	788
Total Phosphorous (mg/L) [b]	9.14	14.1
Total Organic Carbon (mg/L) [b]	283	322
Calcium (mg/L) [b]	47.9	63.6
Magnesium (mg/L) [b]	47.9	59.2
Sodium (mg/L) [b]	129	121
Potassium (mg/L) [b]	97.8	86.2
Iron (mg/L) [b]	22.1	8.08

[a] Determined by the standard 2540 B method [49]

[b] Determined by AGAT Laboratories

2.3.2 Metal precipitate sludge

Two samples of MPS were supplied by the owner of a nickel-copper mine in Ontario, Canada. The first sample, hereafter referred to as the ‘shore sample’, was collected from various locations along the perimeter of the onsite lime treatment system’s polishing reservoir. The individual discrete samples were collected using a shovel and deposited in a 20 L pail to produce a composite for shipment to McMaster University. The second sample, hereafter referred to as the ‘pond sample’, was collected along a transect of the polishing reservoir using a surface sediment sampler. The specific model used was an Ekman dredge; a mechanical device fitted with opposable jaws which are operated from surface. The dredge was slowly lowered through the water column until it reached the MPS. The jaws were then tripped, collecting the discrete sample. The dredge was then retrieved and the MPS was deposited in a 20 L pail. Figure 18 displays a picture of the shore sample after receipt at McMaster University.

Figure 18. Picture of the MPS ‘shore sample’ that was supplied by the owner of a nickel-copper mine in Ontario, Canada.

The TS contents of the shore and pond samples were found to be significantly different; the shore sample had a TS of 19.6%, while the pond sample was measured to have a TS of 6.1%. However -as shown in Figure 19- the chord length distribution for both MPS samples were relatively similar; the median chord length for the shore sample was 14.2 µm while the median chord length for the pond sample was 12.3 µm. WQA was performed on the liquid fraction of the shore and pond samples by AGAT Laboratories. Once again, the supernatant to be analysed was prepared via batch centrifugation at 6000 rpm. The analytical results for these two samples are summarized in Table 4.

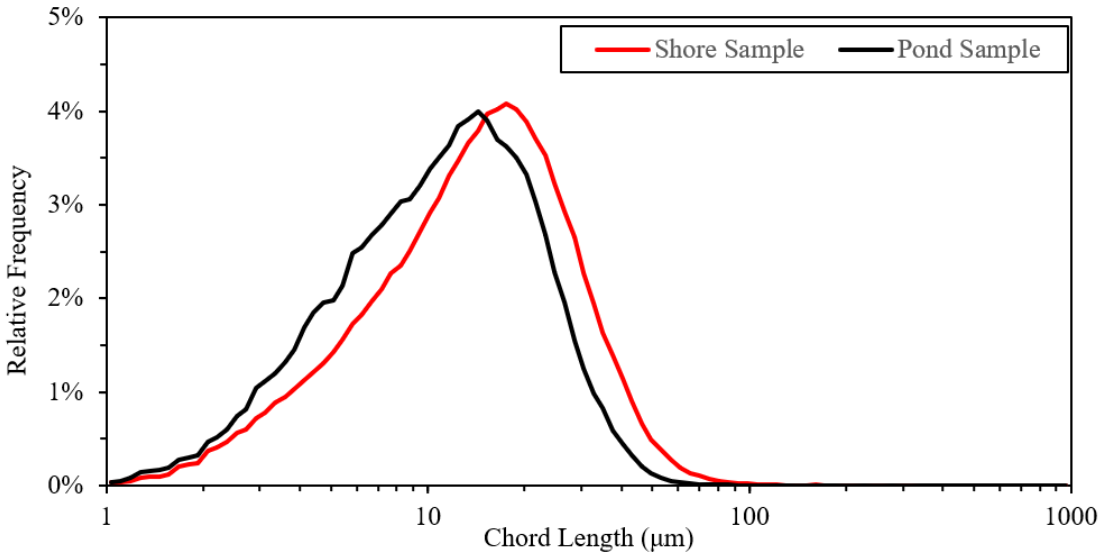

Figure 19. Chord length distributions for the metal precipitate sludge shore and pond samples obtained via focused beam reflectance measurement using a Particle Track G400 instrument (Mettler Toledo).

Table 4. Summary of the analytical results for the metal precipitate sludge samples used to obtain the experimental results presented in Chapter 4.

Property	Shore Sample	Pond Sample
Total Solids (%) [a]	19.6	6.1
Electrical Conductivity (µS/cm) [b]	1650	2860
pH [b]	7.52	7.02
Total Hardness (mg/L) [b]	800	1170
Total Dissolved Solids (mg/L) [b]	1290	2150
Alkalinity (mg/L) [b]	83	26
Chloride (mg/L) [b]	209	231
Sulphate (mg/L) [b]	700	1180
Reactive Silica (mg/L) [b]	3.06	Not Provided
Ammonia as N (mg/L) [b]	1.56	7.3
Total Organic Carbon (mg/L) [b]	11.2	16.8
Calcium (mg/L) [b]	101	342
Magnesium (mg/L) [b]	133	76.3
Sodium (mg/L) [b]	95.3	97.5
Potassium (mg/L) [b]	25.7	30.0
Iron (mg/L) [b]	1.37	2.26
Nickel (mg/L)	1.66	3.77
Strontium (mg/L)	0.875	Not Provided

[a] Determined by the standard 2540 B method [49]

[b] Determined by AGAT Laboratories

2.3.3 Sludge total solids test

The TS content was measured for each of the ADS and MPS samples using the standard 2540 B method [48]. To begin, three aluminum weigh tins (GE Healthcare) were placed in a 105℃ oven for 1 hour. The tins were then removed from the oven, briefly placed on the lab bench to cool, and immediately weighed using an Excellence XS Analytical Balance (Mettler Toledo). Known quantities of sludge were then transferred from the bulk samples to the tins via a 30 mL syringe. To ensure the acquired sludge was representative of bulk properties, a paint mixing rod was used to thoroughly mix the sample contents. The tins were then reweighed and placed back in the oven where the sludge was dried for a minimum of 16 hours. The tins were then removed and weighed for a final time. The TS content of the sludge in each of the three tins was calculated using Equation 1; 'm_{tin}' refers to the initial mass of the tin, '$m_{sludge+tin}$' is the combined mass of the tin and the sludge prior to drying, and '$m_{dried\ sludge+tin}$' is the combined mass of the tin and the sludge after drying. The TS content reported for each sludge sample is the average of the triplicate TS analysis. Figure 20 includes images of the TS Test performed for the MPS shore sample.

$$TS\ (w/w\ \%) = \frac{m_{dried\ sludge+tin} - m_{tin}}{m_{sludge+tin} - m_{tin}} x\ 100\ (\%) \quad (1)$$

(A) **(B)**

Figure 20. Images of the total solids test performed for the metal precipitate sludge shore sample. Panel A depicts the three aliquots transferred from the bulk sample prior to drying, while Panel B depicts the same three aliquots after drying at 105℃ for 16 hours.

2.3.4 Particle size analysis

Particle size analysis of the as-received sludge samples was performed via FBRM using a ParticleTrack G400 instrument (Mettler Toledo). FBRM was first applied to the in-situ characterization of crystallization processes in the early 1990s and, more recently, has been shown to be an effective tool for real-time monitoring of polymer induced flocculation [13]. FBRM was selected to characterize the ADS and MPS samples as it is capable of analysing high SC materials and does not require the suspension to be kinetically stable (external mixing can be applied).

FBRM instruments consist of a cylindrical probe housing a rotating laser, a set of optics, a detector, and a probe window. To acquire a measurement, the probe is inserted directly into the solid-liquid system at a 45-degree angle and the laser (rotating at approximately 2 m/s) is directed down the length of the probe. The focused laser beam exits the probe by way of the probe window and subsequently passes through individual solid particles or particle structures. The interactions between the laser and the solid

particles cause the backscatter of light to the detector. The accompanying software counts the number of backscatter pulses and, for each pulse, calculates the distance across the particle using the pulse duration. This distance is referred to as chord length; a fundamental property of the particle related to its size. As reported by Heath et al., the chord length distributions obtained by way of FBRM are in reasonable agreement with other particle sizing technologies [49].

For each sludge sample, a 100 mL aliquot was transferred from the 20 L pail to a standard 250 mL beaker using a 30 mL syringe. As was performed for the TS Test, a paint mixing rod was used to thoroughly mix the sample contents prior to material transfer to ensure the aliquot was representative of bulk properties. The beaker was then placed on a magnetic stir plate and a cylindrical stir rod measuring 7.9 mm in diameter by 24.9 mm in length was used to stir the aliquot at 300 RPM. The probe was positioned in the center of the beaker and the FBRM software (Mettler Toledo) was configured to measure the ‘unweighted’ chord length distribution at 5 s intervals. Analysis was performed for a period of 3 minutes to ensure the reported distribution was stable. Figure 21 presents a picture of the FBRM instrument.

Figure 21. Image depicting a ParticleTrack G400 instrument (Mettler Toledo) [50].

2.4 Polymer Flocculants

This work utilized a total of ten polymer flocculants; six of which were systematically screened as pre-treatment additives for the dewatering of ADS (Chapter 3), and seven of which were screened for the dewatering of MPS (Chapter 4). Each of these polymers were cationic or anionic polyacrylamides which were supplied from their respective manufacturers (Kemira or SNF) in either powder or emulsion form. The selection of appropriate polymers for evaluation was performed such that those selected possessed a variety of charge densities and molecular weights. A complete list of the ten polymers screened, their respective technical details, and the sludge material(s) for which they were evaluated are presented in Table 5.

Table 5. Technical details for the ten polymer flocculants (from Kemira and SNF) employed in this work.

Supplier	Polymer ID	Charge	Molecular Weight	Charge Density	Sludge Evaluated
SuperFloc (Kemira)	4512	+	Very High	Very Low	ADS
	4516	+	Very High	High	ADS, MPS
	4518	+	Very High	Very High	ADS
	C-1594	+	High	Medium	ADS, MPS
	C-1596	+	High	High	ADS
	C-1598	+	High	Very High	ADS, MPS
	A-1883 RS	-	High	Medium	MPS
	4818 RS	-	Extremely High	High	MPS
FLOPAM (SNF)	1540 CT	+	Very High	Low	MPS
	AN 934 SH	-	Very High	Medium	MPS

The three polymers used most extensively in this work were the SuperFloc 4516, the SuperFloc C-1594 and the FLOPAM AN 934 SH. The SuperFloc 4516 and SuperFloc C-1594, both manufactured by Kemira, were supplied in emulsion form and are cationic copolymers of polyacrylamide and quaternized-N,N dimethylamino ethylacrylate (DMAEA-Q). The SuperFloc 4516 is a very high molecular weight, high charge density polymer with a specific gravity of 1, while the SuperFloc C-1594 is a high molecular weight, medium charge density polymer with a specific gravity of 1.02. The FLOPAM AN 934 SH, from SNF, is an anionic, linear polyacrylamide which was supplied in powder form. It has a very high molecular weight and a medium charge density.

The stock polymers were stored in a lab cabinet (at room temperature) while not in use to minimize their exposure to direct sunlight as per the manufacturers' recommendations. The as-received polymer emulsions were diluted to 0.3% by weight

via two-stage serial dilutions using 10 mM sodium phosphate monobasic buffer according to the following procedure: 40 g of buffer was acquired in a 250 mL glass beaker, placed on a magnetic stir plate, and stirred at 600 RPM using a cylindrical stir rod 7.9 mm in diameter by 24.9 mm in length; next, the appropriate quantity of stock polymer was added to the buffer via a 1000 µL micropipette (Eppendorf) and the contents of the beaker were mixed thoroughly for 10 minutes at a stir rate of 400 RPM; then an additional 40 g of buffer was added to the beaker and mixed for an additional 10 minutes at 400 RPM. The diluted polymer emulsion was removed from the stir plate and placed on the lab bench where it was left to age for at least 30 minutes, but no longer than 24 hours, prior to use. The polymers received in powder form were dissolved in the buffer using the same procedure; the only exception being the use of the Excellence XS Analytical Balance and a weigh boat to add the appropriate quantity of polymer to the buffer.

2.5 Polymer Screening

Two high-throughput methods of polymer screening were employed in this work; a MFT utilizing capillary suction time (CST) measurements was used to select an appropriate polymer to flocculate the ADS in Chapter 3, while an analytical centrifuge (rather than CST measurements) was used select the ‘best’ cationic and anionic polymers to treat the MPS in Chapter 4. A thorough description of both techniques is provided below.

2.5.1 Capillary suction time measurements

The MFT was originally developed by LaRue et al. as an alternative to the conventional ‘jar test’ method of identifying the polymer and polymer dose that yield the

optimal separation of water from suspended solids [14]. This method incorporates both parallel and microscale processing techniques which reduce the amount of time and the volume of sludge material required to screen polymer flocculants and to perform dosage optimization.

The standard MFT integrates CST measurements in order to quantitatively compare the performance of pre-treatment conditions. CST is regarded as a fundamental measure of dewaterability and thus is widely used. Lower CST values are associated with better dewatering performance. It is a purely empirical test without any theoretical analysis that characterizes the filtration phase of the dewatering process. These CST measurements are performed using a specially designed filtration unit which includes a piece of chromatography paper placed between two rectangular blocks. The upper block has a thru-hole milled in its center around which there are two concentric circles made from a conductive material. These circles have three integrated sensors (two on the inner circle and one on the outer circle) connected to a timer. A circular reservoir is placed on top of the paper filter through the hole in the upper block. To obtain a CST measurement, the sludge material of interest is poured into the reservoir and the amount of time required for the filtrate to extend from the inner to the outer circle (referred to as the CST) is recorded.

In this work, the standard MFT was used to screen the effectiveness of six cationic polymers from Kemira (refer to Table 5 for the complete list) to flocculate the ADS. To begin, a handheld paint mixing rod was used to thoroughly mix the bulk ADS sample. Triplicate 3 mL aliquots were then placed within a standard flat-bottom 12-well

microplate using a 5 mL micropipette (Eppendorf). The microplate was then placed on a custom-built stand with an integrated tumble stirrer (V&P Scientific), and magnetic stir rods measuring 7.9 mm in diameter and 12.9 mm in length were placed in each well. The aliquots were then stirred at 70 RPM while the appropriate quantity of dilute polymer was added to each well using a 1000 µL micropipette (Eppendorf). After a period of 10 seconds, the stir rate was reduced to 40 RPM and the samples were mixed for an additional 2 minutes. After the 2 minutes had elapsed, the CST was measured for each individual aliquot using the Model 304M CST instrument (Triton Electronics) with the circular 'slow-filtering' reservoir insert and Whatman No. 17 chromatography papers. This procedure was repeated four times for polymer doses of 4, 6, 8, and 10 kg of polymer per tonne of total suspended solids (kg/TTS). Figure 22 displays images of the equipment used to perform the MFT for the ADS.

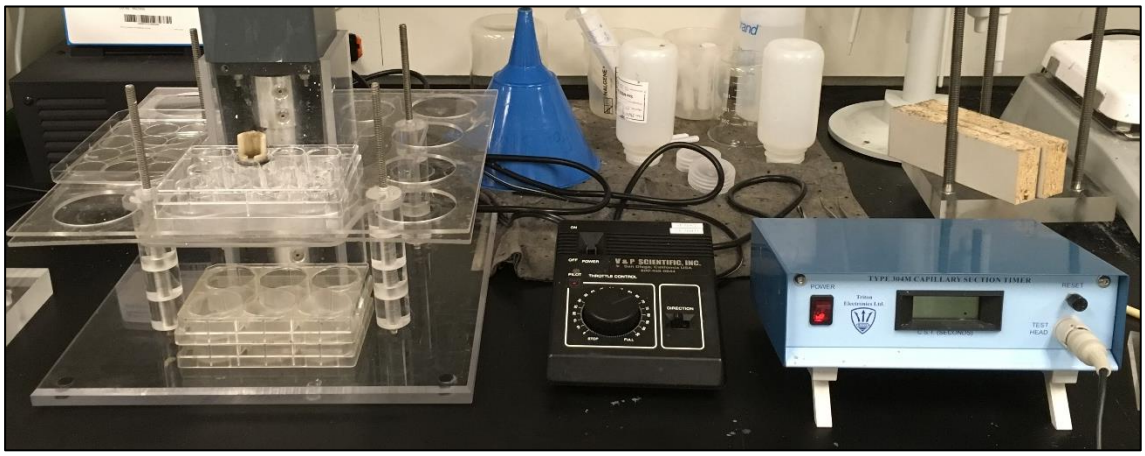

Figure 22. Image depicting the 12-well microplate and custom-built stand with integrated tumble stirrer (left) as well as the capillary suction time filtration unit (right) used to perform the standard MFT. Using this setup, six cationic polymers from Kemira were evaluated for the treatment of anaerobic digested sludge.

2.5.2 LUMiFuge analysis

The MFT was also applied in this work to compare the performance of four cationic and three anionic polymers (refer to Table 5) in treating the MPS. However, rather than using CST measurements, a settling test was performed using a temperature-controlled bench-top stability analyzer (LUMiFuge Model LF110, LUM GmbH). This instrument (which provides a high-throughput alternative to the conventional column settling test) has been used in a wide range of applications including the study of settling characteristics for mature fine tailings, the selection of appropriate flocculants for the dewatering of ADS, and the evaluation of novel biopolymeric flocculants [8] [51] [52].

As shown in Figure 23, the LUMiFuge consists of a light source, a rotor designed to house up to 8 cuvettes in a horizontal orientation, and a charge-coupled device sensor. As the rotor rotates, the centrifuge measures the light transmitted through the sample cuvettes as a function of horizontal position. The regions within the cuvette having higher concentrations of solid particles (i.e. towards the outside of the centrifuge) scatter and absorb a greater quantity of light than those regions in which there is relatively clear water. As a result, a transmission gradient or 'profile' along the length of the cuvette is recorded. Changes in the shape and location of these profiles as centrifugation proceeds provide an indication of the rate at which the solid and liquid fractions of the sample separate under the given flocculation conditions.

Figure 23. Operation of LUMiFuge analytical centrifuge, with light transmission used to determine location of solids front.

Prior to taking samples of the MPS, the handheld paint mixing rod was used to thoroughly mix the bulk material. Four 8 mL aliquots were then transferred from the MPS pail to a standard flat-bottom 6-well microplate using the 5 mL micropipette. The magnetic stir rods measuring 7.9 mm in diameter and 12.9 mm in length were placed in each well, and the microplate was positioned on the tumble stirrer stand. The four samples were mixed at 60 RPM and subsequently dosed using the 1000 µL micropipette at 1, 2, 4 and 8 kg/TTS. After 10 seconds, the stir rate was reduced to 40 RPM, and mixing was continued for an additional 110 seconds. Duplicate 1.5 mL samples from each well were then transferred to the LUMiFuge cuvettes using a MICROMAN® M1000E positive displacement pipette (Gilson). The cuvettes were placed in the LUMiFuge instrument and centrifugation was performed at 500 RPM for 12 minutes at ambient temperature. A total of 48 near-infrared transmission profiles were recorded (15 second intervals) using the SEPView 6 software (LUM GmbH). This procedure was repeated seven times; once for each polymer of interest.

To compare the dewatering rate for each polymer-dose combination, the transmission profiles recorded by the LUMiFuge were analyzed to track the horizontal position of the supernatant-pellet boundary (referred to as the 'solids front') as a function of time. The solids front for each profile was identified as the location along the length of the cuvette at which the measured transmission was 50% of the maximum transmission recorded. The solids front positions were then used to estimate the volume within which the solids were contained at each time interval using a method proposed in a previous work [8]: a linear regression of sample volume onto horizontal position was generated using known quantities (0.30, 0.90, 1.20, and 1.60 mL) of deionized water. The regression is presented in Equation 2, where 'X_n' refers to the position of the solids front for the nth profile.

$$Solids\ Volume\ (mL). = -0.0709(X_n) + 9.2142 \quad (2)$$

Figure 24 displays a representative set of transmission profiles recorded by the LUMiFuge instrument used to identify the position of the solids front as well as the scatter plot of sample volume versus horizontal position produced using the deionized water.

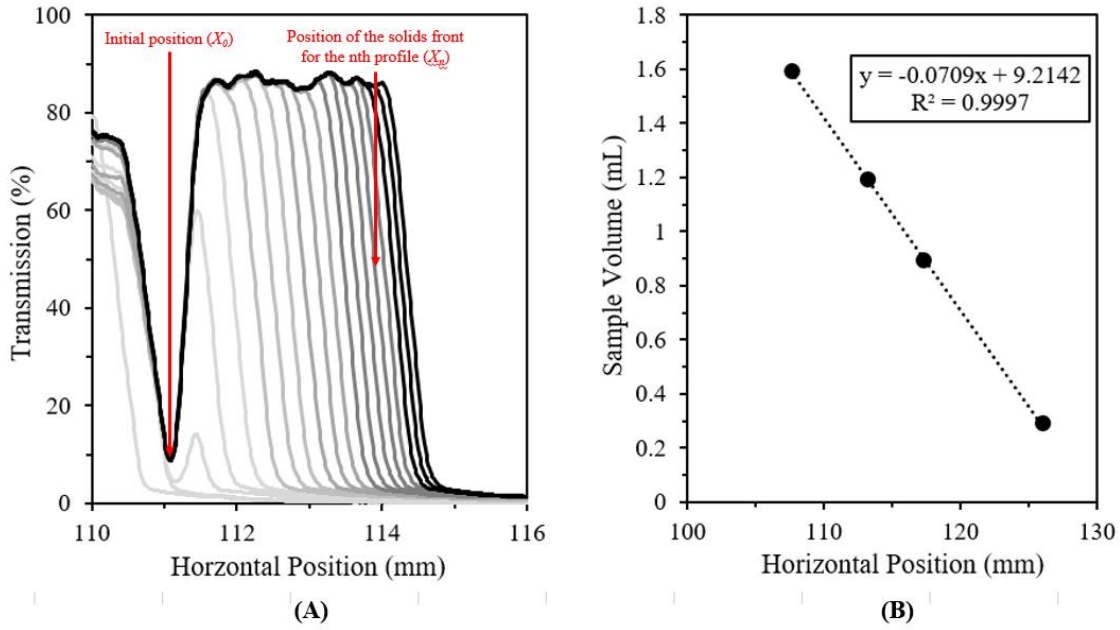

Figure 24. Panel A includes a set of transmission profiles recorded by the LUMiFuge. As centrifugation proceeds, the solids front is forced down the length of the bag, reducing the volume within which the solids are contained. Panel B displays the linear regression of sample volume onto horizontal position generated using the deionized water.

2.6 Dewatering Performance Tests

2.6.1 Lab-scale setup

In this work, the respective performances of the thin-film dewatering filters with ADS and MPS were evaluated using the dewatering performance test (DPT) apparatus, a laboratory-scale geotextile filtration system designed and fabricated ‘in house’. The DPT apparatus can be operated in one of two modes to perform dewatering under conditions of constant pressure (using an overpressure of compressed gas) or constant rate (using a laboratory pump to draw filtrate through the filter medium). A schematic of the DPT apparatus with labels for each of the system’s individual components can be found in Figure 25 below.

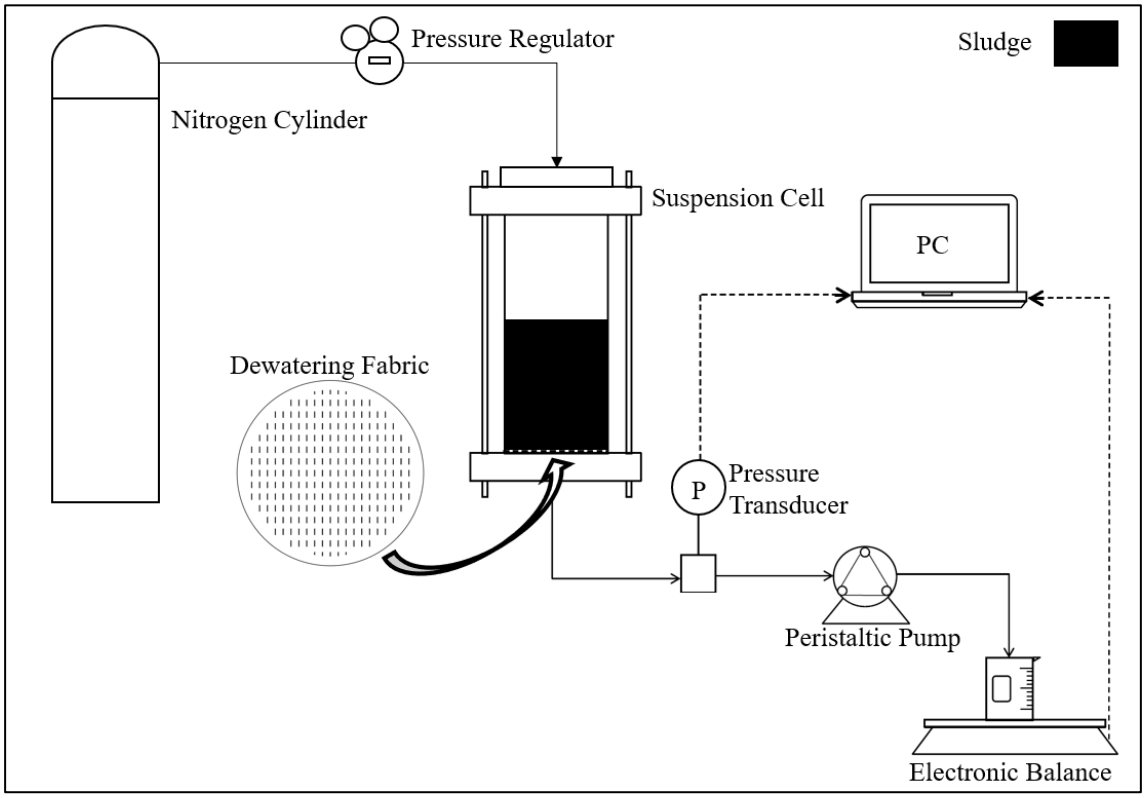

Figure 25. Schematic of the dewatering performance test apparatus used to evaluate the performances of the thin-film dewatering filters with anaerobic digested sludge and metal precipitate sludge.

As shown in Figure 26 below, the cylindrical suspension cell (229 mm height, 82 mm inner diameter) was constructed of clear acrylic and had a maximum capacity of 1.2 L. The lower flange was designed to house the thin-film dewatering filters on top of a porous polypropylene support (85 mm diameter) which was rated by the manufacturer (Scientific Commodities Inc.) as containing pores 200 μm in size. The lower flange incorporated a filtrate collection port complete with a barbed tube fitting of nylon construction (McMaster-Carr). The upper flange had an inlet port 25 mm in diameter used to load the suspension cell with sludge. Three threaded rods running the length of the suspension cell were used (in combination with wingnuts) to compress the O-rings on the

top and bottom of the suspension cell; creating airtight seals with the upper and lower flanges.

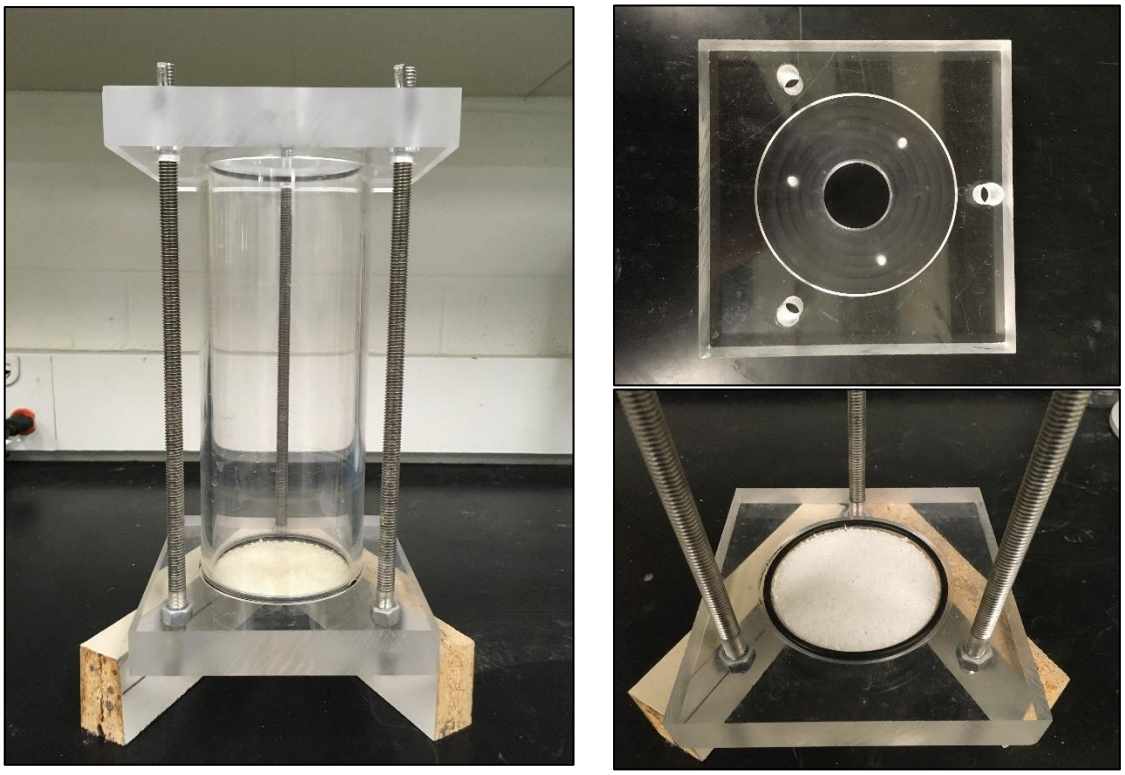

Figure 26. Images of the suspension cell (left) upper flange (top right) and lower flange (bottom right).

To perform dewatering under constant rate conditions, a Masterflex L/S series peristaltic pump (Cole-Parmer) equipped with an easy-load® II pump head (Model 77201-60) was connected to the filtrate collection port using silicone tubing (3.1 mm inner diameter). A PX409 vacuum pressure transducer (OMEGA) having a featured range of 0 to -103 kPa was installed between the suspension cell and the peristaltic pump using a custom 3-way connector. In order to record the vacuum pressure within the DPT apparatus in real-time, the transducer was interfaced to a PC using OMEGA Digital Transducer software. Similarly, a PB1501-S precision balance (Mettler Toledo) was interfaced to the PC using Mettler Toledo BalanceLink software to record the mass of

filtrate collected. Figure 27 displays images of the pressure transducer, peristaltic pump, and precision balance used in this work.

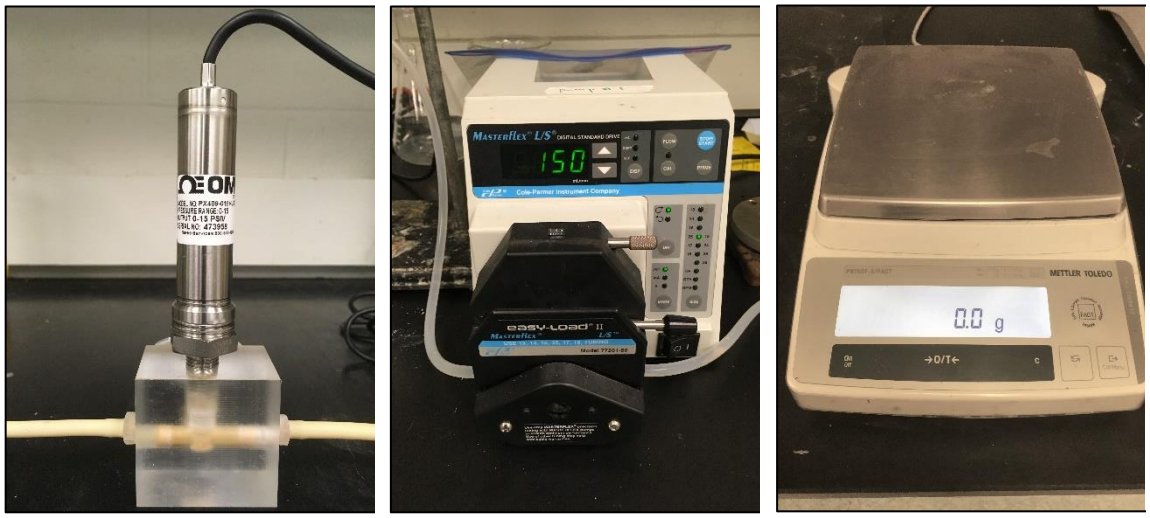

(A) **(B)** **(C)**

Figure 27. Images of the PX409 vacuum pressure transducer (Panel A), Masterflex L/S series peristaltic pump (Panel B), and the PB1501-S precision balance (Panel C).

To perform dewatering under constant pressure conditions, a custom adapter (complete with an O-ring seal and a push-to-connect pneumatic airline fitting) was attached to the upper flange using three bolts. Nylon tubing (3.1 mm inner diameter) was used to connect a nitrogen cylinder (Air Liquide) fitted with a CGA 580 pressure regular (Matheson) to the suspension cell. Once again, the precision balance was used to record the mass of filtrate collected. In this mode of operation, the pressure transducer and peristaltic pump were removed. Figure 28 displays images of the custom adapter and the pressure regulator.

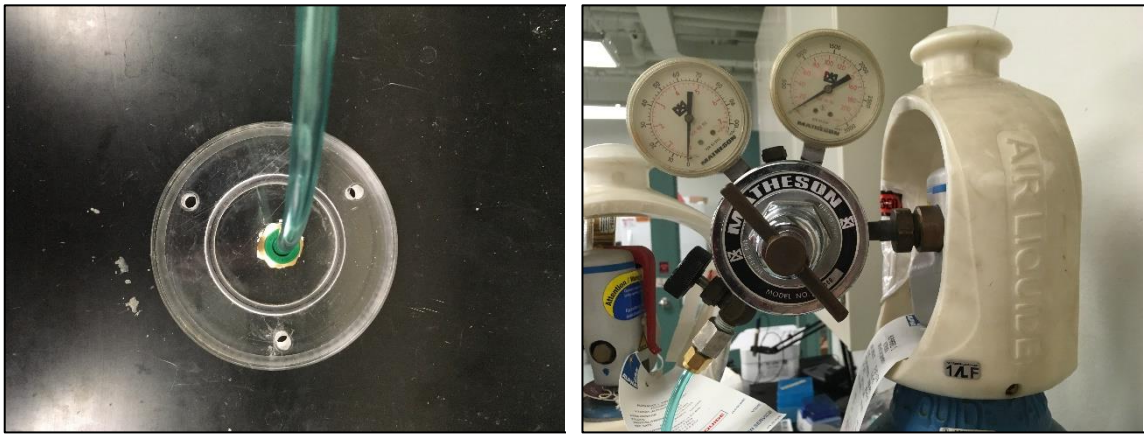

(A) **(B)**

Figure 28. The custom adapter (Panel A) and pressure regulator (Panel B) used to perform dewatering under constant pressure conditions.

2.6.2 Constant-rate dewatering test

Lab-scale constant-rate dewatering tests were performed for the ADS in Chapter 3. An image of the DPT apparatus in 'constant rate mode' is presented in Figure 29. The constant-rate dewatering test was chosen over the conventional PFT for the ADS because it allowed the filtration efficiency, dewatering efficiency, medium resistance, and cake resistance values for each thin-film filter to be established under conditions that are similar to those present in their industrial application. Performing filtration under constant pressure conditions can result in excessive pore blockage, compression of the initial cake layers, and filter cake non-uniformities due to the application of the ultimate pressure drop prior to the development of a filter cake [53]. This issue is particularly prevalent for highly flocculated material. However, since industrial applications of geotextile dewatering use a displacement pump to feed sludge to the dewatering bag, the potential issues associated with the use of constant pressure conditions are avoided.

For each dewatering test, a 200 g aliquot of the ADS was transferred from the sample pail to a 600 mL glass beaker. To ensure the acquired material was representative

of the bulk sample, a handheld paint mixing rod was used to thoroughly mix the pail contents prior to collection. The diluted polymer was then added at the desired dose using a 6 mL syringe, while the ADS was mixed at 300 RPM using an overhead mixer having a 77 mm diameter Standard Pitch P4 impeller (Caframo Lab Solutions). After 10 seconds of mixing, the stir rate was reduced to 190 RPM and mixing was continued for an additional 2 minutes. The flocculated sludge was then poured into the suspension cell where a thin-film dewatering filter had been set up. The peristaltic pump was used to draw the free water through the system at a constant-rate of 150 mL/min. As dewatering proceeded, filtrate was collected in a 250 mL beaker. For all tests, dewatering was performed for a total of 15 minutes.

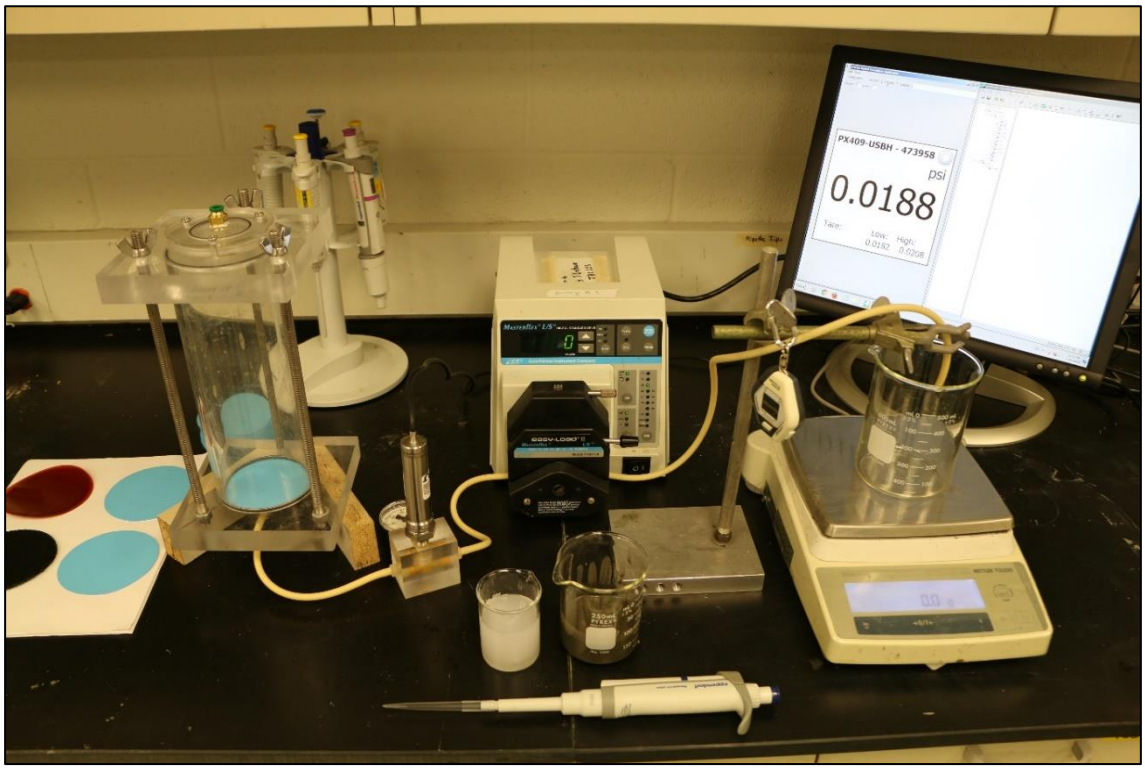

Figure 29. Picture of the dewatering performance test apparatus used to perform the constant-rate dewatering test.

2.6.3 Pressure filtration test

PFTs were performed to evaluate the performances of the thin-film dewatering filters with the MPS in Chapter 4. An image of the DPT apparatus in 'constant pressure mode' is presented in Figure 30. An applied pressure of 35 kPa was selected for use in this work as it represents a common pumping pressure in industrial applications of the geotextile dewatering technology [17].

To begin the PFT, a drill-operated mixing rod was used to thoroughly mix the bulk MPS sample. A 500 g aliquot was then transferred from the bulk sample to a 600 mL glass beaker. For the PFTs performed using a cationic or anionic polymer, the aliquot was stirred using the overhead mixer at 300 RPM, and a 30 mL syringe was used to deliver the appropriate quantity of dilute polymer. After 10 seconds, the mixing speed was reduced to 190 RPM and mixing was performed for an additional 110 seconds. Once the mixing time elapsed, the MPS was immediately transferred to the suspension cell which was then pressurized to 35 kPa by the nitrogen gas supply. As dewatering proceeded, the filtrate was collected in sequential 45 g fractions (identified as F1, F2, F3, and F4) in centrifuge tubes (Fisher Scientific). The PFT was performed until 'breakthrough' (BT), which occurred when the filter cake dried to the point that a crack formed causing a loss of pressure.

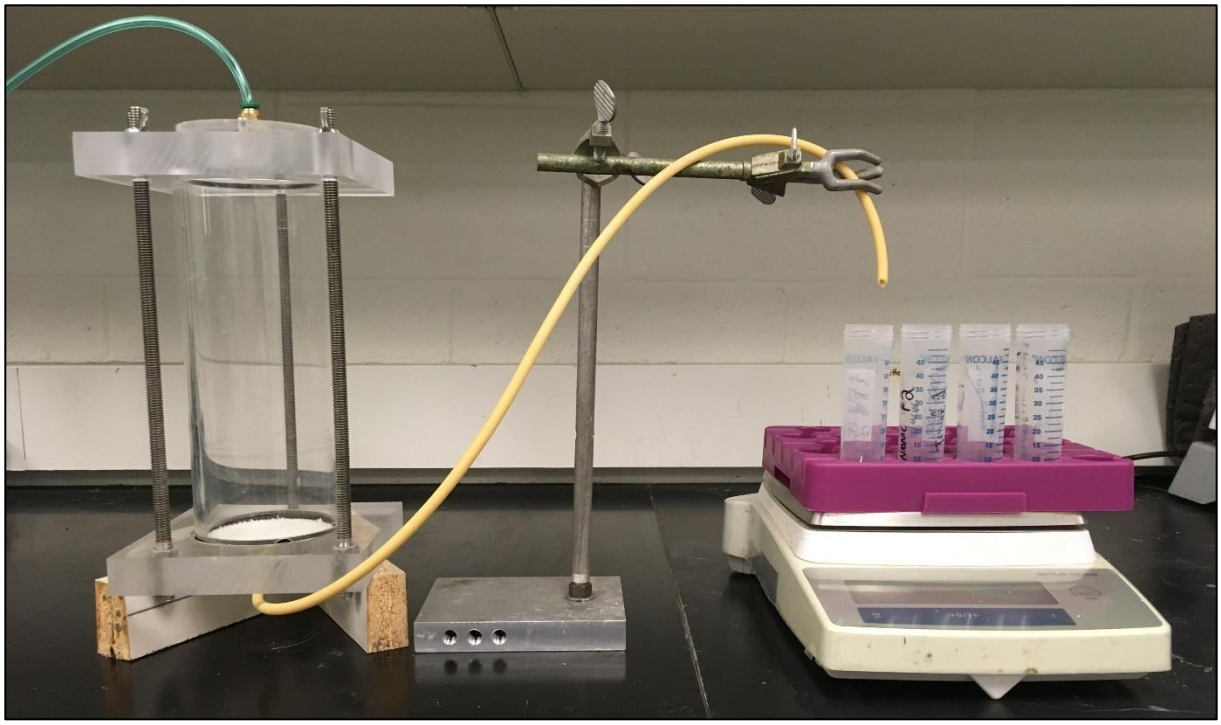

Figure 30. Picture of the dewatering performance test apparatus used to perform the constant-rate dewatering test.

2.6.4 Filter cake total solids test

The principal objective of sludge dewatering is to increase the SC of the sludge by removing as much of the liquid phase as possible. Therefore, the capacity of an engineered dewatering fabric to allow free water to pass through the pore openings is critical to the successful implementation of the geotextile dewatering technology. In this work, the dewatering capacities of the thin-film dewatering filters and the Woven Commercial Textile were assessed by determining the TS of the filter cake at the end of each DPT. TS analysis was performed as per the standard 2540 B method [48].

Section 2.3.3 outlines the TS test (as performed for the as-received sludge samples) in full detail. A description of how this procedure was applied to the filter cake is presented herein: the dewatering apparatus was first disassembled to provide access to

the filter cake; the upper flange was detached, and the cylindrical suspension cell was removed. The filter cake was then divided into three equal-sized fractions and transferred to aluminum weigh tins (GE Healthcare) using a Fisherbrand microspatula (Fisher Scientific). The filter cake was then dried at 105℃ for 16 hours. The TS content of the three filter cake fractions was calculated using Equation 3; 'm_{tin}' refers to the initial mass of the aluminum weigh tin, '$m_{cake+tin}$' is the combined mass of the tin and the filter cake prior to drying, and '$m_{dried\ cake+tin}$' is the combined mass of the tin and the filter cake after drying. The TS content reported is the average of this triplicate TS analysis. Figure 31 displays images of ADS and MPS filter cake retained on the surface of a thin-film dewatering filter, as well as the filter cake fractions placed in aluminum weigh tins for analysis.

$$TS\ (w/w\ \%) = \frac{m_{dried\ cake+tin} - m_{tin}}{m_{cake+tin} - m_{tin}} x\ 100\ (\%) \quad (3)$$

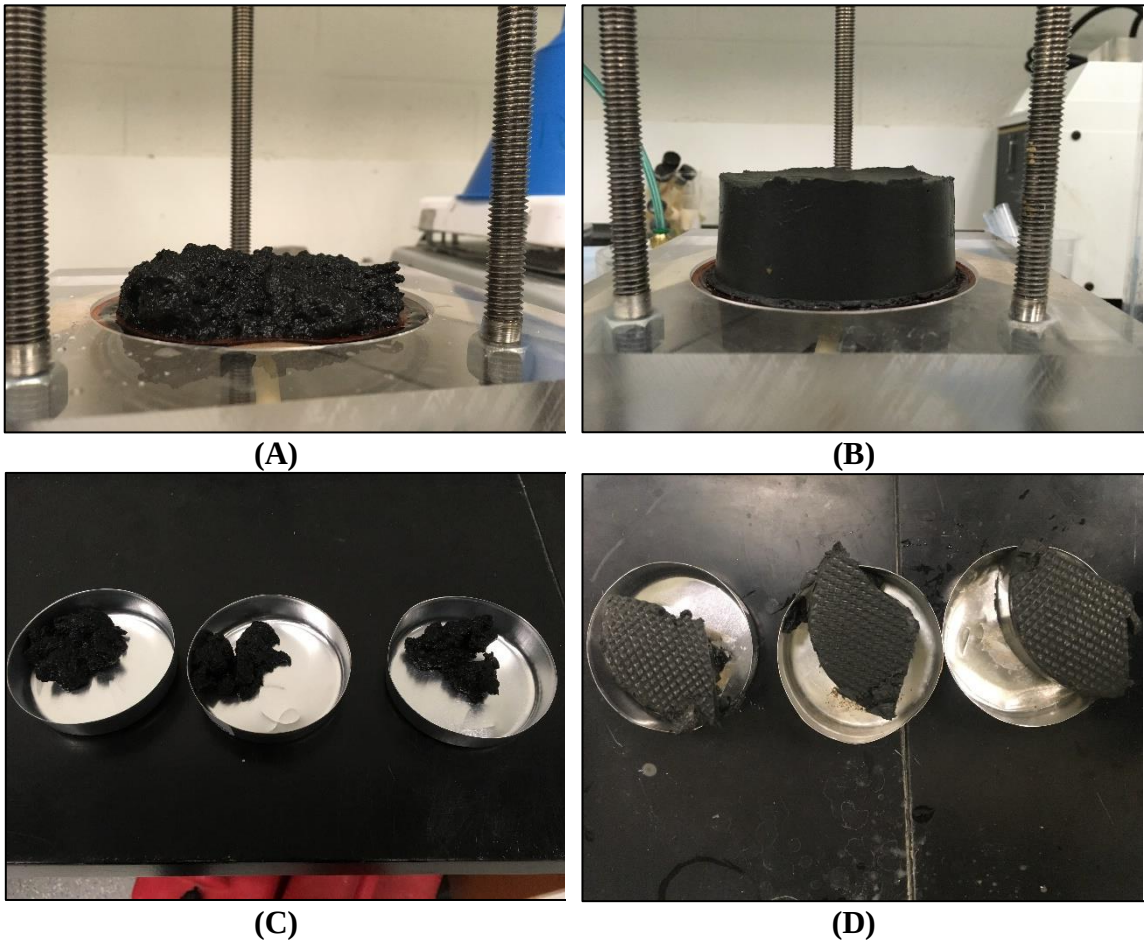

Figure 31. Images of the filter cake retained with the suspension cell at the end of the dewatering performance tests. Panels A and C depict ADS, while Panels B and D depict MPS.

2.6.1 Filtrate total suspended solids test

The capacity of an engineered dewatering fabric to retain the suspended solids is another important performance metric used to assess its viability for a given application. In this work, the solids retention capacities of the thin-film dewatering filters and the Woven Commercial Textile were assessed by determining the concentration of total suspended solids (TSS) present in the filtrate collected. For the constant rate dewatering tests performed in Chapter 3, the average filtrate TSS was determined through analysis of the filtrate collected cumulatively in the 250 mL beaker. Conversely, for the PFTs

performed in Chapter 4, the TSS present in each of the four discrete filtrate fractions was determined to evaluate the impact of filter cake development on solids retention. In either case, TSS analysis was performed as per the standard 2540 D method [48].

To begin, Whatman 934-AH glass microfiber filters (GE Healthcare) measuring 47 mm in diameter were placed in the three filter holders of the filtration apparatus depicted in Panel A of Figure 32. These filters were acquired in the 'ready-to-use' format and thus were pre-washed and pre-weighed by the manufacturer. The vacuum pump was turned on, and a small volume of deionized water was used to 'seat' each of the filters. The filtrate to be analysed was placed in a 250 mL beaker and stirred using a magnetic stir rod 7.9 mm in diameter by 24.9 mm in length. Filtrate was then added to each filter holder using a 5 mL micropipette (Eppendorf); 5 mL samples were analyzed for filtrate which appeared to possess an elevated concentration of suspended solids in order to avoid obstruction of the microfiber filter, while 10 mL samples were analyzed for filtrate having lower TSS. Suction was performed for 3 minutes to ensure filtration reached completion. The filters were then removed from the filtration apparatus, placed in aluminum weigh tins (GE Healthcare), and dried in an oven at 105℃ for 1 hour. After drying, the filters were removed from the oven and weighed using an Excellence XS Analytical Balance (Mettler Toledo). Panel B of Figure 32 includes a picture of the glass microfiber filters after drying. The TSS for each filter was calculated using Equation 4; '$m_{initial}$' refers to the initial mass of the glass microfiber filter, 'm_{final}' is the mass of the filter after drying, and 'V' is the volume of filtrate added to the filter holder. The TSS reported is the average of the triplicate TSS analysis.

$$TSS\ (mg/L) = \frac{m_{final} - m_{initial}}{V} x\ 10^6 \quad (4)$$

(A) **(B)**

Figure 32. Images depicting the filtration apparatus (Panel A) and the glass microfiber filters (Panel B) used to perform TSS analysis on the filtrate produced by the thin-film dewatering filters and the Woven Commercial Textile.

Chapter 3: Anaerobic Digested Sludge

The work presented in this chapter will be published in an forthcoming issue of Environmental Technology.

3.1 Introduction

The implementation of efficient sludge dewatering processes prior to the further treatment or final disposal of high-water-content slurry streams is critical to the economic and environmental sustainability of numerous industrial operations [1]. These dewatering processes apply solid-liquid separation principles in order to increase the SC of the sludge, thus reducing the overall volume of material requiring further handling. As a result, substantial cost savings are generated with respect to sludge pumping, transportation, treatment, storage, and disposal. Furthermore, environmental concerns related to the long-term storage of sludge, such as leachate production during landfilling operations, are mitigated [2].

Sludge dewatering is commonly performed via non-mechanical methods, such as sludge drying beds, or through the use of advanced mechanical systems, such as scroll decanter centrifuges, filter presses, and screw thickeners. Although these separation techniques perform admirably in terms of solids capture and volume reduction, their widespread adoption is restricted due to their respective limitations [2] [5]. Specifically, non-mechanical dewatering methods require large areas of land and favorable climatic conditions, while mechanical dewatering technologies require significant capital investment and ongoing operation and maintenance by highly trained personnel [27].

Recently, geotextile dewatering has emerged as a viable alternative to conventional methods of sludge dewatering. In this process, a feed sludge source is first

chemically conditioned using an appropriate coagulant or flocculant, then fed into an enclosed bag made from an engineered dewatering fabric. The head pressure within the bag forces the free water out through the pores of the fabric while keeping the solids contained within [18]. The size, shape, and distribution of a dewatering fabric's pores are a function of the fiber type and manufacturing processes used in its development [21]. A permeable cake layer develops on the inner surface of the dewatering fabric which then contributes to the retention of fine particles and affects the overall permeability of the system [19]. Offering both a small footprint and simple operation, this technology has been used to dewater sludge materials in municipal water and wastewater treatment facilities as well as in mining and pulp and paper operations [19] [29] [30].

The currently available fabrics for geotextile dewatering applications fall into one of two categories: woven or nonwoven. Woven geotextiles are composed of monofilament, multifilament, or slit-film yarns that are produced using high-tenacity polypropylene or polyester [19]. The weave patterns employed to interlace these yarns create a non-uniform array of pores which are approximately square in shape [22] [23]. Conversely, a nonwoven geotextile is a sheet, web, or batt of fibers or filaments that has been bonded using a combination of mechanical, thermal, or chemical processes creating a complex 3-dimensional pore structure [24] [25]. Conventionally, dewatering fabrics are selected for a given application based on an empirical ratio between the median particle size of the sludge and the AOS of the fabric [22]. The AOS refers to the largest opening and is measured via ASTM D4751-16, which combines the dry-sieving of glass beads and the use of a capillary porometer [26]. Typical AOS values reported in the literature range

from 150 to 850 μm for woven fabrics, and 75 to 210 μm for nonwoven fabrics [23] [25]. However, as previous studies have demonstrated, the size of the smaller pore openings has a direct effect on filtration performance [23] [25]. This is problematic as many currently available methods for measuring pore opening size distributions are unreliable, operator-dependent, or extremely time consuming [23]. Furthermore, this approach to dewatering fabric selection does not consider the relationship between porosity and the permeability of the filter cake or its rate of development.

In this work, an alternative approach was used to study the performance of dewatering fabrics. A series of thin-film dewatering filters were produced using advanced microfabrication techniques to create well-defined slit-pore geometries – the advantage to this approach is that it allows for a comprehensive analysis of the effect of the filter properties on dewatering performance to be made. The idea of using slit-pore geometries was inspired by recent work on the development of polymeric ultrafiltration and microfiltration membranes [35] [36] [37]. A full-factorial DOE was employed to evaluate the effects of slit-pore dimensions and slit-pore spacing on the cake layer development and overall dewatering performance in constant-rate dewatering tests. Three criteria are commonly used to assess the performance of dewatering fabrics: solids retention, permeability, and the extent to which pore openings become blocked over time. Of these criteria, permeability is given the largest weighting in order to ensure the water content of the sludge is removed in a timely manner [19].

3.2 High-throughput Screening of Polymer Flocculants via CST

The CST results obtained via the MFT for the ADS (from Sample 3) dosed with the six Kemira polymers (at values ranging from 4 to 10 kg/TTS) are shown in Figure 33. The error bars presented in this plot represent one standard deviation above and below the average CST result, which was attained via triplicate analysis. The CST values ranged from 280 (+/- 90) s for the 4518 polymer at 4 kg/TTS to 9 (+/- 1) s for the C-1594 polymer at 10 kg/TTS. As a control, 3 ml of the as-received ADS (i.e. without polymer addition) was added to the 'slow filtering' reservoir, resulting in a CST value of 460 (+/- 200) s. Therefore, each of the six polymers yielded CST values for each of the four evaluated doses that were significantly less than that of the control. Furthermore, each polymer displayed an inverse relationship between CST and dose. Therefore, the dewaterability of the ADS was shown to increase incrementally as quantities of each polymer were added between 4 and 10 kg/TTS. As was reported by LaRue et al., the dewatering performance dose-dependent dewatering profile is clearly a function of the polymer type [14]. The C-1594 polymer, which possesses a 'high' molecular weight and 'medium' charge density, was found to be the most effective across the dose range, resulting in CST values ranging from 14 (+/- 1) s at 4 kg/TTS to 9 (+/- 1) s at 10 kg/TTS. Conversely, the 4516 polymer was less effective at 4 kg/TTS, resulting in a CST of 42 (+/- 3) s, but demonstrated similar performance at 10 kg/TTS, yielding a CST of 9.3 (+/- 0.2) s. This polymer is reported to have a 'very high' molecular weight and 'high' charge density. The 4518 polymer, which has a 'very high' molecular weight and 'very high' charge density, produced the highest CST value for each of the four doses, ranging from

280 (+/- 90) s at 4 kg/TTS to 21 (+/- 2) s at 10 kg/TTS. Based on the qualitative information that was supplied by the manufacturer, it is impossible to extract any particular trends with regards to the dewatering performance and polymer molecular weight or charge density.

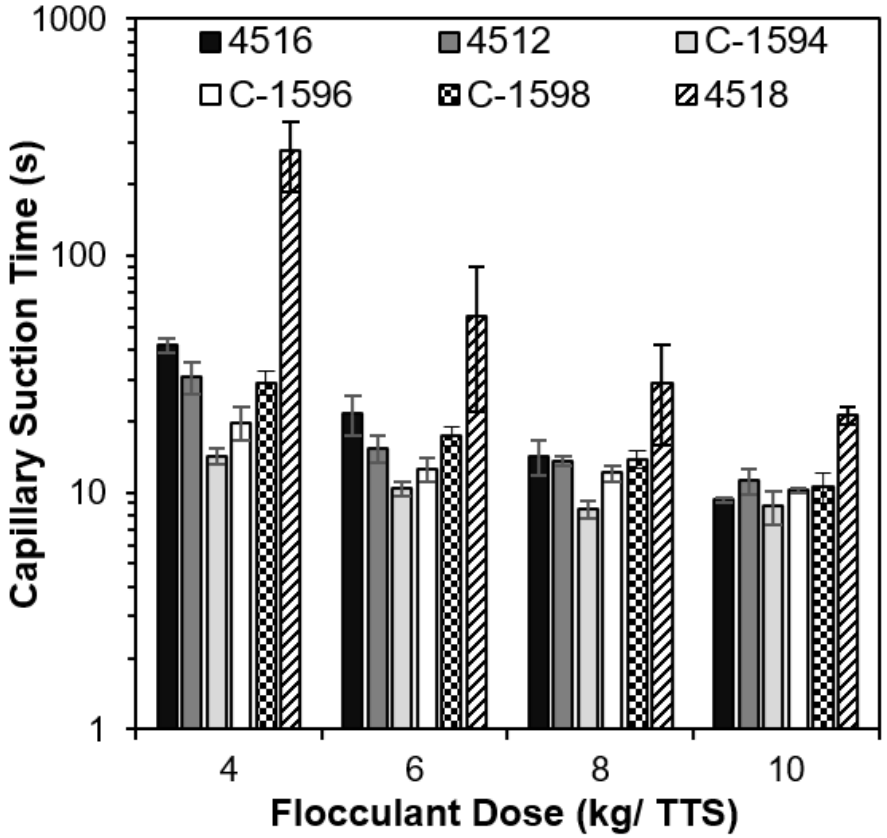

Figure 33. Comparison of the dose-dependent dewatering profile in terms of capillary suction time for the six Kemira Superfloc® polymer flocculants: 4516, 4512, C-1594, C-1596, C-1598, and 4518 (see Table 5 for technical details); the error bars correspond to the standard deviation from the triplicate analysis done at each condition.

The ADS dosed at 10 kg/TTS using the C-1594 and 4516 polymers yielded the two lowest CST results of the twenty-four total conditions evaluated. The observed variance in CST between these two conditions was negligible. Therefore, 10 kg/TTS of either polymer was identified as the OPD for the ADS. As previously discussed, the C-

1594 polymer displayed little variance in CST between 4 and 10 kg/TTS, while the 4516 polymer was significantly more effective at 10 kg/TTS than it was at 4 kg/TTS. The primary objectives of this work were to evaluate the impact of polymer dose on the geotextile dewatering process, to determine if the three design factors influence the response of the thin-film dewatering filters to adverse feed conditions, and to elucidate the relationships between pore structure and dewatering performance at the OPD. Based on this analysis, the 4516 polymer was selected for use in the subsequent stages of this study as it allowed for the constant-rate dewatering tests to be performed at varying levels of pre-treatment effectiveness using a single polymer flocculant.

3.3 Impact of Polymer Dose on Textile Dewatering Performance

The impact of polymer dose on the respective performances of the thin-film dewatering filters and the Woven Commercial Textile were evaluated via duplicate constant-rate dewatering tests performed at 4, 6, and 10 kg/TTS of 4516 polymer. In order to reduce the total number of tests required while also still incorporating a wide range of filter properties, the thin-film filters used in these tests were limited to those that fell within the DOE framework (as described in Table 1) and had a characteristic dimension of 100 μm.

The average filtrate TSS results for each filter at the three evaluated polymer doses are displayed in Panel A of Figure 34, the error bars presented in this plot represent the observed range above and below the average TSS result across duplicate dewatering tests. The measured TSS values for the thin-film dewatering filters ranged considerably from the lowest value of 100 (+/- 10) mg/L for the ‘100×5000_4mm’ filter (pore width =

100 µm; pore length = 5000 µm; pore-to-pore spacing = 4 mm) at a polymer dose of 10 kg/TTS to the highest value of 960 (+/- 200) mg/L for the '100×5000_4mm' filter at a polymer dose of 4 kg/TTS. Filtration efficiency (FE) is a metric used to index the solids retention capacity of a dewatering fabric when assessing the viability of dewatering with geotextile bags; higher FE values indicate a greater capacity to retain solids. FE is calculated from the filtrate TSS and feed TS as shown in Equation 5 [19]:

$$FE = \frac{TS_{initial} - TSS_{final}}{TS_{initial}} x\ 100\ (\%) \quad (5)$$

The range of TSS values reported above for the thin-film dewatering filters corresponds to FEs of 99.6% (for the '100×5000_4mm' filter at 10 kg/TTS) and 95.9% (for the '100×5000_4mm' filter at 4 kg/TTS). In comparison, the Woven Commercial Textile yielded FEs of 99.5% and 96.9% for the 10 kg/TTS and 4 kg/TTS doses, respectively.

The filtrate TSS results indicate that the polymer dose employed during the pre-treatment phase of the constant-rate dewatering test significantly impacted the solids retention capacity of the thin-film dewatering filters and the Woven Commercial Textile. The main reason for this is that an inverse relationship exists between the TSS in the collected filtrate and the polymer dose for each evaluated filter. In other words, during the treatment of ADS, the filtration efficiency of each filter was shown to increase by adding increasing quantities of polymer between 4 kg/TTS and 10 kg/TTS. For example, the '100×5000_4mm' filter produced a filtrate TSS of 960 (+/- 200) mg/L when it was used in combination with a 4 kg/TTS dose. However, when the polymer dose was increased to

10 kg/TTS, that same filter yielded a filtrate TSS of only 100 (+/- 10) mg/L. This observation is consistent with the results presented in Section 3.2 for the MFT.

The average SC values for each filter at the three polymer doses are displayed in Panel B of Figure 34; again the error bars representing the observed range above and below this average across duplicate dewatering tests. The measured SC values for the thin-film dewatering filters ranged from 2.4 (+/- 0.1) % for the '100×5000_4mm' filter at a 4 kg/TTS dose to 14.27 (+/- 0.03) % for the '100×1500_1mm' filter with a 4 kg/TTS dose. The dewatering efficiency (DE) is a useful indicator of dewatering capacity, defined as the relative increase in the SC of the feed achieved during the dewatering process as shown in Equation 6 [19].

$$DE = \frac{SC_{final} - SC_{initial}}{SC_{initial}} x\ 100\ (\%) \tag{6}$$

The range of SC values reported above for the thin-film dewatering filters correspond to DEs of 0% (for the '100×5000_4mm' filter at 4 kg/TTS) and 490% (for the '100×1500_1mm' filter at 4 kg/TTS). In comparison, the Woven Commercial Textile yielded a DE of 320% at 10 kg/TTS and 530% at 4 kg/TTS.

The observed relationship between polymer dose and SC for the thin-film dewatering filters is dependent upon the filter pore structure. Specifically, a positive correlation was observed between polymer dose and SC for the two filters with the lowest porosity, while a negative correlation was observed for the two highest porosity filters. For example, the '100×1500_4mm' filter, which had a porosity of 0.69%, yielded a SC value of 2.4 (+/- 0.1) % at 4 kg/TTS and 9.89 (+/- 0.01) % at 10 kg/TTS. Conversely, the

‘100×5000_1mm’ filter, which had a porosity of 8.81%, yielded SC results of 12 (+/- 2) % at 4 kg/TTS and 9.8 (+/- 0.2) % at 10 kg/TTS. It is hypothesized that this phenomenon is principally due to excessive pore blockage at low polymer dose conditions, which impact the ability of the filters to allow free water to pass through.

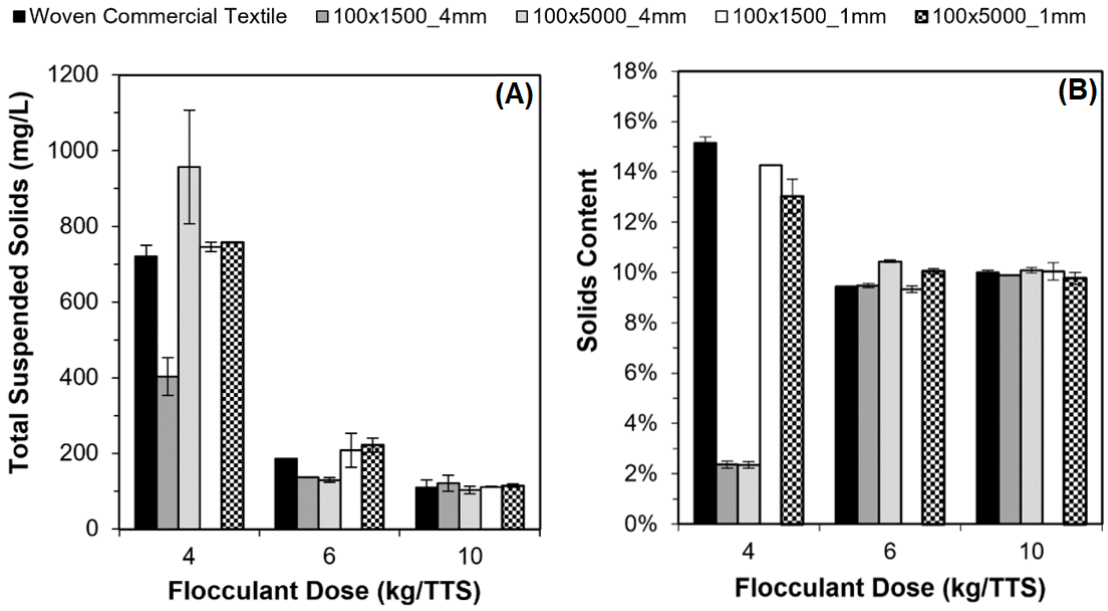

Figure 34. Constant-rate dewatering test results for 2.4% ADS (Sample 4) dosed with Kemira Superfloc® 4516 at 4, 6, and 10 kg/TTS. Panels A and B display the TSS present in the collected filtrate and the SC of the material retained within the suspension cell for the subset of the thin-film dewatering filters (100×5000_1mm, 100×1500_1mm, 100×5000_4mm, and 100×1500_4mm) and the Woven Commercial Textile. The error bars correspond to the range above and below the average result based on triplicate solids analysis performed for duplicate constant-rate dewatering tests.

The vacuum pressure versus filtrate mass plots for the same subset of thin-film dewatering filters and the Woven Commercial Textile are displayed in Figure 35. The slight variation in pressure profiles for duplicate trials indicates that the dewatering behaviours captured by the constant-rate dewatering test are inherent to each of the conditions evaluated. These plots clearly demonstrate that a higher vacuum pressure is required to dewater the ADS dosed at 4 kg/TTS for each filter, which confirms that

greater pore blockage occurs at low polymer dose conditions. Furthermore, the observed relationship between vacuum pressure and filtrate mass at 4 kg/TTS is unique for each of the filters. The two low-porosity thin-film dewatering filters (‘100×1500_4mm’ and ‘100×5000_4mm’), which have relatively few pore openings and are particularly sensitive to pore blockage, produce a dramatic increase in vacuum pressure during the earliest stages of dewatering and, subsequently, a premature end to filtrate collection. Conversely, the high-porosity thin-film dewatering filters (‘100×1500_1mm’ and ‘100×5000_1mm’) are less sensitive and produce a pressure increase significantly later in the dewatering process as well as not ending filtration collection prematurely. In fact, those high-porosity filters exhibit greater DE at 4 kg/TTS than at 10 kg/TTS due to increased cake compression, which arises from the higher vacuum pressures that, in turn, cause more liquid to be released from the ADS.

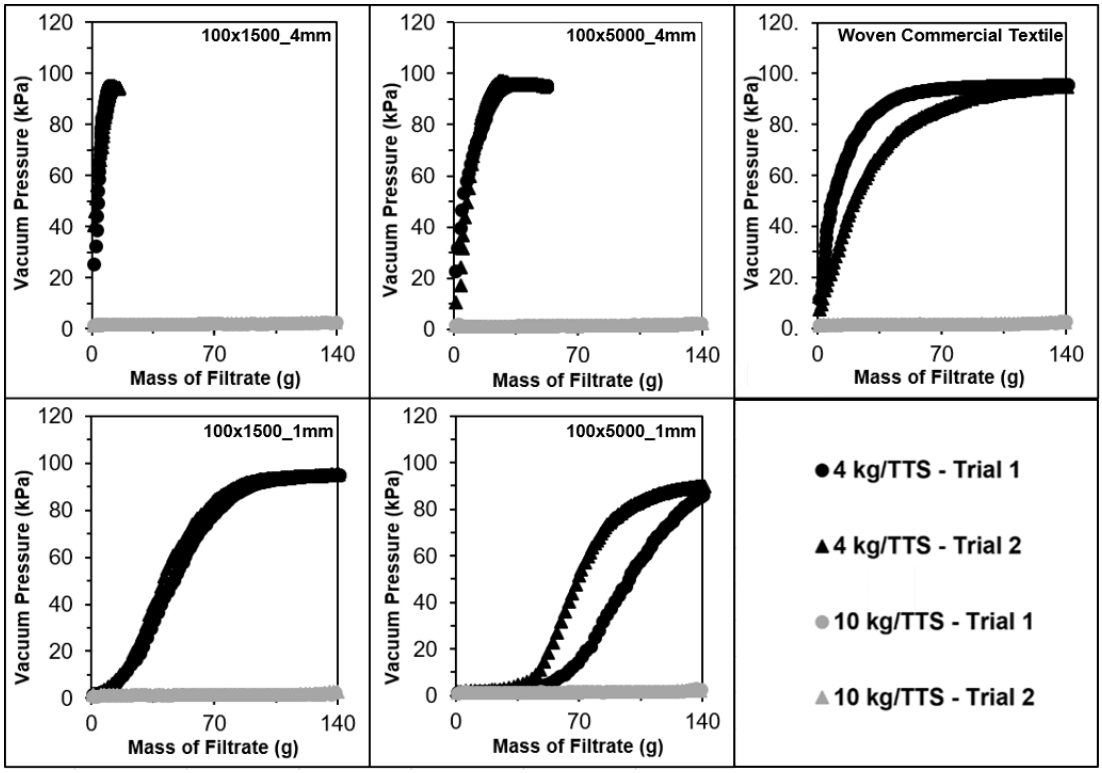

Figure 35. Constant-rate dewatering test results for ADS (Sample 4) treated with Kemira Superfloc® 4516 polymer at doses of 4 kg/TTS (black data points) and 10 kg/TTS (grey data points) using a subset of the thin-film dewatering filters (100×5000_1mm, 100×1500_1mm, 100×5000_4mm, and 100×1500_4mm) and the Woven Commercial Textile.

3.4 Pore Structure, Cake Layer Development, and Dewatering Performance

In order to evaluate the relationship between pore structure, dewatering performance, and filter cake permeability at the OPD, the results from the duplicate constant-rate dewatering tests (performed at 10 kg/TTS of 4516 polymer) for the eight thin-film dewatering filters defined by the 2^3 full-factorial DOE, as well as the Woven Commercial Textile, are analyzed below.

3.4.1 Medium and maximum cake resistances

For constant-rate dewatering experiments, the medium and cake resistances can be calculated from the amount of applied pressure required to maintain a constant filtrate

flow rate and the cumulative volume of collected filtrate. The vacuum pressure profiles for the eight thin-film dewatering filters and the Woven Commercial Textile are displayed in Figure 36. During the initial stages of the constant-rate dewatering test, cake layer development on the surface of the dewatering filter and blockage of the available pore openings are negligible. Therefore, the recorded vacuum pressure during this period is exclusively a function of the medium resistance. The vacuum pressure values recorded after the collection of only 10 mL of filtrate ranged from 1.79 kPa for the '80×1200_1mm' filter to 5.79 kPa for the '80×1200_4mm' filter. As the dewatering test proceeds, the pressure required to maintain a constant flow rate increases as cake accumulates on the surface of the filter and solid particles become lodged within the pore openings. As such, the vacuum pressure recorded during the later stages of dewatering is a function of both the medium and cake resistances, as well as the extent to which pore blockage occurs. The vacuum pressure values recorded after the collection of 120 mL of filtrate ranged from 2.06 kPa for the '80×1200_1mm' filter to 12.27 kPa for the '80×1200_4mm' filter. In comparison, the Woven Commercial Textile yielded a vacuum pressure of 1.86 kPa after 10 mL of filtrate was collected and 2.21 kPa after 120 mL was collected. As shown in Figure 36, the vacuum pressure recorded for the '80×1200_4mm' filter was significantly higher than that of the other filters throughout the dewatering test. This result suggests that the use of this filter requires a greater driving force to maintain a constant filtrate collection rate of 150 mL/min both when the surface of the filter is 'clean', and when cake layer development and pore blockage have occurred. This observation suggests that the pore structure of this filter makes it inherently more difficult

for filtrate to pass through for collection. Previous studies have demonstrated that the porosity of a dewatering fabric is directly correlated to its permittivity [23]. ASTM International defines the permittivity of a dewatering fabric as the volumetric flow rate of water per unit area that passes through the pores of the material at a given pressure [54]. Permittivity is a function of its medium resistance; higher resistance materials yield lower permittivity. By extension, lower porosity dewatering fabrics have higher medium resistance. The '80×1200_4mm' filter had the lowest porosity (0.47%) within the DOE framework. This is a non-ideal scenario for textile dewatering applications, as the use of elevated pressure prior to sufficient cake development can lead to excessive pore blockage and compression of the initial cake layers—both of which would degrade the rate of dewatering in industrial applications of this technology [53]. The results for the '80×1200_4mm' filter reflected this phenomenon, exhibiting a substantial increase in required vacuum pressure as dewatering proceeded.

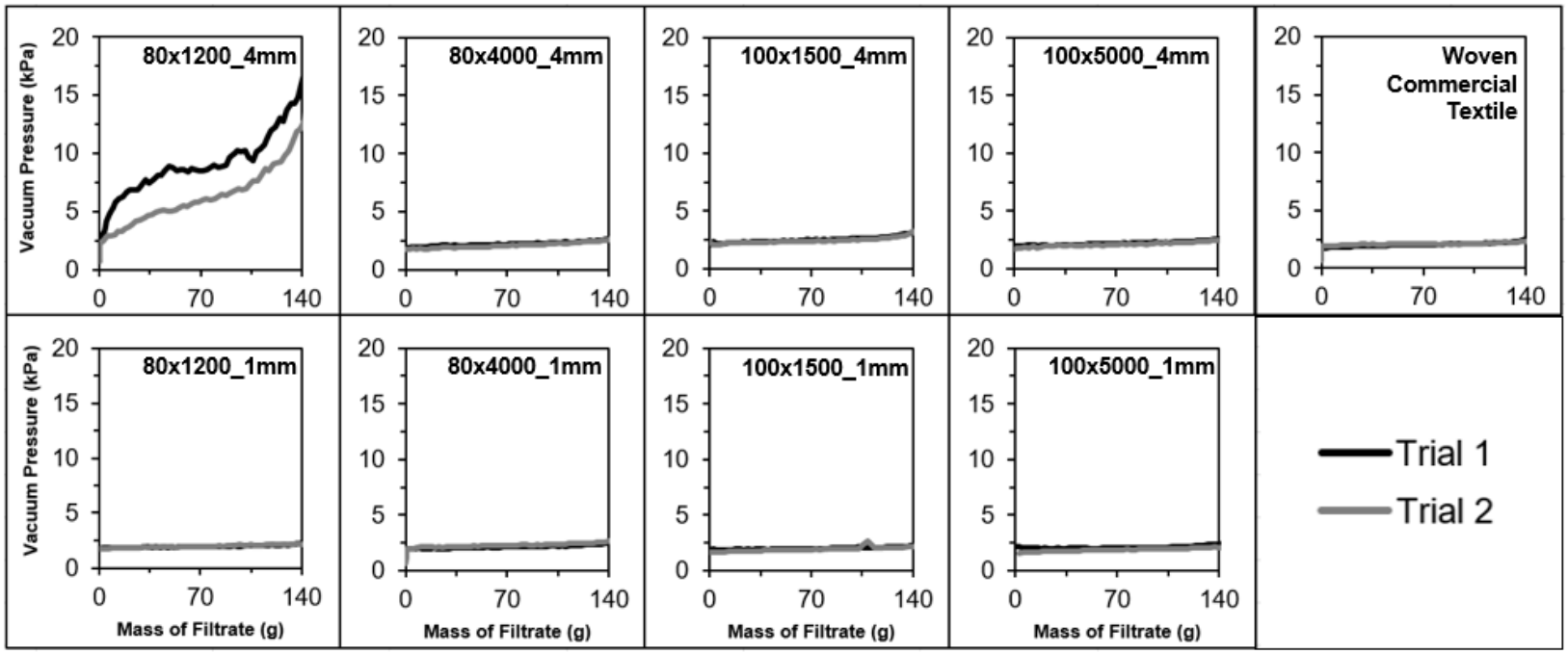

Figure 36. Scatter plots of vacuum pressure versus the mass of filtrate collected for the constant-rate dewatering test results for 1.7% ADS (Sample 3) with a 10 kg/TTS dose of Kemira Superfloc® 4516 polymer.

Medium and cake resistance were calculated using the method proposed by Mahdi and Holdich [53]. Specifically, these two values were derived from a linear regression of vacuum pressure onto the volume of collected filtrate. To convert the recorded filtrate mass data to volume data, the collected filtrate was assumed to have a constant density equal to that of water at 25℃ (997 kg/m^3). Evidence to support this assumption is provided in Section 3.3.2; the TSS present in the filtrate was minimal for each of the DOE filters. The data used to calculate the linear regression was limited to the range of 10 to 120 mL of filtrate, and the results indicated that linearity was strong in this range. The produced regression was of the form shown in Equation 7. The y-intercept was used in combination with the liquid viscosity of the ADS (μ) and the filtration area of the filter (A) in order to calculate medium resistance (Rm). Cake resistance values (α_{av}) were calculated using the slope of the linear regression as well as the liquid viscosity of the ADS (μ), the filtration area of the filter (A), and the dry cake mass per unit volume of filtrate (**c**).

$$\Delta P = \frac{\mu \alpha_{av} c}{A^2} \frac{dV}{dt}(V) + \frac{\mu R_m}{A} \frac{dV}{dt} \tag{7}$$

The medium resistances that were calculated for the thin-film dewatering filters and the Woven Commercial Textile are displayed in Panel A of Figure 37; the results are arranged such that the filters are ordered with respect to filter porosity (refer to Table 2 for exact values). The error bars represent the observed range above and below the average medium resistance obtained via duplicate dewatering tests. The medium resistance of the thin-film filters ranged from 4.05×10^9 (+/- 1×10^7) m^{-1} for the '80×1200_1mm' filter to 10×10^9 (+/- 5×10^9) m^{-1} for the '80×1200_4mm' filter. In

comparison, the medium resistance for the Woven Commercial Textile was 4.3×10^9 (+/- 3×10^8) m^{-1}. The medium resistance and filter porosity are inversely related with lower porosity filters yielding higher medium resistance values. For example, the '80×1200_4mm' and '80×1200_1mm' filters possess pores that have the same characteristic dimension and length-to-width aspect ratios (i.e. 15:1). However, the pore-to-pore spacing, and therefore porosity, of these filters is dissimilar, which results in a substantial change in the observed medium resistance. The '80×1200_4mm' filter had a nominal porosity of 0.47% and was found to have a medium resistance of 10×10^9 (+/- 5×10^9) m^{-1}, while the '80×1200_1mm' filter had a nominal porosity of 4.32% and a medium resistance of only 4.05×10^9 (+/- 1×10^7) m^{-1}. Therefore, a 59% decrease in medium resistance was achieved by reducing the pore-to-pore spacing from 4 mm to 1 mm. Similarly, while the '80×1200_4mm' and '80×4000_4mm' filters had the same characteristic dimensions and pore spacings, their length-to-width aspect ratios were 15:1 and 50:1, respectively. The larger aspect ratio used in the design of the '80×4000_4mm' filter yielded a filter porosity of 1.03%, which resulted in a 57 % decrease in medium resistance compared to the '80×1200_4mm' filter. Further analysis of the relationship between medium resistance and filter porosity is presented in Section 3.4.4.

The maximum cake resistance values, defined as the hydraulic resistance that arises from cake layer development and pore blockage at the point in the dewatering test when 120 mL of filtrate has been collected, are displayed in Panel B of Figure 37. Again, the results are arranged such that the filters are ordered based on their porosity. The error bars represent the observed range above and below the average maximum cake resistance

result that was attained via duplicate dewatering tests. The maximum cake resistance for the thin-film filters ranged from 1.1×10^9 (+/- 3×10^8) m/kg for the '100×1500_1mm' filter to 2.3×10^{10} (+/- 1×10^9) m/kg for the '80×1200_4mm' filter. In comparison, the Woven Commercial Textile was determined to have a maximum cake resistance of 1.1×10^9 (+/- 4×10^8) m/kg. As described above, elevated pressure during the early stages of a surface filtration process can result in excessive pore blockage and the compression of the initial cake layers. Therefore, as was observed for medium resistance, it is intuitive that an inverse relationship must exist between maximum cake resistance and the filter porosities of the evaluated thin-film dewatering filters. The low-porosity filters were found to have higher-than-average medium resistances, which meant that greater driving force was required in order to achieve the desired rate of filtrate collection. As a result, these same filters were found to yield elevated maximum cake resistance due to a greater occurrence of pore blockage and cake compression. For example, the '80×1200_4mm filter', which has the lowest porosity of the filters tested in this stage of the study, was determined to have both the highest medium and maximum cake resistance. Further analysis of the relationship between filter porosity and the occurrence of pore blockage and cake compression is included in Section 3.4.4.

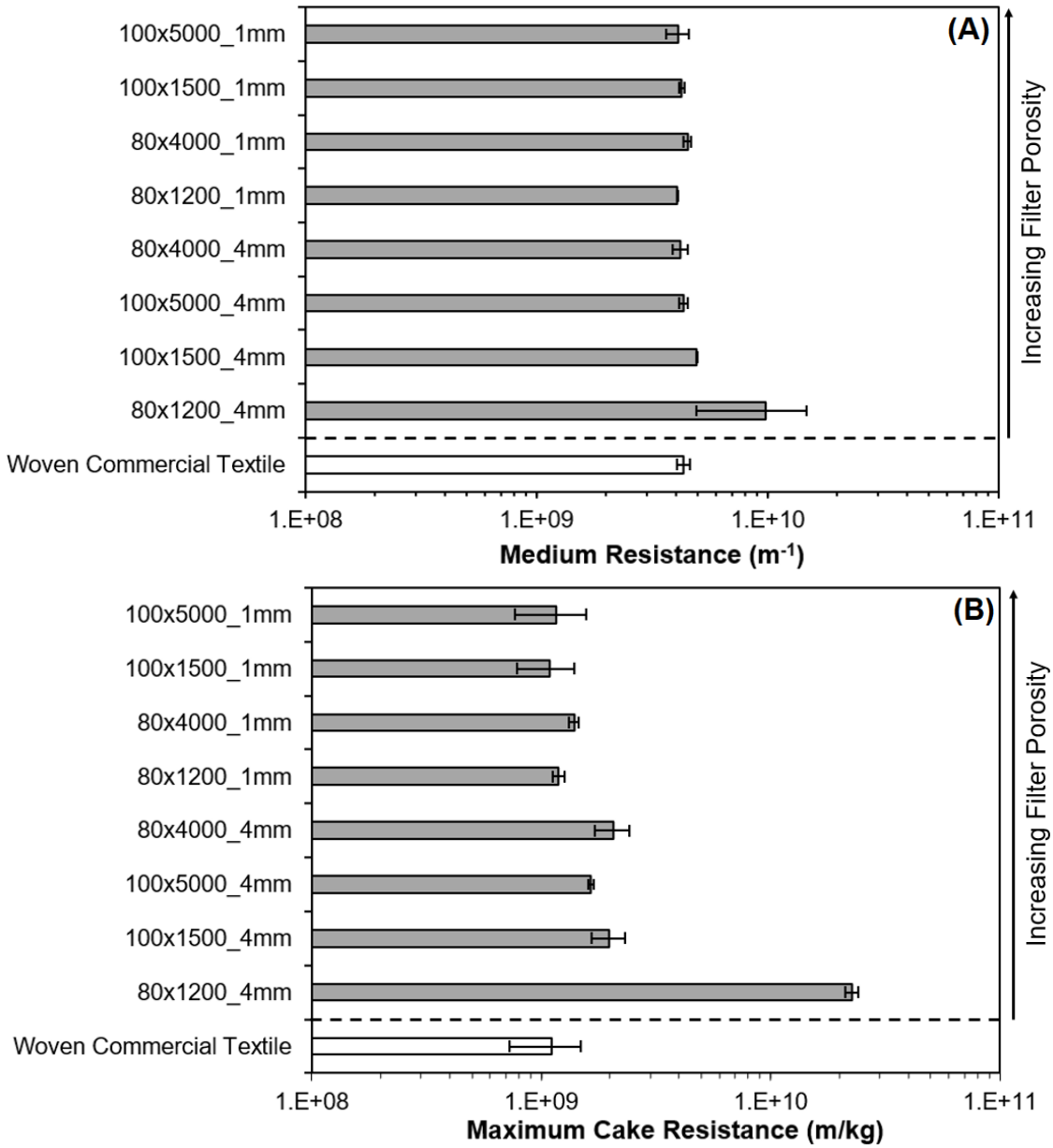

Figure 37. Constant-rate dewatering test results for 1.7% ADS (Sample 3) with a 10 kg/TTS dose of Kemira Superfloc® 4516 polymer. Panels A and B display the calculated medium resistance and maximum cake resistance for each of the thin-film dewatering filters, as well as the Woven Commercial Textile. The error bars correspond to the standard deviation of triplicate solids analysis for the duplicate constant-rate dewatering tests.

3.4.2 Filtrate data and dewatering efficiency

The filtrate TSS results for the thin-film dewatering filters and the Woven Commercial Textile are displayed in Panel A of Figure 38; the error bars represent the observed range above and below the average TSS result, which was based on triplicate analysis for each of the duplicate dewatering tests. The average TSS values ranged from 112 (+/- 8) mg/L for the '80×4000_4mm' filter to 160 (+/- 20) mg/L for the '100×5000_1mm' filter; the corresponding filtration efficiencies for these two filters are 99.2% and 98.9%, respectively. In comparison, the Woven Commercial Textile yielded a filtrate TSS result of 180 (+/- 10) mg/L. As originally reported by Liao and Bhatia, elevated pressure tends to degrade filtration efficiency due to elongation of the textile fabric and the resulting enlargement of the pore openings [55]. Due to the highly compressible nature of the flocculated material, elevated pressures can also result in floc deformation, which can lead to greater solids passthrough. However, these potential issues are not reflected in the results obtained in this study as the '80×1200_4mm' filter, which required the highest vacuum pressure to maintain a constant filtrate flow rate, yielded a filtrate TSS of 150 (+/- 20) mg/L; this result corresponded to a filtration efficiency of 99.0%. In fact, each of the evaluated filters displayed excellent efficacy in retaining solids, and all were able to achieve filtration efficiencies that were greater than that of the Woven Commercial Textile.

The corresponding SC results for the material retained on each thin-film dewatering filter and the Woven Commercial Textile are displayed in Panel B of Figure 38. The average values for the thin-film dewatering filters ranged from 10.0 (+/- 0.3) %

for the ‘100×1500_1mm’ filter to 11.89 (+/- 0.07) % for the ‘80×1200_4mm’ filter; the corresponding dewatering efficiencies for these two filters are 490% and 600%, respectively. In comparison, the material retained by the Woven Commercial Textile was determined to have an average SC of 9.46 (+/- 0.08) %, which corresponded to a DE of 460%. The variance in SC observed between the thin-film dewatering filters was minimal, which indicates that characteristic dimension, pore spacing, and aspect ratio has a negligible impact on dewatering relative to that of the flocculant-dose combination described in Section 3.3.

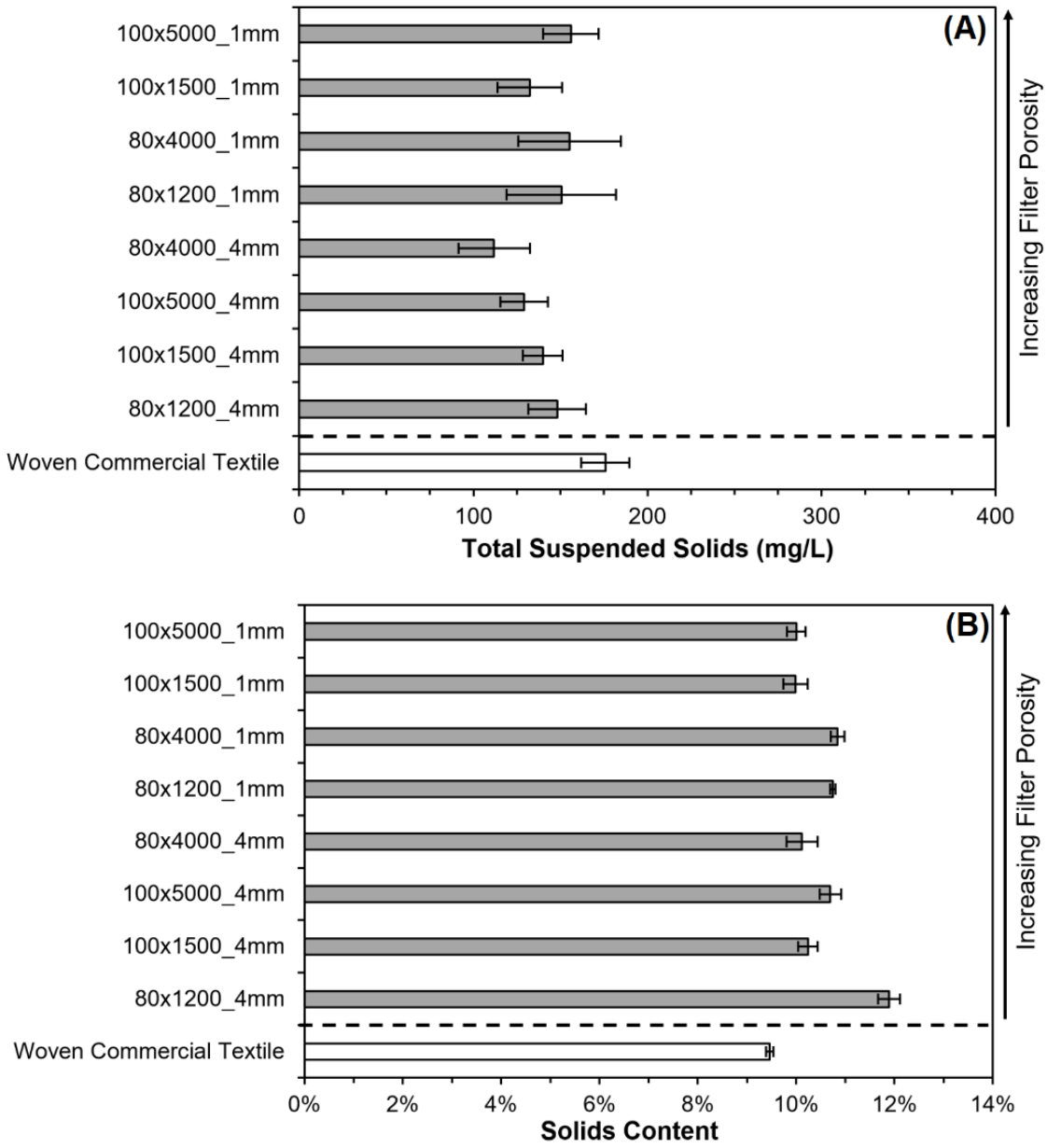

Figure 38. Constant-rate dewatering test results for 1.7% ADS (Sample 3) with a 10 kg/TTS dose of Kemira Superfloc® 4516 polymer. Panels A and B display the TSS present within the collected filtrate and the SC of the material retained within the suspension cell for each of the thin-film dewatering filters and the Woven Commercial Textile. The error bars correspond to the standard deviation of triplicate analysis for the duplicate constant-rate dewatering tests.

3.4.3 Multiple linear regression models

In order to quantify the relationships between pore structure, dewatering performance, and filter cake permeability that were outlined in Sections 3.4.1 and 3.4.2, four multiple linear regression (MLR) models were developed. Each MLR model quantified the correlation structure between the three design factors of interest and one of the key evaluated dewatering performance metrics—specifically, medium resistance, maximum cake resistance, filtrate TSS, and the SC after dewatering. The boundaries of these models consisted of the high and low values that were selected for each design factor, as reported in Table 1. The models took the form presented in Equation 8, where 'x_A', 'x_B', and 'x_C' range from -1 to 1 and define the characteristic dimension, pore spacing, and aspect ratio of a thin-film filter within the design space, while the coefficients 'b_A', 'b_B'and 'b_C' describe the average impact of each variable on the performance metric; 'b_0' defines the average of all measured outcomes for the performance metric, while 'b_{AB}', 'b_{AC}', 'b_{BC}' and 'b_{ABC}' capture the interaction between the three design factors.

$$\hat{y} = b_0 + b_A x_A + b_B x_B + b_C x_C + b_{AB} x_A x_B + b_{AC} x_A x_C + b_{BC} x_B x_C + b_{ABC} x_A x_B x_C \quad (8)$$

The model coefficients for the filtrate TSS are displayed in Panel A of Figure 39. The average TSS across the sixteen experiments was 140 mg/L, which corresponds to a filtration efficiency of 99.17%. The model predicts an average decrease of only 2 mg/L when the characteristic dimension is increased from 80 to 100 μm. This value is trivial in relation to both the TSS of the as-received ADS and the average filtrate TSS result and

thus indicates that such changes in characteristic dimension have no bearing on filtration efficiency. Similarly, a decrease in filtrate TSS of only 5 mg/L is predicted when the length-to-width aspect ratio of the pore openings is increased from 15:1 to 50:1, and a decrease of only 16 mg/L is predicted when the pore-to-pore spacing is increased from 1 mm to 4 mm. Therefore, at the OPD condition, substantial changes can be made to the aspect ratio and spacing of the pores without degrading the capacity of the filter to retain solids. Panel B of Figure 39 displays the coefficients for the SC model. The average SC across the sixteen experiments was determined to be 10.56%, which corresponds to a DE of 520%. As was the case for filtrate TSS, the SC model indicates that the dewatering capacities of the thin-film filters are not significantly impacted by slight changes to the characteristic dimension or substantial variations in pore spacing and aspect ratio.

In contrast, the MLR models developed for medium and maximum cake resistance indicate that substantial correlation exists between the three design factors included in the DOE framework and the permeability of the thin-film filters and the filter cake. The coefficients of the medium resistance model are displayed in Panel C of Figure 39. A negative correlation is observed between both the characteristic dimension and spacing of the pores and the medium resistance of the thin-film filters. Conversely, a positive correlation is observed between the pore-to-pore spacing and medium resistance. Therefore, the regression model indicates that the medium resistance of the thin-film filters can be minimized through the implementation of wider and longer pores that are spaced more closely together. The pore structure's correlation to maximum cake resistance was observed to be the same as its correlation to medium resistance. The model

coefficients for the maximum cake resistance are displayed in Panel D of Figure 39. As the porosity of a thin-film filter is increased through changes to characteristic dimension, pore spacing, and aspect ratio, the occurrence of cake compression and pore blockage are substantially reduced due to lower pressures during the initial stages of dewatering.

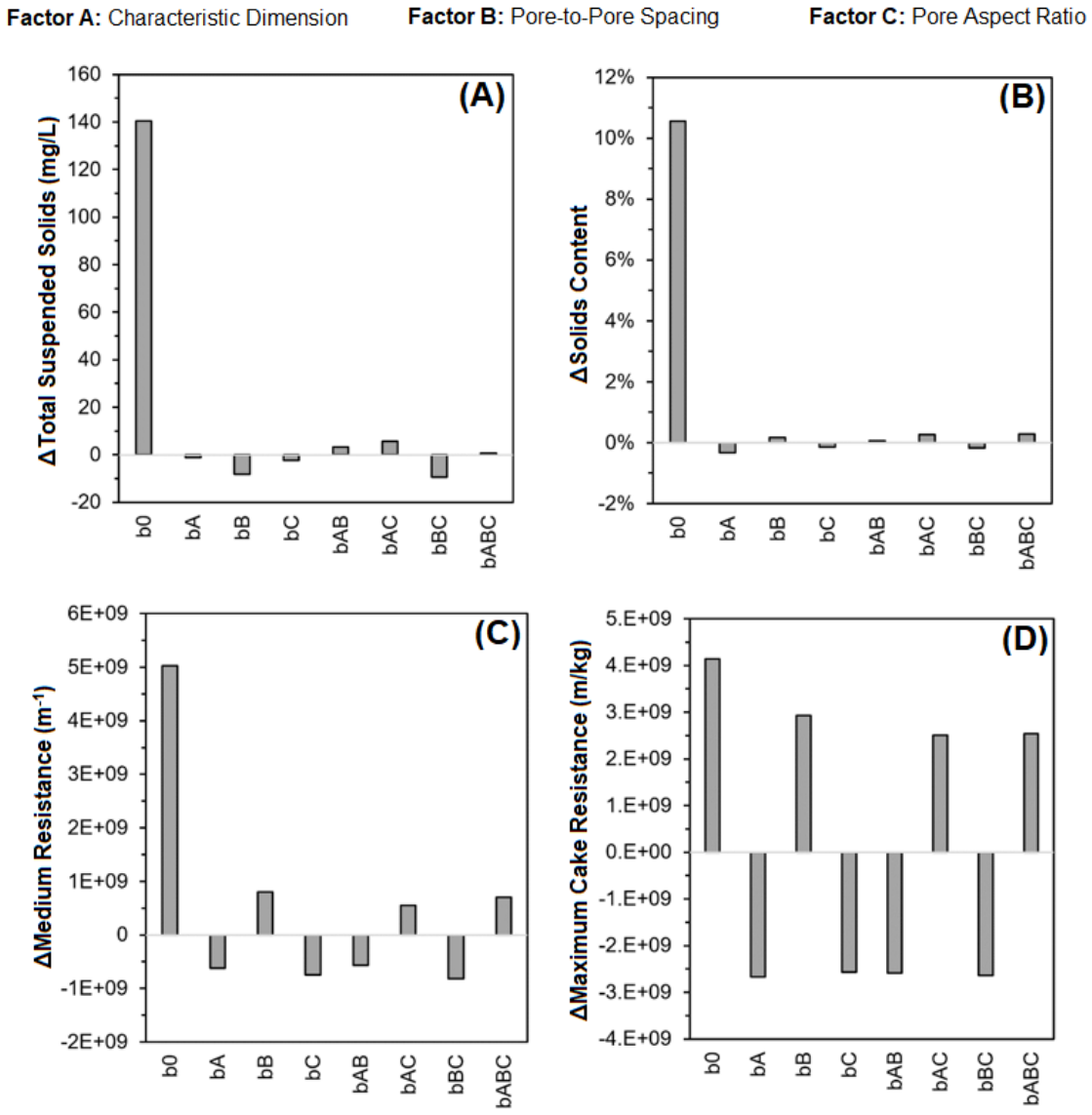

Figure 39. Regression model coefficients for the correlations of characteristic dimension, pore-to-pore spacing, and length-to-width aspect ratio with filtrate TSS (Panel A), SC (Panel B), medium resistance (Panel C), and maximum cake resistance (Panel D). These models were developed using the constant-rate dewatering test results for Sample 3, which was dosed with 10 kg/TTS of Kemira Superfloc® 4516 and dewatered using the 8 thin-film filters defined by the DOE framework in Table 1.

3.4.4 Expanded design space

In order to further elucidate the relationship between the porosity of a thin-film filter and its medium resistance, and to understand how this relationship impacts the permeability of the produced filter cake, six additional thin-film dewatering filters incorporating pore structures outside of the original DOE framework were evaluated. These supplemental filters were designed such that the expanded design space included a wider range of filter porosities. The medium resistance values calculated for each of the thin-film dewatering filters are presented as a function of filter porosity in Panel A of Figure 40; the error bars represent the observed range above and below the average medium resistance values, which were attained via duplicate constant-rate dewatering tests. The results demonstrate that, while a strong inverse relationship does exist between the porosity of a thin-film filter and its medium resistance, this relationship is largely confined to the 0.1 to 1.0 % filter porosity range. Beyond 1.0 %, further increases in porosity obtained by modifying the characteristic dimension, pore spacing, or aspect ratio of the slits pores do not yield significant decreases in medium resistance. For example, the lowest porosity filter evaluated in this study ('40×600_4mm') has a designed porosity of 0.14% and a calculated medium resistance of 5.1×10^{10} (+/- 3×10^{9}) m^{-1}. Adjusting the pore structure of this filter to achieve a porosity of 1.03% (as is the case for the '80×4000_4mm' filter) resulted in a 92% drop in medium resistance. However, increasing the porosity further to 8.81% (as is the case for the '100×5000_1mm') yields only a further 3% drop in medium resistance.

The maximum cake resistance for each of the thin-film dewatering filters as a function of filter porosity is displayed in Panel B of Figure 40; the error bars correspond to the observed range above and below the average maximum cake resistance result from the duplicate dewatering tests. As observed for medium resistance, there exists an inverse relationship between filter porosity and maximum cake resistance between 0.1 and 1.0 % porosity, and that maximum cake resistance is independent of porosity beyond 1.0 %. This observation confirms that the use of thin-film filters having high medium resistances result in the development of a filter cake having elevated hydraulic resistance due to compression of the initial cake layers and the occurrence of pore blockage.

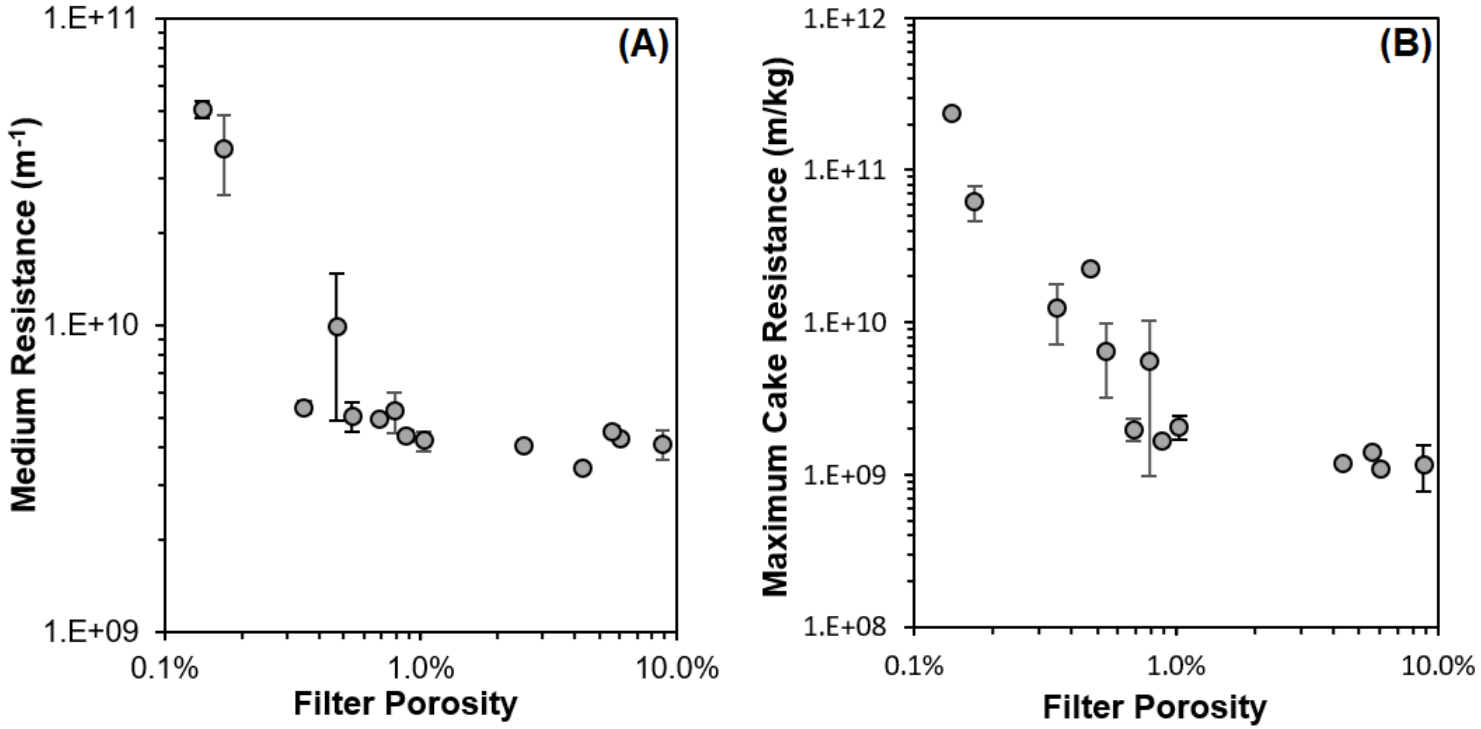

Figure 40. Constant-rate dewatering test results for 1.7% ADS (Sample 3) with a 10 kg/TTS dose of Kemira Superfloc® 4516 polymer. Panels A and B display the calculated medium resistance and maximum cake resistance versus total porosity for the fourteen thin-film dewatering filters within the expanded design space.

3.5 Conclusions

Microfabricated dewatering filters have been shown in this work to effectively facilitate the evaluation of the effects of pore geometry and total porosity on solids retention, permeability, and the occurrence of pore blockage for geotextile dewatering applications. In contrast with the conventional woven and nonwoven dewatering fabrics, these filters possess pore structures which can be exactly defined prior to fabrication, allowing for the application of DOE frameworks and the development of regression models for key performance metrics. Furthermore, the use of solid-state laser technology, in combination with computer aided design software, allows for a rate of prototype development greater than that achievable for conventional fabrics. These benefits are compounded when high-throughput methods of polymer screening and lab-scale dewatering tests are employed to evaluate filter performance. A review of the key findings from the application of this approach to the dewatering of municipal digested sludge is given below:

- The MFT was successfully employed to screen six cationic polymers. Each of the six polymers showed a decrease in CST with increasing dosage. The optimum polymer had a combination of ‘high’ molecular weight and ‘medium’ charge density.
- Polymers were shown to improve the viability of the geotextile dewatering process by increasing solids retention and reducing the occurrence of pore blockage.

- Regression analysis of the dewatering test results revealed that, at the OPD condition, medium and cake resistances can be minimized without sacrificing solids retention using closely spaced, elongated pores to increase filter porosity.
- The dewatering test results for the expanded DOE filters demonstrated that the inverse relationship that exists between the porosity of a dewatering fabric and both medium and cake resistances is confined to the 0.1 to 1.0 % filter porosity range. Beyond 1.0 %, these properties are comparatively independent of pore structure.

In this study, we focused on the geotextile dewatering of municipal digested sludge, however, our methods are applicable to sludge sourced from a wide range of industries including precious metal mining, power generation, oil and gas, and pulp and paper. By extension, this microfabrication approach to filter design could also be applied to the investigation of other dewatering processes which rely on filtration media including filter presses. Overall, the results of this work indicate that the performance of a geotextile dewatering fabric is primarily determined by its porosity and the efficacy of polymer pre-treatment. The microfabrication approach to filter development and the use of high-throughput methods of polymer screening allow for the rapid quantification of these multivariate relationships and the optimization of the geotextile dewatering process.

Chapter 4: Metal Precipitate Sludge

The work presented in this chapter has been accepted for publication as part of the proceedings of the Tailings & Mine Waste '18 Conference to be held October 1-2, 2018 in Keystone, Colorado.

4.1 Introduction

Canada is one of the world's largest producers of base and precious metals. In 2016, the extraction and processing of economic minerals contributed over $50 billion to the country's national gross domestic product and was responsible for the employment of approximately 600,000 people [56]. However, mining operations produce large volumes of hazardous wastes that can pose a significant threat to the environment and human health. Therefore, the treatment and disposal of mine waste in a responsible manner is critical to maintaining the health and overall quality of life of Canadians, as well as the continued growth of the economy.

The two most prevalent waste materials produced by base and precious metal mining operations are mine tailings and waste rock. 'Mine tailings' refers to the fine particulate matter left over after extractive processes have been used to remove valuable constituents from ore. 'Waste rock' refers to the broken rock or overburden -ranging in size from fine sand to large boulders- removed from the ground along with the ore which contains minerals in concentrations too low for economic recovery. The ever-growing inventory of mine waste presents a major ongoing concern for the mining industry due to the potential environmental effects on receiving water bodies and inhibition of mine site reclamation strategies associated with AMD. Mine tailings and waste rock contain sulphide minerals -such as pyrite- which readily react with atmospheric oxygen and water

to form AMD. These effluents contain elevated concentrations of toxic substances such as: cyanides, arsenic, heavy metals, and other by-products of ore extraction. These substances can cause widespread damage to surrounding ecosystems [57]. The Kam Kotia Mine -located in Timmins, Ontario- is a notable example of the environmental and economic impacts of AMD. At this copper mine, a 'killzone' was created in which nearly all vegetation was destroyed as AMD flowed through the groundwater and ultimately contaminated a nearby river. Despite entering closure in the 1970s, AMD production onsite persists and is expected to continue for the indefinite future. The estimated cost to fully remediate the Kam Kotia Mine is $40.8 million [41]. Across Canada, it is estimated that as much as $5 billion will be required to remediate all existing AMD sites [42].

Conventional treatment options for AMD begin with the addition of an alkali - such as lime or caustic soda- to raise the pH [43]. The targeted pH is typically between 9.5 and 11 to precipitate metals out of solution as metal hydroxides [44]. The metal hydroxide suspension is pumped to settling ponds wherein the metal hydroxides are removed. Polymer flocculants may also be added to the process to agglomerate the solids into larger particles and improve the separation efficacy. To maintain the capacity of the AMD treatment system, the material which accumulates at the bottom of the ponds is removed periodically via dredging and subsequently sent for disposal in on-site engineered 'ponds' or transported to off-site processing facilities. The AMD precipitates produced by conventional pond treatment systems are typically 5% solids by weight [58]. Therefore, a pre-disposal precipitate dewatering process should be applied to reduce the

overall volume of material and thus minimize the land use requirements and handling costs.

Sludge dewatering is commonly performed via non-mechanical methods such as sludge drying beds. Sludge dewatering is also done via advanced mechanical systems such as: scroll decanter centrifuges, filter presses, and screw thickeners. Geotextile dewatering is a promising alternative to both methods. It uses less land than the non-mechanical methods and requires less capital and operating expenditures than the mechanical technologies. In this process, sludge is hydraulically pumped into an enclosed bag -or series of bags- made from an engineered dewatering fabric. The pumping pressure forces the free water out through the pores of the fabric while keeping the solids contained within. As dewatering proceeds, a filter cake develops on the inner surface of the bag which contributes to the retention of fine particles. In contrast to the conventional sludge dewatering methods, geotextile bags are economical, simple to use, easily transported, and can be fabricated in site specific sizes. These benefits make them particularly attractive for nomadic or transitory applications [17].

This paper explores the efficacy of thin-film dewatering filters -incorporating well-defined slit-pore geometries- to treat AMD precipitates from a nickel-copper mine in Ontario, Canada. A high-throughput screen of cationic and anionic polymer flocculants was performed to identify the best one to use in lab-scale constant PFTs. A full-factorial DOE was employed to evaluate the effects of slit-pore dimensions and spacing on dewatering performance in terms of: dewatering rate, extent of dewatering, and solids retention.

4.2 High-throughput Screening of Polymer Flocculants via LUMiFuge

The panels in Figure 41 display the solids volume versus time curves from the LUMiFuge analysis of the polymer flocculants with the MPS. Cationic polymers were found to be effective flocculants in that the rate of dewatering increased incrementally as quantities of cationic polymer were added between 1 and 8 kg/TSS. For the low polymer dose conditions (1 to 2 kg/TTS), the increase in the rate of dewatering relative to the 'no polymer' condition was slight. The polymers which displayed the best flocculation performance at these doses possess 'high' or 'very high' charge density and 'high' or 'very high' molecular weight. When the polymer dose was increased to 4 kg/TTS, the rate of dewatering was significantly increased and the observed relationship between relative solids volume and time became nonlinear; indicating a fundamental change in the separation behaviour of the MPS. A further increase in the rate of dewatering was observed for all cationic polymers with an increase in dose to 8 kg/TTS. Ultimately, 4 kg/TTS of the Kemira C-1594 polymer was identified as the optimum cationic polymer-dose combination as this condition combines excellent polymer performance and industrial practicality (i.e. acceptable treatment costs). As reported in Table 5, the C-1594 polymer has a combination of 'medium' charge density and 'high' molecular weight.

The three anionic polymers produced only minor improvements in dewatering rate with increasing dose. The lone exception to this observation was the Kemira A-1883 RS polymer at an 8 kg/TTS dose which, while able to significantly increase the rate of dewatering, was deemed impractical due to the excessive quantities of polymer required. The SNF AN 934 SH polymer at a 4 kg/TTS dose was selected as an optimum anionic

polymer and used in the PFTs to directly compare the performance of anionic and cationic polymers for the geotextile dewatering of MPS. AN 934 SH has a combination of 'medium' charge density and 'very high' molecular weight.

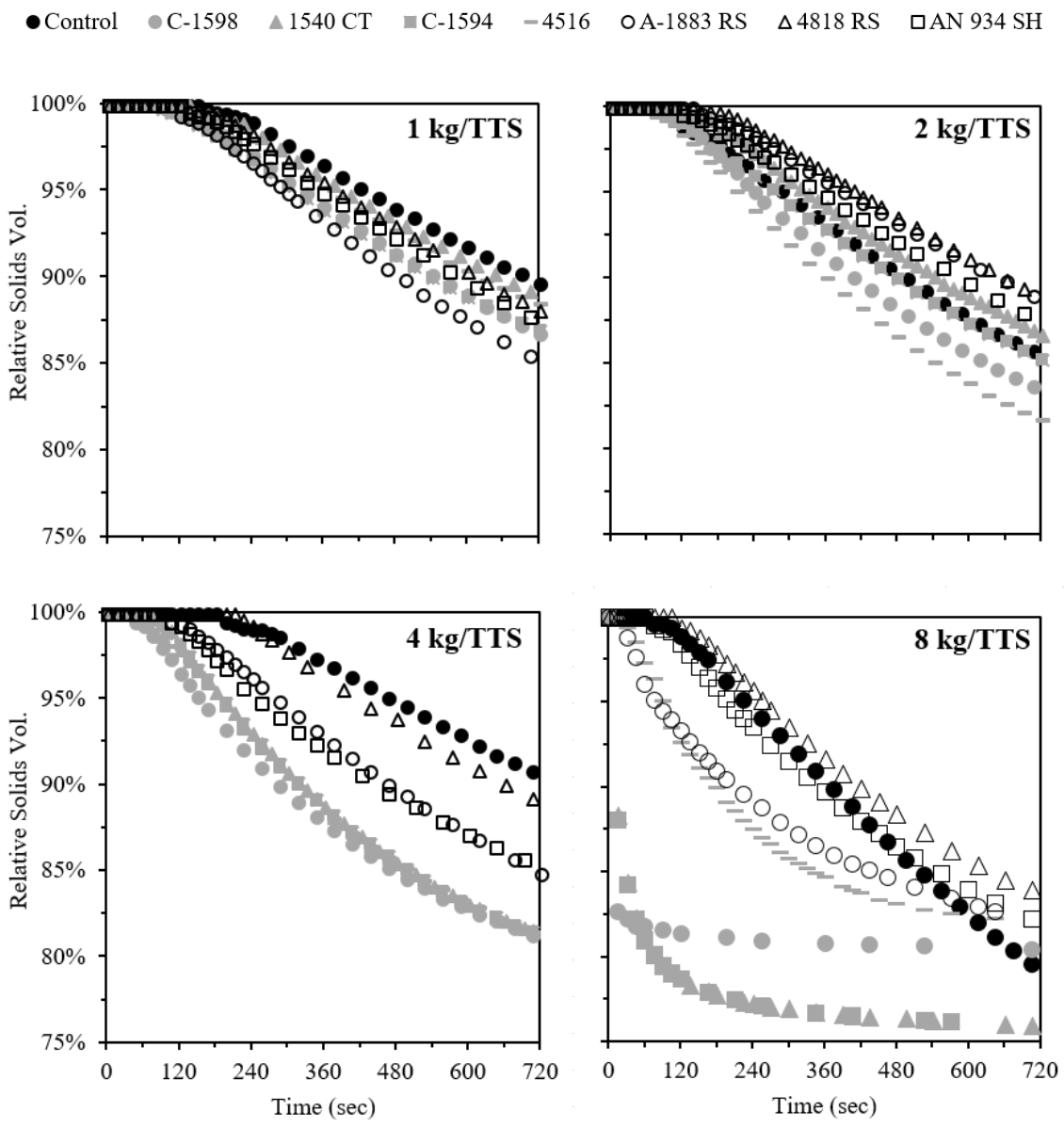

Figure 41. LUMiFuge stability analysis results for MPS treated with four cationic and three anionic polymers at four different doses.

The best flocculation conditions were further evaluated using FBRM to assess the change in particle aggregation. As shown by the chord length distributions for the as-received and treated samples of AMD precipitates in Figure 42, neither polymer-dose combination resulted in a meaningful aggregation of the MPS particles.

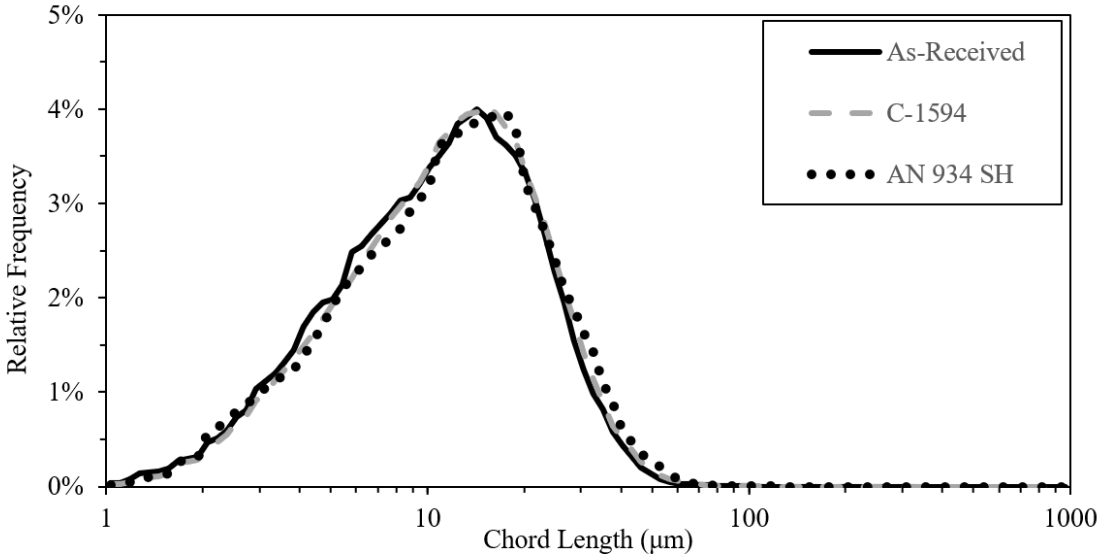

Figure 42. FBRM results depicting the impact of polymer addition on the chord length distribution of MPS. Results are shown for the pond sample as well as MPS treated with polymers C-1594 and AN 934 SH at a 4 kg/TTS dose.

4.3 Pressure Filtration Test Results

4.3.1 Woven commercial textile

The results from the duplicate PFTs performed using the Woven Commercial Textile for untreated MPS as well as those treated with 4 kg/TTS of the C-1594 and AN 934 SH polymers are shown in Figure 43. Panel A of Figure 43 includes mass of filtrate versus time curves which illustrate the rate of dewatering achieved at an applied pressure of 35 kPa. Overall, geotextile dewatering of the MPS using conventional engineered dewatering fabrics was shown to be a slow process. Without polymer pre-treatment, the Commercial Woven Textile required an average of 200 (+/- 20) min to reach BT; the

specified error representing the observed range above and below the average BT across duplicate tests. The application of a polymer pre-treatment step using C-1594 was only able to reduce the required dewatering time to 190 (+/- 10) min while AN 934 SH reached BT in 196 (+/- 9) min. Therefore, neither the cationic nor the anionic polymer were able to improve the rate of dewatering to a degree that would justify the additional operating cost associated with their use.

Despite requiring an extended amount of time to perform dewatering, the Commercial Woven Textile was able to significantly increase the SC of the MPS. Panel B of Figure 43 displays the SC of the filter cake after dewatering; the error bars representing the observed range above and below the average across duplicate tests. Without polymer pre-treatment the average SC was 18.5 (+/- 0.6) % while the use of C-1594 and AN 934 SH yielded SC values of 17.0 (+/- 0.8) % and 17.0 (+/- 0.2) %, respectively. The SC values correspond to DEs of 179 % (with either C-1594 or AN 934 SH) and 203 % (without polymer pre-treatment). Therefore, despite the significant difference in separation performance between cationic and anionic polymers observed in the LUMiFuge results, both polymer-dose combinations yielded the same dewatering capacity. Furthermore, the use of either polymer type was shown to decrease the dewatering capacity of the Woven Commercial Textile relative to the 'no polymer' condition.

Panel C of Figure 43 displays the average filtrate TSS measured for each of the four sequential 45 g filtrate fractions collected; the error bars represent the range above and below the average across duplicate tests. Without polymer pre-treatment, the woven

textile yielded an average filtrate TSS of 4200 (+/- 200) mg/L for F1, 97 (+/- 0) mg/L for F2, 16 (+/- 1) mg/L for F3, and 40 (+/- 20) mg/L for F4. The dramatic decrease in filtrate TSS suggests that, over time, an effective filter cake was developed on the surface of the Commercial Woven Textile which served as the dominant mechanism by which solids were retained. For context, the 'daily concentration limit' of TSS for effluent originating from metal mining operations in Ontario, Canada is 30 mg/L (as per O Reg 560/94). Therefore, the Commercial Woven Textile was able to meet the discharge limit after sufficient filter cake development without the use of polymer flocculants. The range of TSS values reported above for the Woven Commercial Textile without polymer pre-treatment correspond to FEs of 93.4 % (for F1) and 99.9 % (for F4). Therefore, the Commercial Woven Textile was able to retain nearly all the suspended solids present in the MPS after the filter cake was established. The use of a cationic polymer to pre-treat the MPS was shown to provide a modest improvement in FE during the initial stages of dewatering. Specifically, a 4 kg/TTS dose of C-1594 increased the average FE calculated for F1 from 93.4% to 96.6%. The FEs calculated for F2, F3, and F4 were comparable to the 'no polymer' condition. Conversely, pre-treating with AN 934 SH yielded a FE of only 92.0 % for F1. Hence, the cationic polymer provided a slight improvement in solids retention during the earliest stages of dewatering, while no improvement was observed for the anionic polymer. After the establishment of the filter cake, the Commercial Woven Textile displayed excellent solids retention with or without polymer pre-treatment.

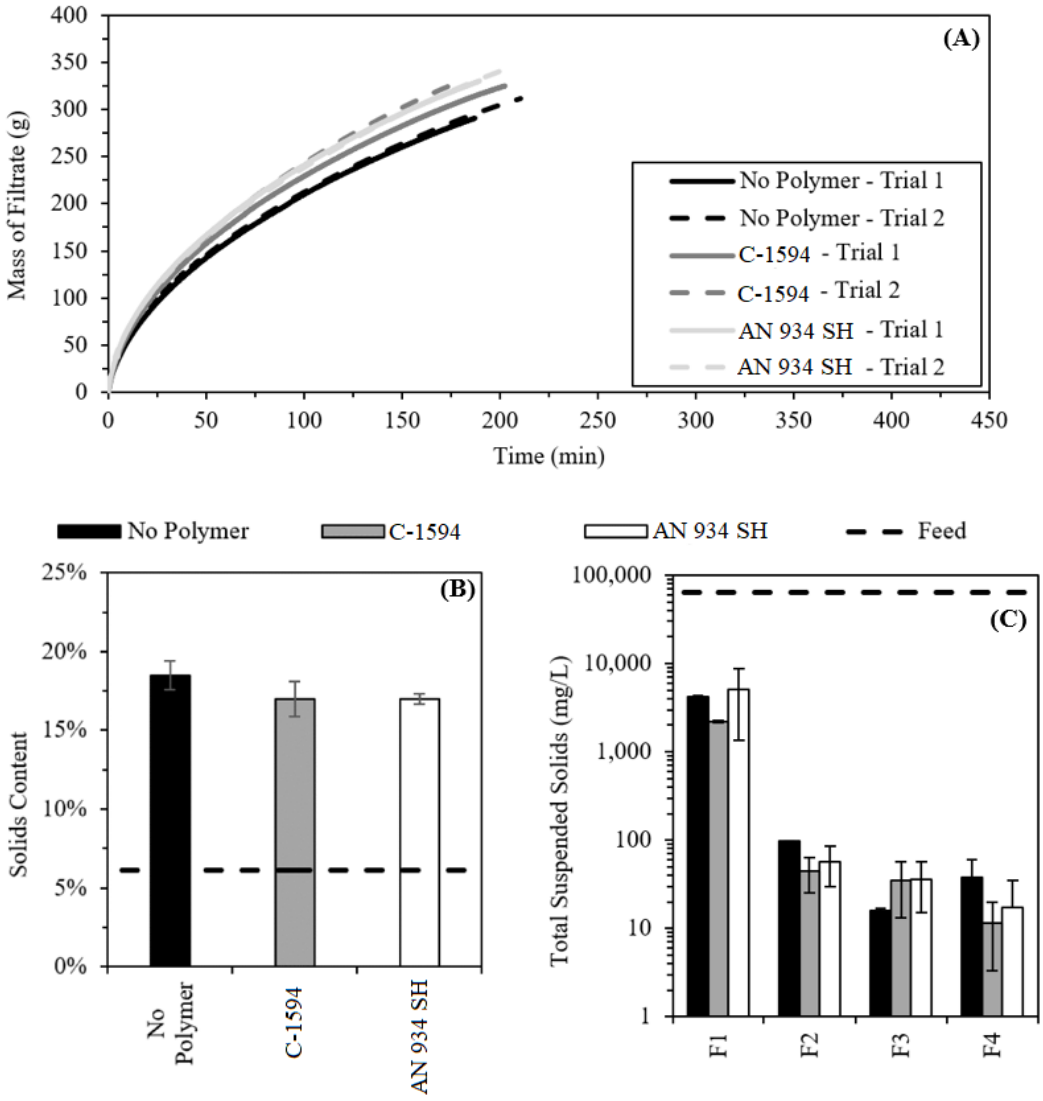

Figure 43. PFT results using the Commercial Woven Textile for the pond sample without polymer pre-treatment, with a 4 kg/TTS dose of C-1594, and with a 4 kg/TTS of AN 934 SH. Panel A displays the mass of filtrate versus time curves, Panel B displays the SC of the material retained within the suspension cell after dewatering, and Panel C displays the total suspended solids of the four filtrate fractions.

4.3.2 Thin-film dewatering filters without polymer pre-treatment

Figure 44 displays the results of the PFTs performed using the thin-film dewatering filters for untreated MPS. Panel A of Figure 44 displays the mass of filtrate versus time curves for each filter. These results indicate that a negative correlation exists between the time required to reach BT and filter porosity. For example, the

‘100×1500_4mm’ filter (having a porosity of only 0.69%) required 425 min to dewater the 500 g sample. Conversely, the ‘100×5000_1mm’ filter, having a porosity of 8.81%, required only 138 min. Therefore, by increasing the aspect ratio of the slit-pores from 15:1 to 50:1 and reducing the pore-to-pore spacing from 4 mm to 1 mm, the BT time was reduced by 70%. The power regression of the BT times versus porosity (P) for the treatment of AMD precipitates is presented as Equation 9:

$$BT\ (min) = 327.55(P)^{-0.382} \tag{9}$$

The coefficient of determination was 0.95. As previously discussed, the Commercial Woven Textile required 200 (+/- 20) min to reach BT; this result falls between the 173 min required by the ‘100×1500_1mm’ filter (which has a porosity of 6.03%) and the 299 min required by the ‘100×5000_4mm’ filter (having a porosity of 0.88%). Therefore, although not reported by the manufacturer, the effective porosity of the woven textile is estimated to be 3.64% using Equation 9.

Filter porosity was also shown to impact DE. Panel B of Figure 44 displays the SC of the material retained within the suspension cell at the end of the PFT for each of the thin-film dewatering filters without polymer pre-treatment. The measured SC values for the two highest porosity filters (‘100×5000_1mm’ and ‘100×1500_1mm’) were 19.6% and 18.1% which correspond to DEs of 221% and 197%, respectively. Conversely, the two lowest porosity filters (‘100×5000_4mm’ and ‘100×1500_4mm’) yielded DEs of only 179% and 189%. Therefore, increasing the porosity of a thin-film filter using longer, more densely spaced pores not only increases the rate at which dewatering occurs, it also provides a modest improvement to the extent of dewatering achieved.

Panel C of Figure 44 displays the TSS of the four sequential filtrate fractions collected using the thin-film dewatering filters. Although increasing filter porosity results in greater solids passthrough during the initial stages of the dewatering process, excellent solids retention is achieved irrespective of filter porosity once a stable filter cake is established. For example, the '100×1500_4mm' filter yielded a TSS of 4027 mg/L for F1; a value which corresponds to a FE of 93.7%. However, FE quickly improved to 99.9% for F2. Conversely, the '100×5000_1mm' filter yielded a TSS of 41,547 mg/L for F1, 50,580 mg/L for F2, 18,767 mg/L for F3 and, finally, 40 mg/L for F4. These values correspond to FEs of 26.5%, 17.5%, 63.1%, and 99.9%, respectively. Hence, a stable filter cake was not established on the surface of this filter until after the collection of 135 g of filtrate (F3). However, according to Panel A of Figure 44, this cake development period corresponds to only the first 5 min of dewatering, indicating that excellent solids retention was achieved for the majority of the PFT. Therefore, for full-scale applications where large volumes of MPS are to be dewatered, the period of reduced solids retention during cake layer development is expected to be limited to the initial filling of the dewatering bag and be negligible in the overall operating life of the dewatering textile.

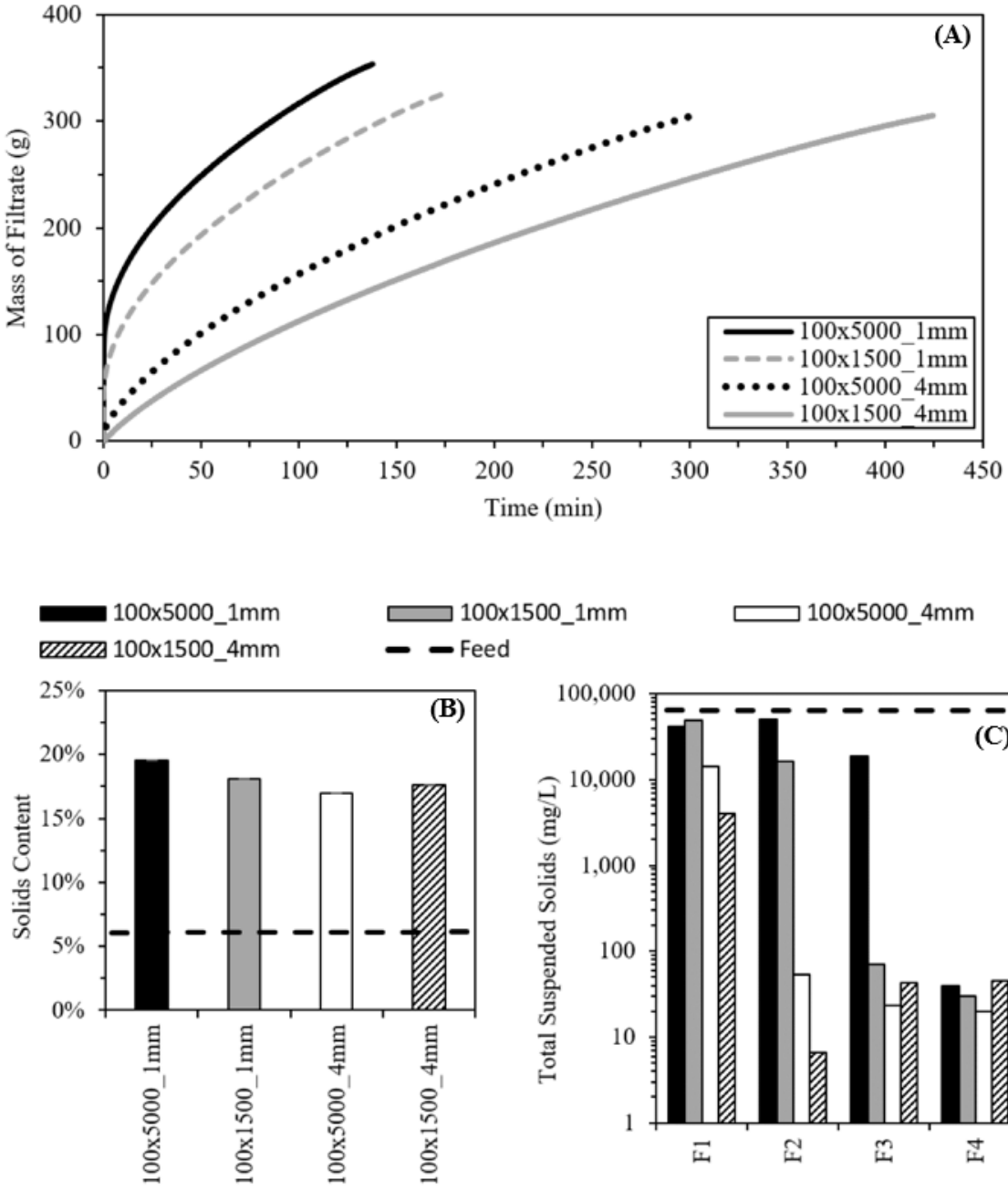

Figure 44. PFT results using the four thin-film dewatering filters for the pond sample without polymer pre-treatment. Panel A displays the mass of filtrate versus time curves, Panel B displays the SC of the material retained within the suspension cell after dewatering, and Panel C displays the total suspended solids of the four filtrate fractions.

4.3.3 High-porosity thin-film dewatering filters with polymer pre-treatment

Additional PFTs were performed to determine if polymer pre-treatment can be applied to promote more rapid filter cake development for the high porosity thin-film dewatering filters. Figure 45 displays the average TSS for the sequential filtrate fractions collected using the '100×5000_1mm' and '100×1500_1mm' filters in combination with 4 kg/TTS doses of C-1594 and AN 934 SH. Once again, the error bars represent the observed range above and below the average TSS result for duplicate tests. The obtained results indicate that a stable filter cake was established significantly earlier in the PFT for the high porosity thin-film dewatering filters when polymer pre-treatment of the MPS was employed.

As previously discussed, the '100×5000_1mm' filter did not develop a filter cake capable of retaining the MPS particles prior to the collection of 135 g of filtrate without polymer pre-treatment. However, applying a 4 kg/TTS dose of either C-1594 or AN 934 SH significantly reduced filtrate TSS during the initial stages of dewatering. Specifically, C-1594 resulted in 36%, 84% and 99 % reductions in TSS for F1, F2, and F3, while Polymer A3 produced decreases of 19%, 95%, and 99% compared to the no-polymer trials. Similar observations can be made for the '100×1500_1mm' filter which displayed poor solids retention for the first two filtrate fractions without polymer pre-treatment. In this case, C-1594 yielded reductions of 41% and 99% for F1 and F2, while AN 934 SH produced decreases of 46% and 99%. Therefore, filter cake development was shown to occur significantly earlier in the dewatering process for the high porosity thin-film

dewatering filters when either the cationic or the anionic polymer were used to pre-treat the MPS.

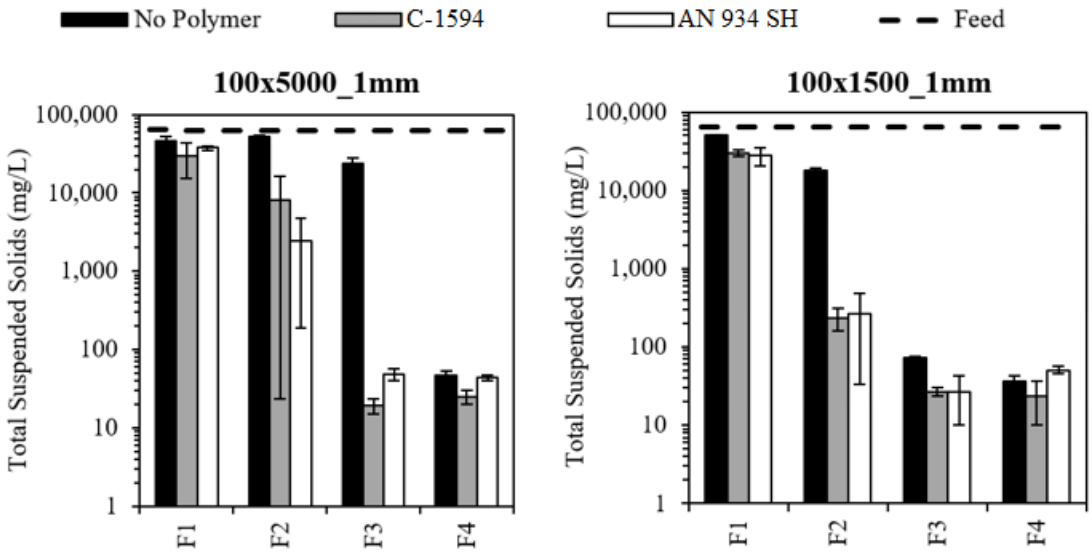

Figure 45. Filtrate TSS results using the '100×5000_1mm' and '100×1500_1mm' filters for the pond sample without polymer addition, with a 4 kg/TTS dose of C-1594, and with a 4 kg/TTS dose of AN 934 SH

4.4 Conclusions

In this study, we investigated the efficacy of microfabricated thin-film dewatering filters for treating AMD precipitates through the performance of lab-scale PFTs. The effects of optimized polymer pre-treatment and the pore geometry, as well as total porosity of the filters, were studied. The dewatering rate, solids retention, and extent of dewatering results were compared to those for a commercially available woven dewatering textile. A review of the key findings from this research is given below:

- A LUMiFuge analytical centrifuge was used to screen four cationic and three anionic polymers. The cationic polymers significantly increased the rate of

dewatering of AMD precipitates, while the use of the three anionic polymers yielded minimal benefit.

- The woven textile was able to retain 99.9 % of the suspended solids after filter cake development and increase the SC of the AMD precipitates by up to 203%. However, permeability was low, resulting in a slow dewatering process. The use of polymer pre-treatment did not provide a meaningful improvement in dewatering rate, but cationic polymers did provide a slight improvement in the rate of filter cake development.
- The PFT results for the thin-film dewatering filters demonstrated that the use of closely spaced, elongated pores -which results in a high porosity- significantly improved the rate of dewatering and provided moderate improvements in DE relative to conventional engineered dewatering fabrics. Furthermore, although increasing porosity was shown to delay filter cake development, excellent solids retention was achieved irrespective of porosity once a stable filter cake was established.
- Cationic and anionic polymers significantly increased the rate of filter cake development for the high porosity, thin-film dewatering filters; minimizing solids passthrough during the initial stages of dewatering.

Overall, this work provides new insights into the importance of pore geometry, porosity, and polymer performance on filter cake development. The dewatering of AMD precipitates is an important and often overlooked facet of mine waste management. The results presented herein indicate that the use of high-porosity dewatering fabrics

incorporating slit-pore geometries is a viable method of performing AMD precipitate dewatering in a manner that is both environmentally and economically responsible.

Chapter 5: Conclusions and Future Work

5.1 Conclusions

Sludge dewatering is conventionally performed via non-mechanical methods or advanced mechanical systems. Although these technologies perform admirably, their inherent limitations restrict their widespread adoption; non-mechanical dewatering methods require large areas of land, appropriate site topography, and favorable climatic conditions, while mechanical dewatering technologies require significant capital and operating expenditure. Engineered dewatering fabrics represent a simple, low cost alternative to the conventional methods of sludge dewatering and have been successfully applied to both small and large-scale operations.

However, there are limitations to the usefulness of the engineered dewatering fabrics available on the market today. To begin, these dewatering fabrics are selected for a given application based on empirical ratios between the dewatering characteristics of the sludge and the porous properties of the textile material. This is problematic as the methods available for characterizing dewatering fabrics are unreliable, operator-dependent, and extremely time consuming. Furthermore, this approach does not consider the relationship between the properties of the fabric and the permeability of the filter cake, or its rate of development. The conventional dewatering fabrics are also prone to fouling. Depending on the dewatering characteristics of the feed material and the efficacy of the pre-treatment conditions employed, the pore openings of the fabric can become blocked with solid material and cause a premature end to the dewatering process.

In this work, a series of next-generation dewatering fabrics featuring well-defined slit-pore geometries were produced using advanced microfabrication techniques. In

contrast with the conventional woven and nonwoven dewatering fabrics, these microfabricated fabrics possess pore structures which can be exactly defined prior to fabrication, allowing for the application of DOE frameworks and the development of regression models for key performance metrics. Furthermore, the use of solid-state laser technology, in combination with computer aided design software, allows for a rate of prototype development greater than that achievable for conventional fabrics. These benefits are compounded when high-throughput methods of polymer screening and lab-scale dewatering tests are employed to evaluate filter performance.

Full-factorial DOE frameworks and laboratory-scale DPTs were employed in this work to evaluate the effects of slit-pore dimensions, slit-pore spacing, and pre-treatment conditions on key dewatering performance metrics and filter cake properties for two sludge sources: ADS and MPS. The results of these two studies demonstrated that increasing the length of the pore openings -or decreasing the distance between adjacent pores- increased the permeabilities of the dewatering fabrics without degrading their ability to retain small particles. Furthermore, the improved permeabilities were maintained throughout the dewatering process, indicating the higher porosity fabrics were less prone to fouling. These fabrics were also found to be less sensitive to pre-treatment conditions; deviations from the OPD did not result in a pre-mature end to dewatering of the ADS for the fabrics having longer, more closely spaced pores.

Overall, this work provides new insights into the importance of a dewatering fabric's pore geometry and porosity, the dewatering characteristics of the sludge material, and the efficacy of polymer pre-treatment in optimizing the geotextile dewatering

process. The results presented in Chapters 3 and 4 indicate that the use of high-porosity dewatering fabrics incorporating slit-pore geometries is a viable method of dewatering both ADS and MPS. These fabrics were also shown to provide substantial advantages over the traditional woven dewatering fabrics.

5.2 Future Work

The next phase of this research project will be the development of pilot-scale geotextile dewatering bags integrating the slit-pore geometries assessed in this work. The flatbed fiber laser cutting system used to produce the thin-film dewatering filters is ideally suited for prototype development. However, such microfabrication techniques are not appropriate for full-scale manufacturing given their high cost and limited throughput. Therefore, a new technology must be applied in order to transition to the next phase of product development. An option for manufacturing dewatering fabric samples having elongated pore openings of various sizes is perforation. The samples would be made from polyvinyl chloride or thermoplastic polyolefin which are inert to biological degradation, resistant to both alkalis and acids, and have sufficient mechanical properties to remain intact throughout the dewatering process.

The prototype samples will first be evaluated with ADS and MPS at the laboratory scale using the DPT apparatus. The results from these tests will be compared to those for the thin-film dewatering filters as well as the woven commercial textile. Following the laboratory scale testing, the next step will be transferring this technology to the pilot-scale. Field tests will be performed following the ‘TenCate Geotube GDT Test’ procedure [59]. This will be accomplished through the construction of dewatering bags that are 46

cm wide by 92 cm long. On one side of each bag a large opening will be included to accommodate the installation of a flange connected to a stand pipe 92 cm long. In addition, a zipper will be installed in order to empty, clean, and re-use the bags multiple times. For each dewatering experiment, the assembly will be positioned on a custom-made stand directly over a large plastic reservoir to collect the filtrate as shown in Figure 46. Approximately 100 L of feed material will be continuously added to the bags via the stand pipe to generate enough head pressure to push the liquid fraction through the fabric. A variety of metrics will be used to assess dewatering performance and statistical tools will be used to identify the critical process parameters.

Figure 46. Image of the TenCate Geotube GDT Test [59].

References

[1] S. K. Bhatia, "Sustainable Management of Dredged Sediments and Waste Using Geotextile Tube Dewatering System," in *Geoenvironmental Practices and Sustainability*, M. Datta, A. De, K. Reddy and G. Sivakumar Babu , Eds., Springer, Singapore, 2017, pp. 91-97.

[2] Ontario Ministry of the Environment, "Design Guidelines For Sewage Works," Toronto, 2008.

[3] L. Svarovsky, Solid-Liquid Separation, England: Butterworth & Co, 1977.

[4] M. Collard, B. Teychené and L. Lemée, "Comparison of three different wastewater sludge and their respective drying processes: Solar, thermal and reed beds – Impact on organic matter characteristics," *Journal of Environmental Management,* vol. 203, pp. 760-767, 2017.

[5] L. K. Wang, N. K. Shammas and Y. Hung, "Drying Beds," in *Biosolids Treatment Processes*, 2007, pp. 403-430.

[6] B. J. Kim and E. D. Smith, "Evaluation of Sludge Dewatering Reed Beds: A Niche for Small Systems," *Water Science & Technology,* vol. 35, no. 6, pp. 21-28, 1997.

[7] E. Tilley, L. Ulrich, C. Lüthi, P. Reymond and C. Zurbrügg, Compendium of Sanitation Systems and Technologies, 2nd Revised Edition ed., Duebendorf (SUI): Swiss Federal Institute of Aquatic Science and Technology (Eawag), 2014.

[8] F. Zafari, "Development of the Next-Generation of Dewatering Technologies for Mature Fine Tailings (MFTs) from Oil Sands Processing," McMaster University, Hamilton (ON), 2016.

[9] A. Records and K. Sutherland, Decanter Centrifuge Handbook, Oxford (UK): Elsevier Science Ltd., 2001.

[10] R. J. Wakeman, "Separation technologies for sludge dewatering," Journal of Hazardous Materials, vol. 144, no. 3, pp. 614-619, 2007.

[11] J. Gregory, "Flocculation Fundamentals," in Encyclopedia of Colloid and Interface Science, Heidelberg, Springer, 2013, pp. 459-624.

[12] N. K. Shammas, "Coagulation and Flocculation," in Handbook of Environmental Engineering, Vol 3: Physiochemical Treatment Processes, New Delhi, Humana Press, 2005, pp. 103-139.

[13] J. Cobbledick, A. Nguyen and D. R. Latulippe, "Demonstration of FBRM as process analytical technology tool for dewatering processes via CST

correlation," Water Research, vol. 58, no. 1, pp. 132-140, 2014.

[14] R. J. LaRue, J. Cobbledick, N. Aubry, E. D. Cranston and D. R. Latulippe, "The microscale flocculation test (MFT) - A high-throughput technique for optimizing separation performance," *Chemical Engineering Research and Design,* pp. 85-93, 2016.

[15] S. K. Dentel, M. M. Abu-Orf and C. A. Walker, "Optimization of slurry flocculation and dewatering based on electrokinetic and rheological phenomena," Chemical Engineering Journal, vol. 80, no. 1-3, pp. 65-72, 2000.

[16] R. Costa, J. L. Pereira, J. Gomes, F. Gonçalves, D. Hunkeler and M. G. Rasteiro, "The effects of acrylamide polyelectrolytes on aquatic organisms: relating toxicity to chain architecture," Chemosphere, vol. 112, pp. 177-184, 2014.

[17] B. W. Maurer, A. C. Gustafson, S. K. Bhatia and A. M. Palomino, "Geotextile dewatering of flucculated, fiber reinforced fly-ash slurry," Fuel, vol. 97, pp. 411-417, 2012.

[18] K. R. Morgan, "Geotextile Tubes and Their Application to Dewatering," Georgia Southern University, Statesboro (GA), 2014.

[19] H. K. Moo-Young , D. A. Gaffney and X. Mo, "Testing procedures to assess the viability of dewatering with geotextile tubes," *Geotextiles and Geomembranes,* vol. 20, no. 5, pp. 289-303, 2002.

[20] GEI Works, "Geotextile Dewatering Tubes," 2018. [Online]. Available: https://www.erosionpollution.com/geotextile_dewatering_tubes.html. [Accessed 18 June 2018].

[21] J. Smith and S. K. Bhatia, "Geotextile Characterization and Pore-Size Distribution: Part I. A Review of Manufacturing Processes," Geosynthetics International, vol. 3, no. 1, pp. 85-105, 1996.

[22] A. H. Aydilek, "Geotextile Pore Structure Characterization Using Image Analysis," in Proceedings of the 4th International Conference on Filters and Drainage in Geotechnical and Environmental Engineering, Stellenbosch (RSA), 2004.

[23] A. H. Aydilek and T. B. Edil, "Evaluation of Woven Geotextile Pore Structure Parameters Using Image Analysis," Geotechnical Testing Journal, vol. 27, no. 1, pp. 99-110, 2004.

[24] W. W. Muller and F. Saathoff, "Geosynthetics in geoenvironmental engineering," Science and Technology of Advanced Materials, pp. 1-20,

2015.

[25] A. H. Aydilek, S. H. Oguz and T. B. Edil, "Digital Image Analysis to Determine Pore Opening Size Distribution of Nonwoven Geotextiles," Journal of Computing in Civil Engineering, vol. 16, no. 4, pp. 280-290, 2002.

[26] ASTM International, "Standard Test Methods for Determining Apparent Opening Size of a Geotextile," West Conshohocken (PA), 2016.

[27] M. G. A. Guimaraes, D. C. Urashima and D. M. Vidal, "Dewatering of sludge from a water treatment plan in geotextile closed systems," Geosynthetics International, vol. 21, pp. 310-320, 2014.

[28] Parsons Corporation, "Onondaga Lake Sediment Consolidation Area (SCA) Dewatering Evaluation," Liverpool (NY), 2009.

[29] J. Fowler, R. M. Bagby and E. Trainer, "Dewatering sewage sludge with geotextile tubes," Geotechnical Fabrics Report, vol. 15, no. 7, pp. 26-30, 1997.

[30] A. D. Sobrino, T. Stephens and C. Timpson, "Containment and Dewatering of Mine Tailingswutg Geotextile Tubes at a Silver Mine in San Luiz, Mexico," in *Proceedings of the 20th International Conference on Tailings*

and Mine Waste, Keyston (CO), 2016.

[31] B. Visser, L. Charlie , B. Timothy , H. Vicki , N. Deanna , S. Rebecca and V. d. V. John , "Vegetable and Fruit Washwater Treatment Manual," Ontario Ministry of Agriculture Food and Rural Affairs, Toronto (ON), 2017.

[32] T. Hein, "Improving water quality," Fruit & Vegetable, pp. 12-13, April 2016.

[33] B. Visser, Technology Investigation: Filter Bags, Holland Marsh Growers Association, 2016.

[34] F. Da Silva and M. Graham, "Geotextile bags for enhanced dewatering and accelerated consolidation of oil sands mature fine tailings," in Proceedings Tailings and Mine Waste 2014, Keystone (CO), 2014.

[35] M. Chandler and A. Zydney, "Effects of membrane pore geometry on fouling behaviour during yeast cell microfiltration," Journal of Membrane Science, vol. 285, no. 1-2, pp. 334-342, 2006.

[36] A. J. Bromley, R. Holdich and I. W. Cumming , "Particulate fouling of surface microfilters with slotted and circular pore geometry," Journal of Membrane Science, vol. 196, no. 1, pp. 27-37, 2002.

[37] D. M. Kanani, W. H. Fissell, S. Roy, A. Dubnisheva, A. Fleischman and A. l. Zydney, "Permeability-selectivity analysis for ultrafiltration: Effect of pore geometry," *Journal of Membrane Science,* vol. 349, no. (1-2), pp. 405-410, 2010.

[38] United States Environmental Protection Agency, "Primer for Municipal Wastewater Treatment Systems," Washington (DC), 2004.

[39] M. E. Ersahin, H. Ozgun, R. K. Dereli and I. Ozturk, "Anaerobic Treatment of Industrial Effluents: An Overview of Applications," in Waste Water Treatment and Reutilization, InTech, 2011, pp. 3-28.

[40] Canadian Council of Ministers of the Environment, "Guidance Document for the Beneficial Use of Municipal Biosolids, Municipal Sludge and Treated Septage," 2012.

[41] C. D. Hamblin and M. G. Kord, "The Rehabilitation of Ontario's Kam Kotia Mine: an Abandoned Acid Generating Tailings Site," in *Proceedings of the Sudbury 2003 Conference on Mining and the Environment III*, Sudbury (ON), 2003.

[42] Environment Mining Council of BC, "Acid Mine Drainage: Mining & Water Pollution Issues in BC," 2000. [Online]. Available:

http://www.protectfishlake.ca/media/amd.pdf. [Accessed June 2018].

[43] M. A. Barakat, "New trends in removing heavy metals from industrial wastewater," *Arabian Journal of Chemistry,* vol. 4, no. 4, pp. 361-377, 2011.

[44] B. Aubé, "The Science of Treating Acid Mine Drainage and Smelter Effluents," Québec (QC), 2004.

[45] A. W. Miller, P. L. Sibrell and T. R. Wilderman, "Comparison of Sludge Characteristics Between Lime and Limestone/Lime Treatment of Acid Mine Drainage," in 30 Years of SMCRA and Beyond, Gillette (WY), 2007.

[46] P. Kaye, "Successful Dewatering of Acid Mine Drainage Materials," 26 April 2016. [Online]. Available: https://www.bishopwater.ca/a/uploads/case_studies/20160426124132_acid-tailings.pdf. [Accessed 21 June 2018].

[47] B. Dowsley, W. Sandes and C. Hambling, "Treatment and Discharge of Acid Mine Drainage at the Kam Kotia Abandoned Mine Site," Stantec, Sudbury (ON), 2007.

[48] L. S. Clescerl, A. E. Greenberg and A. D. Eaton, Eds., Standard methods for the examination of water and wastewater, 20th ed., Washington (DC): American Public Health Association, 1999.

[49] A. R. Heath, P. D. Fawell, P. A. Bahri and J. D. Swift, "Estimating Average Particle Size by Focused Beam Reflectance Measurement (FBRM)," Particle & Particle Systems Characterization, vol. 19, no. 2, pp. 84-95, 2002.

[50] Mettler Toledo, "ParticleTrack G400," [Online]. Available: https://www.mt.com/ca/en/home/products/L1_AutochemProducts/FBRM-PVM-Particle-System-Characterization/FBRM/fbrm-g400.html#documents. [Accessed 14 August 2018].

[51] T. Sobisch and D. Lerche, "Use of Analytical Centrifugation for Evaluation of Solid-Liquid Separation in Decanter Centrifuges: Application to Selection of Flocculants for Sludge Dewatering," Filtration, pp. 270-274, 2004.

[52] J. Sirviö, A. Honka, H. Liimatainen, J. Niinimäki and O. Hormi, "Synthesis of highly cationic water-soluble cellulose derivative and its potential as novel biopolymeric flocculation agent," Carbohydrate Polymers, vol. 86, no. 1, pp. 266-270, 2011.

[53] F. M. Mahdi and R. G. Holdich, "Laboratory cake filtration testing using constant rate," Chemical Engineering Research and Design, vol. 91, no. 6, pp. 1145-1154, 2013.

[54] ASTM International, *ASTM D4491 / D4491M-17, Standard Test Methods for Water* Permeability *of Geotextiles by Permittivity,* West Conshohocken,

PA, 2017.

[55] K. Liao and S. Bhatia, "Evaluation on filtration performance of woven geotextiles by falling head, pressure filtration test, and hanging bag tests.," in *Proceedings of the 8th International Conference on Geosynthetics*, Yokohama (JP), 2006.

[56] The Mining Association of Canada, "Facts and Figures 2017," 2018. [Online]. Available: http://mining.ca/sites/default/files/documents/Facts-and-Figures-2017.pdf. [Accessed June 2018].

[57] N. T. Sithole, "Removal of heavy metals from aqueous acidic mineral effluents by reductive precipitation," University of Johannesburg, Johannesburg (RSA), 2015.

[58] Mine Environment Neutral Drainage Program, "Characterization and Stability of Acid Mine Drainage Treatment Sludges," 1997.

[59] TenCate Geosynthetics, "TenCate Geotube GDT Test," 2006.

[60] J. P. B. Cobbledick, "Lab-Scale Recuperative Thickening: Dewatering Optimization," McMaster University, Hamilton (ON), 2016.